Modeling structural acoustic properties of loudspeaker cabinets

Luan, Yu

Publication date:
2011

Document Version
Publisher's PDF, also known as Version of record

Technical University of Denmark

Yu Luan

Modeling structural acoustic properties of loudspeaker cabinets

PhD thesis, March 2011

DTU Electrical Engineering
Department of Electrical Engineering

Modeling structural acoustic properties of loudspeaker cabinets

Technical University of Denmark
Department of Electrical Engineering
Acoustic Technology
DK-2800 Kgs. Lyngby
Denmark

Bang & Olufsen
Peter Bang's Vej 15
DK-7600, Struer
Denmark

Submitted in partial fulfillment of the requirements for the degree of Doctor of Philosophy at the Technical University of Denmark.

Preface

This dissertation is the documentation of my work carried out in partial fulfillment of a PhD study. This work has been carried out from February 15th 2008 to March 31 2011 at Acoustic Technology, Department of Electrical Engineering, Technical University of Denmark (DTU) and at Bang & Olufsen (B&O). The topic of this dissertation is on modeling structural acoustic properties of loudspeaker cabinets. The project has been carried out under the supervision of Mogens Ohlrich (main supervisor) and Finn Jacobsen (co-supervisor) both from DTU, and from B&O supervision have been given by Søren Bech, Mogens Brynning (for the first year and three months), Frank Bastrup Jørgensen (for remaining two years) , Sylvain Choisel (for the first year), Lars Falk Knudsen and Gert Kudahl Munch. The published/submitted papers during my Ph.D. study are attached at the end of the dissertation.

Yu Luan

Kgs. Lyngby, 31 March 2011

Acknowledgements

The author would like to express his sincere acknowledgements to all supervisors for their suggestions, support and encouragement during the project, especially to Mogens Ohlrich and Finn Jacobsen. He also gratefully acknowledges the support, both academic and financial, from Bang & Olufsen. Tremendous tributes are paid to the family members, especially to his mother, who encouraged the author and watched him gradually making progress with great patience.

Abstract

In this dissertation, a theoretical/numerical methodology is presented for coarse and fast predictions of cabinet vibrations. The study is focused on vibrations of rib-stiffened panels by improving a smearing technique and employing it into finite element modeling. The computationally efficient smearing technique for a cross-stiffened flat thin rectangular plate has been known for many years, but so far the accuracy of predicted natural frequencies has been inadequate. To improve predictions, all stiffeners including the ones neglected in the ordinary smearing technique are taken into account in the calculation of bending stiffness in this dissertation. The improved smearing technique results in good accuracy for predicted natural frequencies and forced vibrations of flat stiffened plates. Another improvement concerns the orientation of the stiffeners. The original smearing technique presupposes that the stiffeners are parallel to the edges of the plate, but simple considerations make it possible to relax this requirement. Whereas the improved smearing technique is well established for stiffened flat panels, there is no similar established technique for doubly curved stiffened shells. In an additional study, the improved smearing technique is combined with the equation of motion for a doubly curved thin rectangular shell, and a solution is offered for using the smearing technique for stiffened shell structures. Finally, the developed smearing technique is employed in a finite element modeling for estimating the vibrational properties and associated sound radiation of models including stiffened panels. Overall, the developed technique is found to be a good method for fast estimations of cabinet vibrations.

Contents

Contents

1 Introduction

1.1 Problem formulation

Un-intended audible vibrations of the cabinet of a loudspeaker system deteriorate its sound quality and are therefore not acceptable in high-quality products. The optimal design of a loudspeaker consists of speaker units with magnetic armatures and vibrating membranes for producing the wanted sound, and with these membranes resiliently mounted in an otherwise rigid and motionless cabinet. With traditional loudspeakers, high quality has been accomplished by mounting the speaker units in a heavy wooden cabinet made of thick compressed wood panels. Many modern loudspeaker cabinets, however, are often of moulded design and fabricated using plastic composites. An advantage of employing moulded plastic cabinets is the ease with which rib-stiffeners can be integrated in the cabinet panels. Such rib-stiffened cabinets are light-weighted and of considerable stiffness because of the rib-stiffeners. Even though membranes of the speaker units are resiliently mounted in the cabinet, they may result in the transmission of unwanted vibrations to the cabinet walls that give rise to audible sound radiation, in particular for transient excitation, and hence a deterioration of the sound quality of the loudspeaker. This also applies to the vibration transmitted via the steel suspension frame of the loudspeaker unit. The purpose of this project is to develop a theoretical/numerical methodology that can be used early in a design process for coarse and fast predictions of the level of such unwanted cabinet vibrations, so that suitable measures and structural modifications of the loudspeaker cabinet can be implemented to minimize the vibration problem.

Finite element analysis (FEA) is nowadays a standard tool for dynamic analyses of complex structures. The analysis involves partitioning a structure into several substructural elements, describing the behavior of each element in a simple way, and then reconnecting the substructural elements at nodes [1]. Advanced commercial software such as ANSYS and ACTRAN can be used for ‘building’ the numerical finite element (FE) models which can estimate the unwanted vibration and associated sound radiation of a loudspeaker cabinet. However, it takes a long time for an engineer to establish an FE model, and also for a computer to calculate the result. Even though computers become more and more powerful, the engineer’s working hours for making drawings and ‘building’ a realistic dynamic FE model have almost not changed. For complex structures, which generally includes rib-stiffeners, the time for an FE estimating could be even longer than making and measuring on physical prototypes. Thus, it is very useful if the geometry can be simplified, for example, by employing a smearing technique, which treats the three-dimensional rib-stiffened plate as an equivalent orthotropic plate by smearing the rib-stiffeners into the plate [2].

The study focuses on improving the smearing technique for rib-stiffened plates, and employing the technique in FE modeling. By utilizing a smearing technique, an FE model can be simplified considerably by replacing the rib-stiffened plate with a smeared orthotropic plate of corresponding properties. This is, therefore, an effective way to save time for generating the FE model as well as for computer calculating. However, the existing smearing technique is not accurate enough to make the FE prediction. Therefore, the first task of the PhD project is to improve the smearing technique. After this, an effective way of employing the improved smearing technique into FE modeling is found.

1.2 Contributions

This work has mainly investigated three important issues:

- Improvements of the smearing technique for estimating vibration of cross-stiffened flat plates
- Extending the smearing technique to doubly-curved cross-stiffened shells
- Applying the smearing technique in a simplified finite element modeling of stiffened structures

For the first issue, an improved smearing technique for cross-stiffened thin rectangular plates is developed. This has been reported in two conference papers and in a journal paper. It should be mentioned that the contents of the conference papers (A.1 and A.2) are included in the journal paper (I):

A.1 Y. Luan, and M. Ohlrich, "An improvement of the smeared theory for stiffened plates," *Proceedings of Noise and Vibration: Emerging Methods 2009, Oxford, England,* 2009.

A.2 Y. Luan, M. Ohlrich and F. Jacobsen, "Vibration of panels with angled stiffeners: A numerical study of the smearing technique," *Proceeding of 17th International Congress on Sound and Vibration, Cairo, Egypt,* 2010.

I. Y. Luan, M. Ohlrich and F. Jacobsen, "Improvements of the smearing technique for cross-stiffened thin rectangular plates," *Journal of Sound and Vibration,* 2011 (in press).

In the investigation of the second issue, the smearing technique was extended, so it could deal with doubly-curved cross-stiffened rectangular shells. This work has been published in a conference paper (A.3) and a journal paper (II):

A.3 Y. Luan, "The structural acoustic properties of stiffened shells," *Proceedings of Acoustics '08, Paris, France,* 393-398, 2008.

II. Y. Luan, M. Ohlrich, and F. Jacobsen, "Smearing technique for vibration analysis of simply supported cross-stiffened and doubly curved thin rectangular shells," *Journal of Acoustical Society of America* **129** (2), 707-716, 2011.

The third issue was an application for the improved smearing technique for cross-stiffened plates in FE models. This work has been submitted as a letter to the editor of a journal (III).

III. Y. Luan, M. Ohlrich and F. Jacobsen, "Applying a smearing technique for cross-stiffened rectangular plates for developing a general type of smeared finite element," *Journal of Acoustical Society of America* , 2011 (Submitted).

1.3 Structure of the dissertation

The dissertation is divided into the following chapters.

Chapter 2 provides the historical background of the smearing technique, and the development of the improved smearing technique for cross-stiffened rectangular plates and for doubly curved cross-stiffened shells.

Chapter 3 presents an evaluation of the improved smearing technique for a number of test cases. The predicted natural frequencies and forced responses for both flat stiffened plates and doubly

curved stiffened shells are tested. Also, the limitations and assumptions of the improved smearing technique are indicated.

Chapter 4 discusses the application of the smearing technique for cross-stiffened rectangular plates when implemented in a general type of FE analysis.

Chapter 5 concludes this dissertation and provides suggestions for future work.

Papers (I-III) are included as part of the framework in Chapters 2 to 4.

Appendix introduces a study of modeling the structural acoustic properties of a loudspeaker system which comprises the cabinet and loudspeaker unit.

2 Smearing technique

This chapter presents a new development of the smearing technique for modeling vibration of cross-stiffened, thin rectangular flat plates and doubly curved shells.

2.1 Historical background

2.1.1 Rib-stiffened plate

Plates reinforced by ribs represent a class of structural components that are widely used in loudspeaker cabinets as well as in other engineering applications such as ship hulls and decks, bridges, land and space vehicles, and buildings. Vibrations of stiffened plates have been extensively studied using various analytical and numerical techniques. The smeared orthotropic plates method (also called the smearing technique) and grillage approximations are two common models used in the early literature [3,4]. While the former treats the stiffened plate as an equivalent orthotropic plate by smearing the stiffeners into the plate, the latter approximates the stiffeners as a grid attached to the plate. Other approaches, such as wave propagation techniques [5-9], transfer matrix methods [10], Rayleigh–Ritz methods [11-15], the finite difference methods [16,17], and the finite element methods [18-22] have also been developed to investigate various aspects of vibrations of stiffened plates.

Even though all these approaches are well developed, the early discovered smearing technique is the most suitable method as an approximate tool for fast prediction of the vibrations of loudspeaker cabinets. Since the smearing technique models the stiffened plate as an equivalent orthotropic plate, the standard theories for an orthotropic plate can be applied to the smeared orthotropic plate without any additional study. This gives an opportunity to replace a stiffened plate with an equivalent orthotropic smeared plate in a model, and the properties of the model can be estimated in any commercial programs that deal with orthotropic plates. The smearing technique was originally developed in 1970s [3], and it has been thoroughly summarized a few years ago by Szilard [2]. In the following, this smearing technique is also called the Szilard's technique.

The smearing technique has some weaknesses. Obviously, the technique cannot be used for stress-strain analysis of the stiffeners, since the stiffeners are smeared out. Moreover, the smearing technique is not expected to work when the frequency becomes so high that the spacing between the stiffeners is comparable to or larger than half a wavelength in the base plate. In short, the smearing technique works only for low frequency predictions. However, the weakness of the smearing technique has only a limited effect on the modeling in this project. Since the vibration power of a woofer unit is much stronger than the midrange and tweeter units in a loudspeaker system, the vibration transmission from units to the cabinet is mainly considered to be at low frequencies, and therefore, the corresponding modeling can employ the smearing technique within its working frequency range. So far, the predicting accuracy of the smearing technique has been inadequate. Therefore, the work in this chapter is to improve the smearing technique.

2.1.2 Doubly curved stiffened shell

Even though rib-stiffened panels have been studied for many years, the smearing technique has never been successfully used for doubly curved stiffened shells. In the last forty years researchers

have paid a great deal of attention to the dynamic behavior of stiffened shells. Work have been done on cylindrical shells [23-48] and on conical shells [49,50]. Since doubly curved shells need more degrees of freedom for analysis researchers mostly use the FEA to deal with such cases. The application of FEA to the vibration analysis of a stiffened shell makes it possible to model discrete stiffeners, variable curvature and irregular geometry. However, FEA calculations based on the detailed geometries of such panels have been found to be very time-consuming. Thus, it is very useful if the geometry can be simplified, for example by the smearing technique.

2.2 Ordinary theories

The ordinary smearing technique for flat cross-stiffened plates, and the equation of motion for a doubly curved homogeneous shell are introduced in this section as a background for later derivations. Only panels of rectangular shape will be considered herein.

2.2.1 Outline of Szilard's smearing technique

A cross-stiffened rectangular plate is considered with geometrical parameters as shown in Figure 2-1. The overall length of the plate is a in the x direction and b in the y direction, and the plate thickness is h. In the x direction the stiffeners have the width w_{sx}, height h_{sx}, and spacing b_s, and in the y direction the corresponding values are w_{sy}, h_{sy}, and a_s.

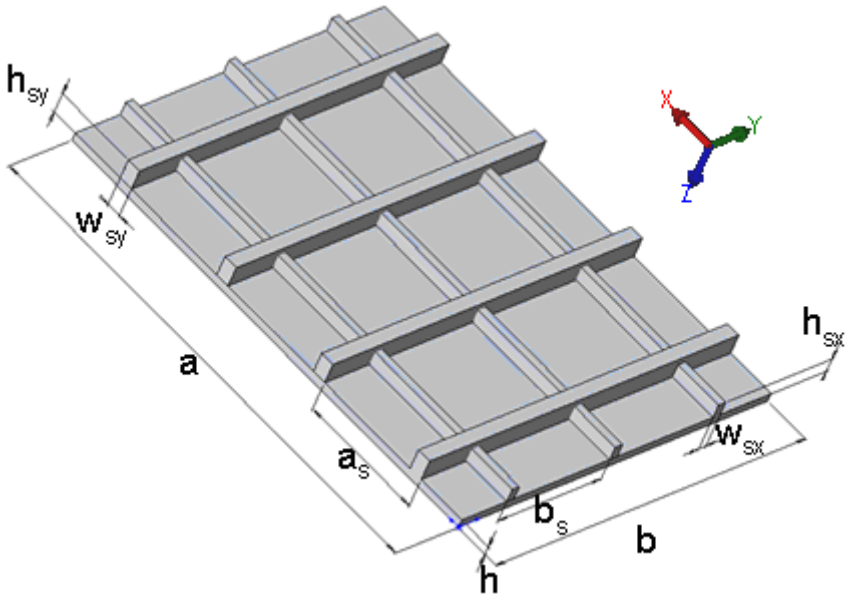

Figure 2-1. Geometrical parameters of a cross-stiffened rectangular plate.

The governing equation of motion for an equivalent smeared orthotropic plate of the actual stiffened plate structure has been derived by Szilard [2] by using the ordinary Kirchhoff bending theory for small transverse deflections, see for example [5]. For the transverse displacement $w(x,y,t)$ the equation reads

$$D_x \frac{\partial^4 w(x,y,t)}{\partial x^4} + 2H \frac{\partial^4 w(x,y,t)}{\partial x^2 \partial y^2} + D_y \frac{\partial^4 w(x,y,t)}{\partial y^4} + \rho'' \frac{\partial^2 w(x,y,t)}{\partial t^2} = p(x,y,t), \qquad (2.1)$$

where D_x and D_y are the equivalent bending stiffness per unit width in the x and y direction, H is the effective torsional rigidity, and $\rho'' = \rho\, h_e$ represents the smeared average mass per unit area, ρ being the mass density of the material and h_e the equivalent thickness of the smeared plate. Finally, $p(x,y,t)$ is the external forcing of the structure. In the following it is assumed that the base plate of the rib-stiffened structure is homogeneous and that the plate and the stiffeners are made of the same material. The bending stiffness of the structure, D_y, is determined by EI_y, where E is the Young's modulus of the material, and I_y is the area moment of inertia in the y direction. Szilard assumed that the stiffeners in the x direction have a negligible little effect on the bending stiffness in the y direction. Therefore, only stiffeners in the y direction were taken into account in his evaluation of I_y, which is given by

$$I_y = I_p + I_{sy}, \tag{2.2}$$

where I_p and I_{sy} represent the area moment of inertia of plate and stiffeners [2].

2.2.2 Outline of Soedel's theory for doubly curved shell

Soedel studied vibrations of a doubly curved rectangular homogeneous shell that is simply supported [51]. Here, the shell has a constant radius of curvature R_x in the x direction, and a constant radius of curvature R_y in the y direction. The x-y coordinate system is selected on the projected flat base plate. The curved edge lengths of the shell are a in the x-z plane, and b in the y-z plane, and the thickness of the shell is h. In what follows E is the Young's modulus, ν is the Poisson's ratio, and ρ is the density of the shell.

Assumptions such as Donell-Mushtari-Vlasor's simplification and the infinitesimal distance assumption are used in Soedel's derivation. The first basic assumption of Donell-Mushtari-Vlasor's simplification is that contributions of in-plane deflections can be neglected in the bending strain expressions but not in the membrane strain expressions. The second assumption is that the influence of inertia in the in-plane direction can be neglected. Thirdly, the infinitesimal distance assumption is taken to be

$$(ds)^2 \cong (dx)^2 + (dy)^2, \tag{2.3}$$

where ds is the magnitude of the differential change [51].

With these assumptions, the equation of motion for forced transverse vibration $w(x,y,t)=U_3 e^{i\omega t}$ normal to the surface of a homogenous shell becomes [51]

$$D\nabla^8 U_3 + Eh\nabla_k^4 U_3 - \rho''\omega^2\nabla^4 U_3 = \nabla^4 p, \tag{2.4}$$

where

$$D = \frac{Eh^3}{12(1-\nu^2)}, \tag{2.5}$$

$$\nabla^2(\cdot) = \frac{\partial^2(\cdot)}{\partial x^2} + \frac{\partial^2(\cdot)}{\partial y^2}, \tag{2.6}$$

$$\nabla_k^2(\cdot) = \frac{1}{R_x}\frac{\partial^2(\cdot)}{\partial x^2} + \frac{1}{R_y}\frac{\partial^2(\cdot)}{\partial y^2}, \tag{2.7}$$

in which $\rho'' = \rho h$ is the mass per unit area, D is the bending stiffness, and p is the external forcing applied on the panel in its normal direction.

2.3 Improved smearing technique

2.3.1 Improvement of the smearing technique for flat stiffened plate

The accuracy of the predicted dynamic properties such as natural frequencies obtained with the Szilard's technique [2] is not completely adequate for engineering purposes, especially for cast or molded plates with wide stiffeners. The reason is that only the stiffeners arranged at a right angle to the axis of angular motion are taken into account when the bending stiffness of the equivalent plate is calculated, whereas the stiffeners that are parallel to this axis of angular motion are neglected, since these stiffeners are assumed to have a negligible influence on the bending stiffness in question. Another limitation of Szilard's technique is that it assumes that the stiffeners are parallel to the edges of the plate. Thus the purpose of this section is to improve the smearing technique by including the parallel stiffeners in the analysis, and to extend the smearing technique to include modeling of panels with angled stiffeners.

In order to improve the smearing technique, the influence of stiffeners in the x direction is also taken into account in the calculation of I_y. A repeating section of the stiffened plate is shown in Figure 2-2(a), and Figure 2-2 (b) shows how the stiffener in the x direction is smeared into a thin layer attached to the top of the base plate. A side view of the geometry is shown in Figure 2-3. Figure 2-3(a) shows the actual repeating section, whereas Figure 2-3 (b) shows the repeating section with the x stiffener smeared into a layer of thickness h_{ey}.

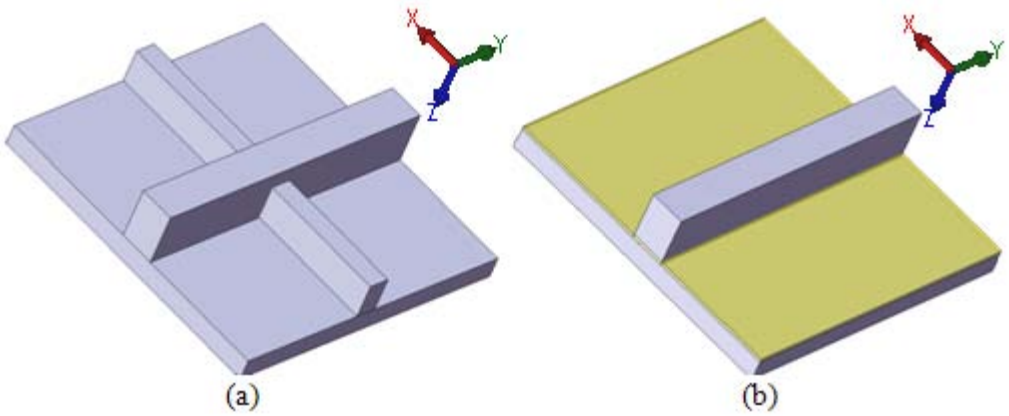

Figure 2-2. (a) A repeating section; and (b) the repeating section with the *x* stiffener smeared.

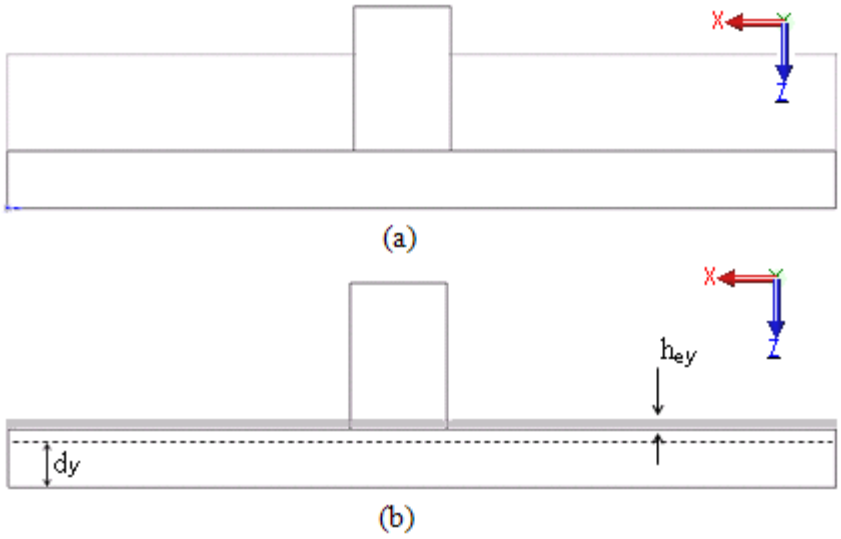

Figure 2-3. (a) Side view of the repeating section; and (b) the repeating section with the *x* stiffener smeared. The dashed line shows the neutral axis for the direction in question.

This smearing of the rectangular shaped *x* stiffeners has two effects: the mass of the *x* stiffener changes the position of the neutral axis slightly and thus results in a new value of the distance to the neutral axis d_y, and the smearing increases the area moment of inertia because of the added layer. Thus the Eq. (2.2) is updated to be

$$I_y = I_p + I_{sy} + I_{sx}, \tag{2.8}$$

where the third term in the right hand side of the equation is the area moment of inertia of the added plate layer with respect to the new neutral axis. Thus, this results in an improved version of the bending stiffness $D_y = EI_y$. An improved value of I_x is obtained in a similar manner, and this results in a new value of $D_x = EI_x$. Substituting these updated values for D_x and D_y into Eq. (2.1) results in an improved equation of motion for the equivalently smeared plate. The detailed equations are illustrated in Section 2.2 of Paper (I) included in this dissertation.

In the development of the smeared properties of the cross-stiffened plate it has been tacitly assumed that the stiffeners are parallel to the edges of the plate. However, in practice the stiffeners may be angled relative to the edge. In this study the angle is therefore included in the calculation of bending stiffness and effective torsional rigidity. Also, as the stiffeners are angled they become longer with increasing added mass, which is also taken into account in the calculation. However, apart from the changes in directional stiffness and added mass, the smearing technique necessarily assumes a modal pattern that is symmetric with respect to the main-axis, that is, the same modal pattern as in the case with stiffeners parallel to the edges of the plate. For details of the equations, please refer to Section 2.3 of Paper (I) included in this dissertation.

2.3.2 Extending the smearing technique to doubly curved stiffened shell

With the smearing technique being improved as shown in the last section, it is the purpose of this section to extend the improved technique to include doubly curved rectangular shells with periodically arranged small stiffeners. The extended technique allows for determining the natural frequencies, mode shapes and forced vibrations.

The improved smearing technique is combined with the equation of motion for a doubly curved thin rectangular shell, Eq. (2.4) in Section 2.2.2. After some algebra, an expression for the frequency dependent bending stiffness is obtained to be

$$D_e = \frac{D_x(\frac{m\pi}{a})^4 + 2H(\frac{m\pi}{a})^2(\frac{n\pi}{b})^2 + D_y(\frac{n\pi}{b})^4}{\left[(\frac{m\pi}{a})^2 + (\frac{n\pi}{b})^2\right]^2}, \tag{2.9}$$

where *m* and *n* are the mode numbers corresponding to the numbers of half-sinusoidals in the *x* and *y* directions, respectively. In what follows, Eq. (2.4) can represent an equation of motion for a stiffened shell, provided that the parameters *D, h,* and $\rho'' = \rho h$ are replaced by the corresponding properties of an equivalent *smeared* shell, that is, by D_e given in Eq. (2.9), the equivalent thickness h_e, and the associated density per unit area $\rho'' = \rho h_e$. The equation of motion of the equivalent smeared shell therefore becomes

$$D_e\nabla^8 U_3 + Eh_e\nabla_k^4 U_3 - \rho''\omega^2\nabla^4 U_3 = \nabla^4 p. \tag{2.10}$$

The dynamic properties of the doubly curved cross-stiffened shells is then derived from Eq. (2.10). The detailed derivation is given in Paper (II), Chapter III.

3 Evaluating the smearing technique

In this chapter, the improved smearing technique is evaluated for a number of test cases. The predicted natural frequencies and forced responses for both flat stiffened plates and doubly curved stiffened shells are compared with either experimental results or FE results that include the exact modeling of the cross-sectional geometries of the stiffened panel. Next, the limitations and assumptions of the improved smearing technique is indicated.

3.1 Natural frequencies

Fist considered is the prediction of natural frequencies of a rectangular, cross-stiffened plate. The structure is similar to the model shown in Figure 2-1. The pattern of the cross-stiffening is chosen to be spatially periodic, and with half end-spacing it follows that there are three stiffeners in the *x* direction and four stiffeners in the *y* direction. The plate is simply supported along all four edges (SSSS) for the first model, whereas the plate of the second model is clamped on all edges (CCCC). Both models have small stiffeners in the *x* direction and larger stiffeners in the *y* direction.

The natural frequencies are calculated for a plate with both simply supported and clamped boundary conditions by using the improved smearing technique, and the results obtained are compared with Szilard's technique. The accuracy of the predicted results is evaluated against reference data obtained by FE calculations with the commercial software package ANSYS. It is found that the improved smearing technique gives smaller deviations in the predicted natural frequencies for both models: about half the deviations as obtained by Szilard's technique. For details, please refer to Paper (I), Chapter 3.

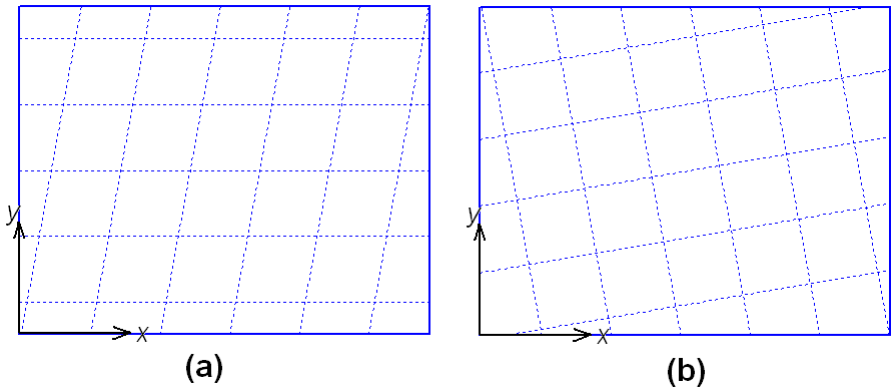

Figure 3-1. Sketches of panels with angled stiffeners. (a) The first series with only the *y* stiffeners angled; and (b) the second series with both the *x* and *y* stiffeners angled.

Secondly, results for the natural frequencies of plates with stiffeners that are angled relative to the edges of the plate are presented. Two series of panel models are investigated as illustrated in Figure 3-1. The first series is for only the *y* stiffeners angled, and results are presented for three small values of angle, see Figure 12a in Paper (I). The second series is for both the *x* and *y* stiffeners rotated for three set of small angles, respectively. The natural frequencies calculated using the smearing technique are compared with FE results, as determined with all the details of the angled stiffeners taken into account. The deviations in natural frequencies reveal a reduced and biased accuracy of the smearing technique with increasing angle. For details, please refer to Paper (I), Section 4.2.

Finally, the evaluation of predicted natural frequencies is made for a series of doubly curved cross-stiffened shells. Several values of panel curvature are examined and Figure 3-2 shows examples of geometries of four of these models. With different values of curvature radii R_x, the predicted natural frequencies are compared to results obtained with 'exact' FE models that contain all details of the structure. All in all, it may be summarized that for the current series of simulations, the natural frequencies are well predicted with the smearing technique even for highly curved panels of a relatively small radius. For details, please refer to Paper (II), Section IV. B.

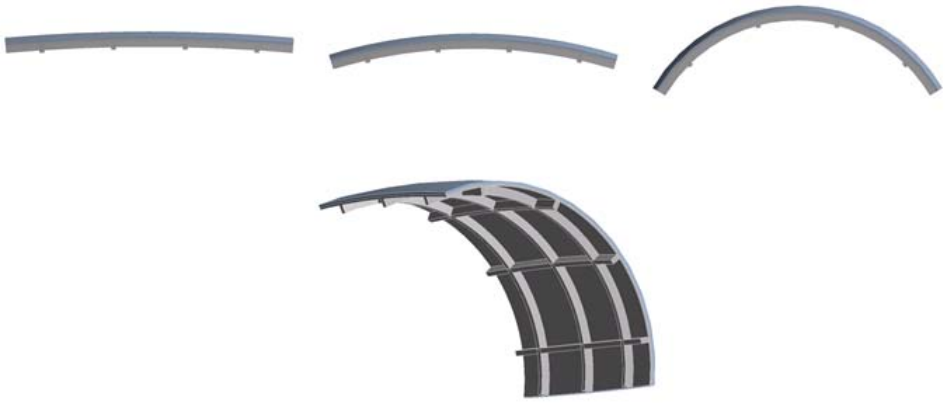

Figure 3-2. Geometries of four panel models. The upper models from left to right have a curvature radius R_x of 2.0 m, 1.0 m, 0.6 m, respectively, while the lower model has a radius of R_x = 0.2 m. For all cases R_y= 1.5 m.

3.2 Forced vibrations

The improved smearing technique is readily applied for predicting the forced vibration of a cross-stiffened plate structure. Experimental investigations have also been conducted in an attempt to validate the improved smearing prediction technique. Figure 3-3 shows the experimental setup

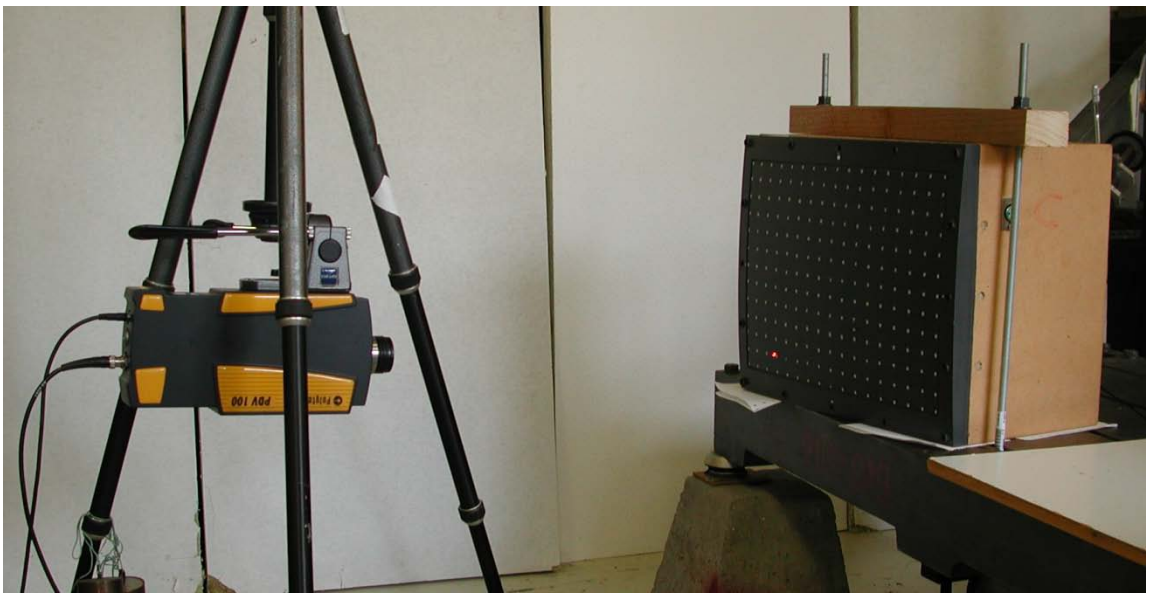

Figure 3-3. Experimental arrangement for vibration tests of a doubly curved cross-stiffened panel.

used for vibration measurements. The tested models were a flat cross-stiffened panel and a doubly curved cross-stiffened shell. Both models were fabricated (milled out) from a solid block of hard

PVC material. The simply supported boundary condition was attempted accomplished by a machined groove around the plate perimeter. This means that the plate was supported by a thin strip that was connected to an almost rigid supporting edge. Moreover, the supporting edge was mounted on a thick-walled hard-wood box, which was bolted to a steel stand of 300 kg. Both types of cross-stiffened panels were driven via a stringer at a stiffener by an electrodynamic exciter. The input force was measured with a force transducer of type B&K 8200, and the response velocities were measured with a laser vibrometer at 192 points evenly spread over the panel. Experimental results of the point mobility, transfer mobilities, and modal patterns were obtained for both models.

The analytical results determined by the improved smearing technique were compared to the experimental results for both models. The results for the point mobility, transfer mobilities and modal patterns have been evaluated. Overall the agreement is found to be good between the predicted and measured results. Moreover, the analytical results are validated by FE results, which estimated the vibration of the inner part of the models with simply supported boundary conditions. Again, good agreement was obtained. This is illustrated by the example in Figure 3-4, which is taken from Figure 11 in Section 4.1.2 of Paper (I).

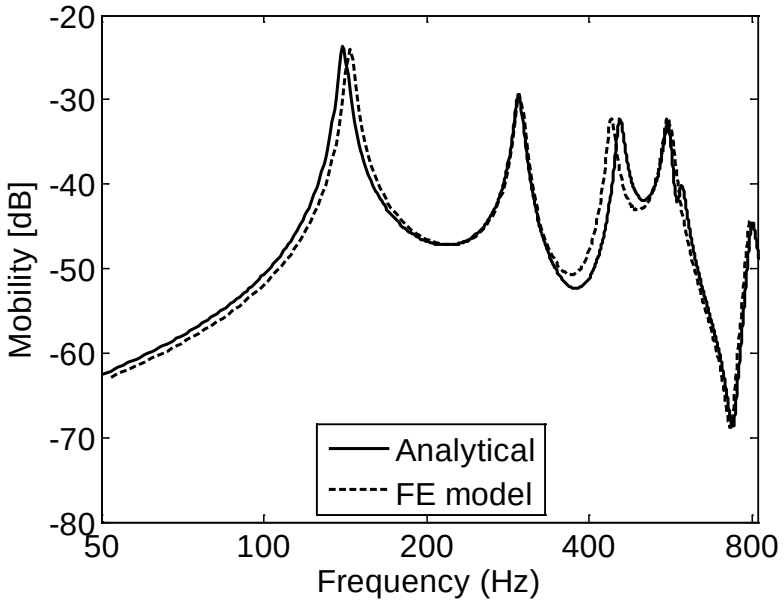

Figure 3-4. Transfer mobility at a position in a plate field of a doubly curved cross-stiffened panel. Magnitude shown in dB re 1 m/Ns.

The mean square velocity has also been calculated using the smearing technique. The two series of models with angled stiffeners introduced in Section 3.1 are now considered again. For each model the spatially averaged mean square velocity of the panel is calculated for each of a large number of individual point force excitations, and these results are finally averaged. In this way the mean square velocity becomes independent of the mode shapes of the panel [52]. The frequency variations of the mean square velocity are obtained in this way for the different models when it is assumed that the excitation force has a squared amplitude of 1 N^2 at each frequency. The results for the first series is illustrated in Figure 3-5, which is taken from Figure 14 in Section 4.2.1 of Paper (I). It is seen that angling the stiffeners by up to 15 degrees has a very limited influence on the narrow-band mean square velocity and practically no influence on one-third octave band levels of

the mean square velocity. For details for the flat cross-stiffened plate, please refer to Section 4.1 of Paper (I) included in the dissertation; whereas for curved panels, reference is made to Section IV. A of Paper (II).

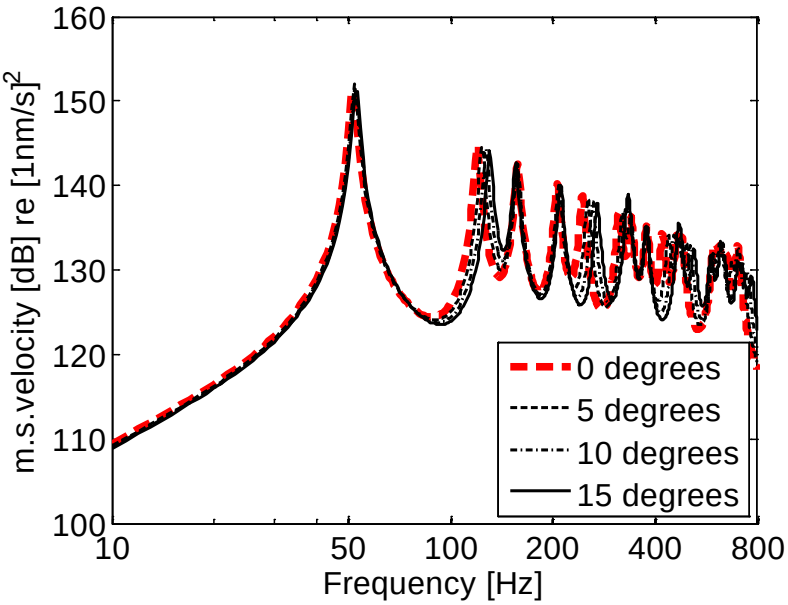

Figure 3-5. Predicted frequency variation of the mean square velocity per squared unit force of panel models with *y* stiffener angled with β = 0, 5, 10, 15 degrees.

3.3 Limitations and assumptions

The smearing technique is based on the ordinary Kirchhoff bending theory in which out-of-plane motion is uncoupled from in-plane motion. In-plane extension and normal-shear coupling are therefore neglected in the smearing technique. Moreover, the smearing technique determines the dynamic properties of thin rectangular plates and shells with periodically arranged small stiffeners, and therefore, the technique does not apply for plates with arbitrary arrangements of stiffeners. Since the technique smears the stiffeners into the base plate, it cannot be used for a local stress-strain analysis of the stiffeners. Furthermore, the technique becomes unreliable at high frequencies, where half a bending wavelength in the base plate becomes comparable to – or smaller than – the stiffener spacing.

Apart from these general limitations, a few other assumptions are made in this study. The smearing technique for angled stiffeners necessarily assumes a main-axis symmetric modal pattern, which is the same as in the case with stiffeners parallel to the edges of the plate. Furthermore, for doubly-curved shells, the Donell-Mushtari-Vlasor's simplification and the infinitesimal distance assumption are used as mentioned in Section 2.2.2, and this gives a considerable error in the estimation of the fundamental natural frequency of a panel [30].

However, the proposed technique is found to be useful for making a fast estimate, although its application is limited to the lower number of vibrational modes. Still, the smearing technique is readily applied as an approximate tool for a fast prediction of the vibrations of loudspeaker cabinets as discussed in Section 2.1.

4 Applying the smearing technique in an FEA program

This chapter presents a new application of the smearing technique for cross-stiffened thin rectangular plates when implemented in a general type of FE analysis. As shown in the previous chapters, the vibration of cross-stiffened plates can be estimated by using equivalent orthotropic smeared plates. In this chapter the *equivalent values* of the material properties of these orthotropic smeared plates are derived, and then used in an FE model of a corresponding smeared panel modeled with a standard type of solid/shell finite element.

4.1 The material parameters

So far, the presentation has been dealing with the improvement of the smearing technique and its application as an approximate tool for fast prediction of the vibrations of loudspeaker cabinet panels. However, there has been no simple way of implementing this smearing technique in a standard FE modeling. In order to implement such an equivalent technique, the general procedure is to calculate the property matrices. In this way, for instance, Rao *et al.* have studied free flexural vibration of stiffened plates [53], and Berry *et al.* have predicted the sound radiation from rectangular baffled plates with arbitrary boundary conditions [54]. Berry and Locqueteau have also computed the vibration and sound radiation of fluid-loaded stiffened plates with consideration of in-plane deformation using a Ritz method [55]. However, these methods are not suitable for coarse estimations of vibration, since one has to write computer codes in order to use these techniques in an FE modeling. The purpose of this section is to propose and examine an effective method for a coarse estimation of the vibration and sound radiation of rib cross-stiffened plates by using smeared properties for the finite element of the model.

Instead of writing the computer code for an FE model, the present method develops a simple way of applying the smearing technique in a general type of FE that is used for orthotropic thin flat plates, in the same way as the element of type Hex08 [56]. (The Hex08 element is a common type of solid/shell element, which is used for structural modeling in commercial FE software packages such as ACTRAN [56] and ANSYS [57].) By using the smearing technique one can calculate the corresponding bending stiffnesses, effective torsional rigidity, and equivalent thickness of an equivalent smeared plate. From these results, the *equivalent material parameters* are determined, that is, the equivalent values of Young's modulus, shear modulus, etc. With these equivalent material parameters, the smeared orthotropic plate can be used to replace the cross-stiffened plate in an FE model by using an existing, conventional element type for orthotropic plates.

In a general type of element for orthotropic plates the following material parameters are required: the different Young's moduli, E_x, E_y, E_z, shear moduli, G_{xy}, G_{zx}, G_{yz}, Poisson's ratios, ν_x, ν_y, ν_z, and the material density, ρ. In order to model the smeared orthotropic plate with an equivalent plate thickness of h_e, these parameters should be replaced by *equivalent* material parameters denoted by $E_{x,e}$, $E_{y,e}$, $E_{z,e}$, $G_{xy,e}$, $G_{zx,e}$, $G_{yz,e}$, together with assumptions of $\nu_e=\nu_x=\nu_y=\nu_z$ and $\rho_e=\rho$.

The equivalent bending stiffnesses, $D_{x,e}$ and $D_{y,e}$, the effective torsional rigidity, H_e, and the equivalent thickness, h_e, can be calculated using the equations in Section 2.3.1, in which they were denoted as D_x, D_y, H, and h_e. By substituting these smeared properties into ordinary formulae of

the general stiffness properties for an orthotropic flat plate, the equivalent material parameters are obtained. As a result, the equivalent Young's modulus is obtained to be

$$E_{i,e} = D_{x,e}\frac{12\left(1-\nu_e^2\right)}{h_e^3}, \qquad i = x, y. \tag{4.1}$$

It is assumed that there is no change in Young's modulus in the normal direction of the plate after smearing, and therefore,

$$E_{z,e} = E, \tag{4.2}$$

where E is the original Young's modulus of the material. The equivalent shear modulus in the x-y plane is

$$G_{xy,e} = \frac{3\left(2H_e - D_{x,e}\nu_e - D_{y,e}\nu_e\right)}{h_e^3}. \tag{4.3}$$

Moreover, the equivalent shear moduli in the x-z plane and y-z plane are

$$G_{iz,e} = \frac{\sqrt{E_{i,e}E_{z,e}}}{2\left(1+\nu\right)}, \qquad i = x, y. \tag{4.4}$$

With these equivalent material parameters, the FE model of a smeared orthotropic plate can represent the vibrational behavior of the stiffened plate. For details, please refer to Chapter II of Paper (III) included in the dissertation.

4.2 Evaluation of the finite element for smeared plates

This section analyses and evaluates the performance of the proposed method of elements with smeared properties for several different cases of rib-stiffened panels. Forced vibrations and sound radiation have been estimated for a physical panel, and the results have been compared with measurements. Finally, the natural frequencies of stiffened plates with a circular hole are examined.

4.2.1 Vibration and sound radiation of stiffened plates

The first case considered is a stiffened flat plate similar to the first model in Section 3.1, but of somewhat larger size. Forced flexural vibration of the panel is considered in the simulation, which computes the point mobility of the panel and its spatially averaged mean-square velocity. Vibration results of the smeared FE model, which is modeled as an equivalent smeared plate, are compared to an "exact" FE model that contains all stiffener details of the structure. The equivalent material parameters of the smeared FE model is calculated according to Eqs. (4.1) to (4.4). It is found that good agreement is achieved except for minor deviations, especially at higher frequencies; this is presumably because the upper frequency limit of the smearing technique is reached. As an example of the results, a comparison between the analytical point mobility and the 'exact' FE results is shown in Figure 4-1. For details, please refer to Section III. A of Paper (III) included in the dissertation.

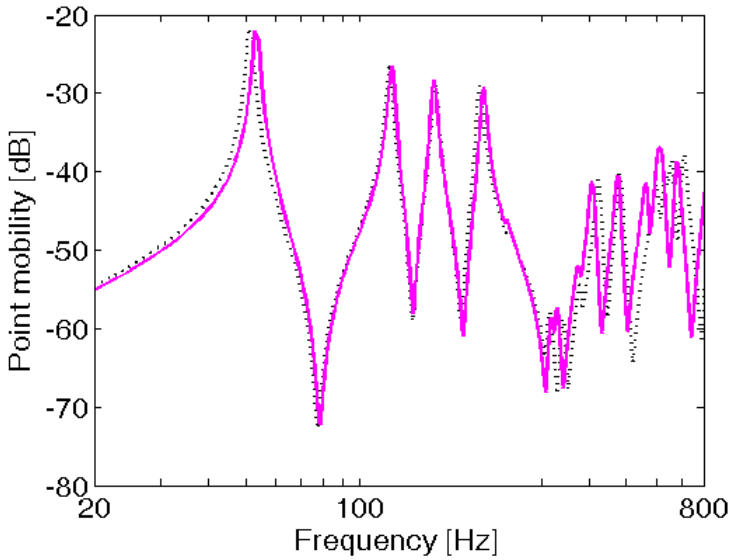

Figure 4-1. Calculated point mobility of a simply supported cross-stiffened rectangular plate. The solid line represents the result for the "exact" FE model; the dotted line is for the smeared FE model. Magnitude shown in dB re 1 m/Ns.

Predictions of the radiated sound are also of interest. The physical model in Section 3.2 is used again for the sound radiation validation. The experimental investigation of the sound radiation from the panel was carried out in a large anechoic room (with a free volume of 1000 m^3) with the box placed in an free-standing IEC baffle; see Figure 4-2. In the experiments the plate was driven by an electrodynamic exciter acting via a stringer at a stiffener. The input force was measured with a force transducer, and the sound pressure was measured with a ½ in. microphone at observation points at a distance of 1 m and 0.3 m from the center of the radiating surface. Vibration estimations determined with an "exact" FE model which includes all details of the stiffened PVC-panel as well as the co-vibrating wooden box are also used as the reference.

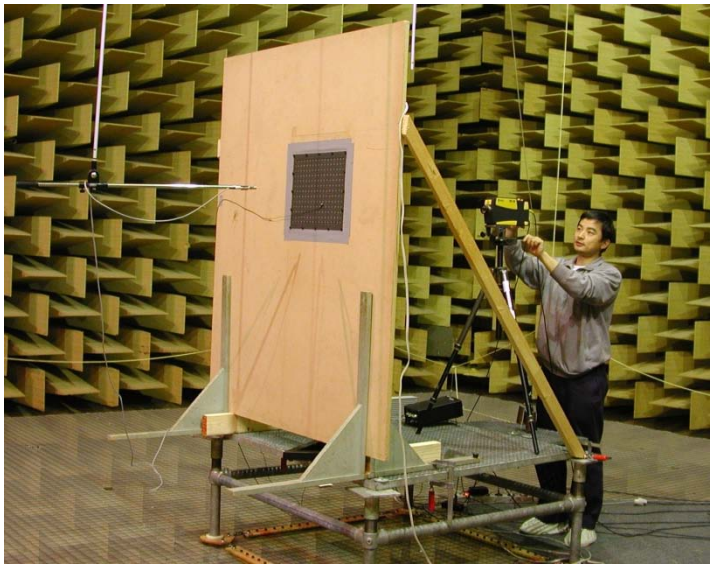

(a)

(b)

Figure 4-2. The experimental setup of an PVC-panel placed in an IEC baffle in a large anechoic room. (a) Front side. The PVC-panel was located flush with the baffle and the gap between the baffle and the PVC-panel was resiliently sealed. (b) Back side. The box was resiliently suspended on soft foam and the panel was driven by a free-standing exciter.

A smeared FE model for the same case was made with the cross-stiffened PVC-panel modeled as a smeared plate; the co-vibrating wooden box was included in the model, and the air in front of the PVC-panel was modeled as a half sphere as illustrated in Figure 4-3. The equivalent material properties of this smeared model were obtained as described above in the modeling of the vibration. The resulting frequency responses of the sound pressure level (normalized by the driving force) at the receiving positions are compared with both the experimental results and the “exact” FE estimations. Almost perfect match is found between the two FE models, and an overall good agreement is obtained between the smeared FE model and experimental results. For details, please refer to Section III. B of Paper (III) included in the dissertation.

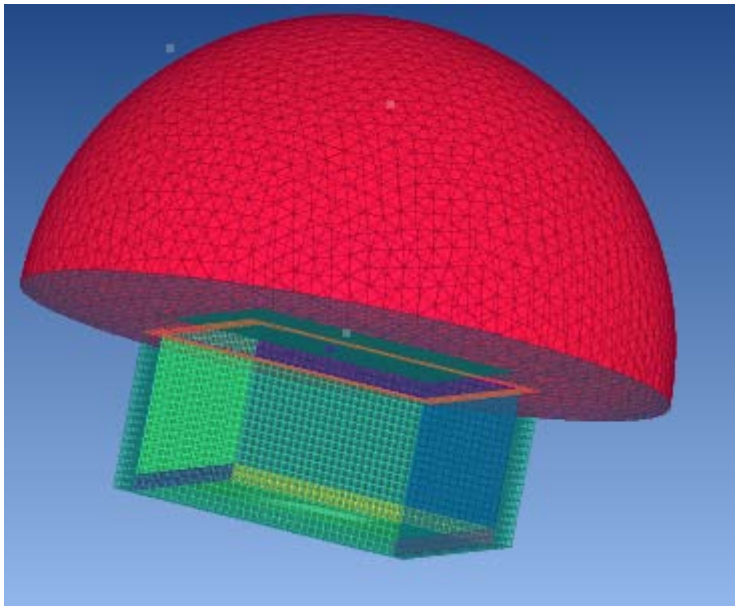

Figure 4-3. An FE model of the smeared panel with box and air, as modeled in ACTRAN.

4.2.2 Cross-stiffened thin rectangular plates with a circular hole

The 'front' panel in a loudspeaker cabinet must have one or more holes for mounting the loudspeaker units. In order to evaluate the application accuracy of the smeared FE model for such cases, this section presents a comparison of the natural frequencies predicted by the smeared FE model and the "exact" FE model of a number of cross-stiffened thin rectangular plates with a circular hole. The dimensions of this cross-stiffened plate are a = 516 mm, b = 430 mm, h = 6 mm, a_s = 86 mm, b_s = 86 mm, $h_{sx} = h_{sy}$ = 9 mm, and $w_{sx} = w_{sy}$ = 6 mm. The material properties are $E = 3\times10^9$ N/m^2, υ = 0.33, and ρ = 1360 kg/m^3. The edges of the plate are simply supported. Figure 4-4 shows panels with a centrally placed hole. The radii of the hole are taken to be 25 mm, 50 mm, 75 mm and 100 mm.

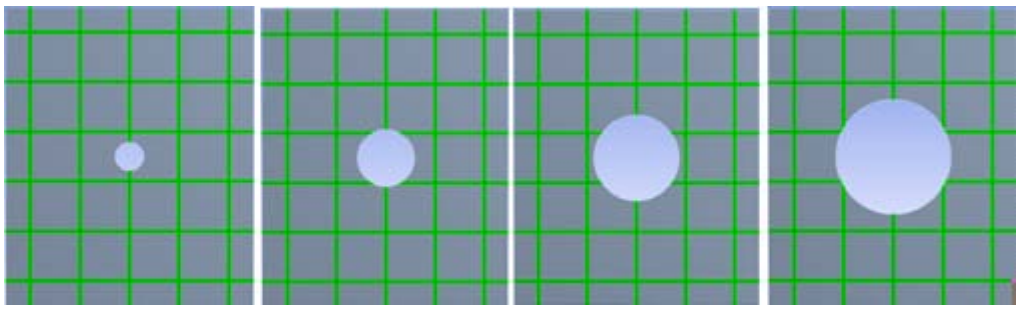

Figure 4-4. A series of panel models with a circular hole of radius 25 mm, 50 mm, 75 mm and 100 mm.

Similar to the element size used for the FE models in Chapter 3 and Section 4.21 (not mentioned in the main text but in Papers (I - III)), the mesh size limit of the FE calculation is taken to be ten times [56] smaller than the bending wavelength [52] in the base plate at a frequency of 800 Hz in order to predict the bending vibration of the panel accurately up to this frequency. This means that at least ten elements are included per wavelength of motion below 800 Hz. For the given material parameters, the wavelength of a bending wave is 155 mm at 800 Hz, and 15 mm is therefore chosen to be the maximum mesh size in the FE models. Figure 4-5 shows the mesh of the two FE models of a cross-stiffened plate with a hole of radius 100 mm.

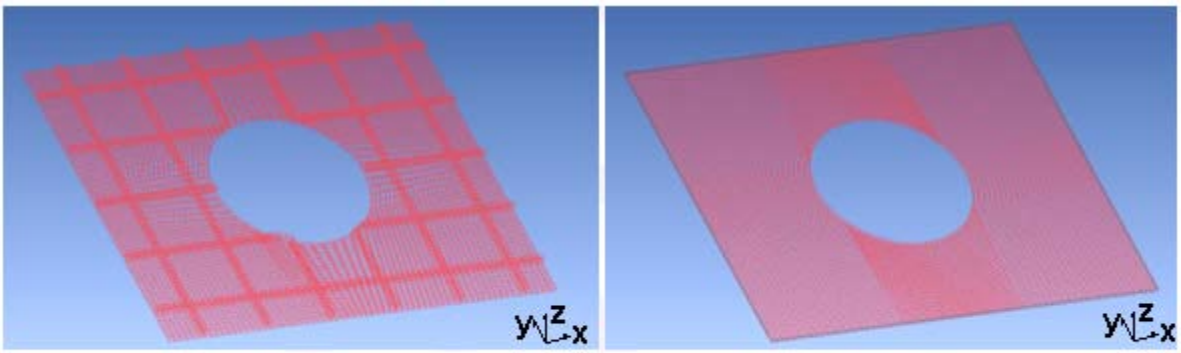

Figure 4-5. The mesh of the 'exact' FE model of a cross-stiffened plate with a hole (left subfigure) and its smeared FE model (right subfigure).

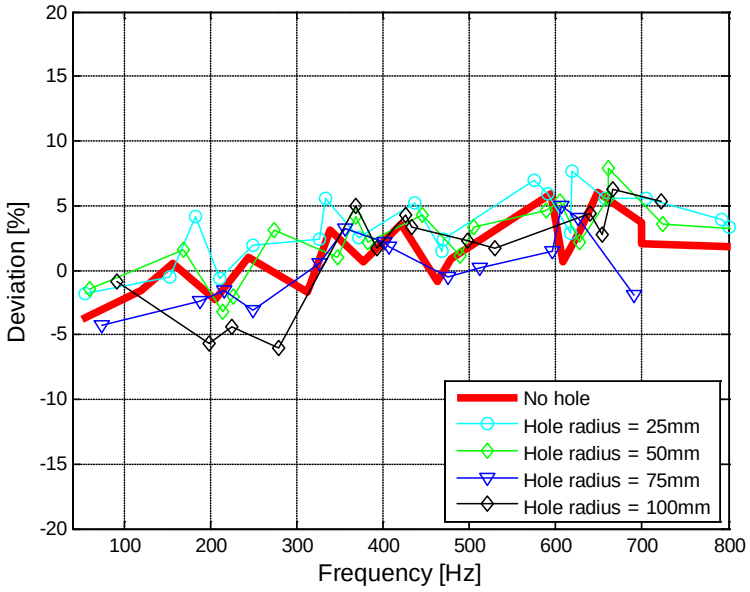

Figure 4-6. Deviations in natural frequencies between the smeared FE models (f_{sm})and 'exact' FE models (f_{ex}). The deviation is calculated in percentage as $100\cdot(f_{sm} - f_{ex}) / f_{ex}$. The plate is simply supported along all four edges, and the boundary conditions at the hole edge are modeled as sliding.

First, the models are analyzed with the boundary of the hole to be sliding, which means that the hole edge is free to move in the transverse *z* direction, that is, with motion normal to the base plate, and with zero slope in the radial direction. The corresponding results for the calculated natural frequencies are denoted f_{sm} for the smeared model and f_{ex} for the "exact" model, respectively. The deviations in natural frequencies are calculated in percentage as $100\cdot(f_{sm} - f_{ex}) / f_{ex}$, and the results for each model are plotted in Figure 4-6. The deviations are seen to be within -6% to +8%, and they have the same tendency of getting larger at higher frequency because of the limitation of the smearing technique mentioned in Section 3.3. Also shown for comparison is the deviation for the panel with no hole (thick red curve).

A structural model that is somewhat closer to a real design of the front panel of a loudspeaker cabinet, is obtained by adding a stiffening ring of the same PVC material to the edge of the hole, and thereby simulating a mounting flange. Further, at its inside surface is attached a steel ring to simulate the frame of a loudspeaker unit. The two rings extrude from the bottom of the base plate to the top of the stiffeners; whereas the width of the PVC stiffening ring is 6 mm, and the steel ring is

2 mm. Moreover, the center of the hole is placed asymmetrically as shown in Figure 4-7, at a position of 129 mm from the longer edge of the plate and 172 mm from the shorter edge. Similarly to the previous comparisons, the results are within -2% to 8% as illustrated in Figure 4-8. These results, however, are seen to deviate less from the no-hole results (red curve) at low frequencies.

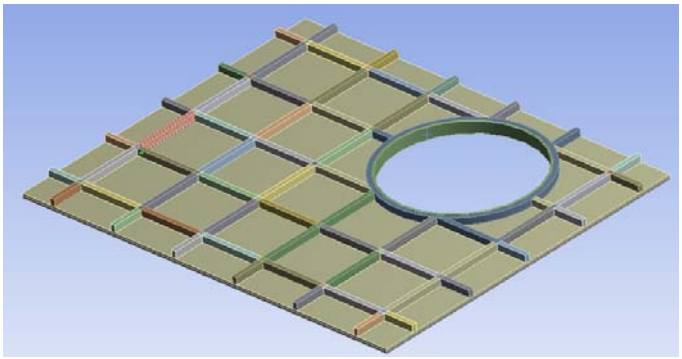

Figure 4-7. Geometry of model with a PVC stiffening ring (flange) and a thin steel ring.

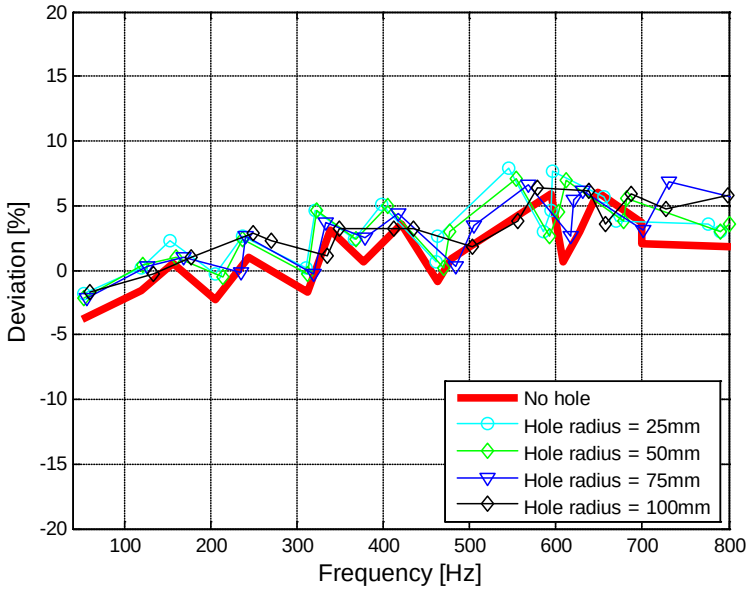

Figure 4-8. Deviations in natural frequencies between the smeared FE models and 'exact' FE models. The plate is simply supported along all four edges. A stiffening ring is added on the hole edge and a steel ring is attached on the inside surface of the stiffening ring, see Figure 4-7.

In conclusion, the deviations in natural frequencies of the considered cases are obtained approximately within -6% to +8% for models with sliding boundary condition at the hole edge; while the deviations is within -2% to 8% for the models with stiffening rings. This can be considered as an acceptable accuracy for a fast estimation.

4.3 Time consumption of FE models

The analysis of a smeared FE model takes less computer time than its corresponding "exact" FE model. It is of interest to investigate differences of the computer time for the mentioned models. The computer in which the FE models are made in this study has an Intel Xeon CPU E5540 @ 2.53GHz and 48 GB of RAM. The computation in Section 4.2.2, which use the "Modal analysis" module in ANSYS for each of the smeared FE models takes about 1 min, whereas it takes

approximately 2 min for the “exact” FE model; the computation in Section 4.2.1 for the forced vibration, which use “Frequency analysis” module in ANSYS with the smeared FE model takes 28 min, whereas it takes 76 min for the “exact” FE model. The estimation for sound radiation using either of the two FE models in ACTRAN is 15 hours and 24 hours, respectively. The models for sound radiation includes the structural vibration (of the stiffened panel and the box), the coupling between the radiating surface and the exterior air volume, and the corresponding pressure in the air volume. Obviously, calculations of the vibration of the box, the coupling and air volume are the same for both the smeared model and the “exact” model, and therefore, the difference between computing time for the two models is not as large as for the previous comparisons. It can be concluded that a smeared FE model saves at least half of the computer time of the corresponding “exact” FE model.

From an engineering point of view, it is of interest to access the whole time it takes to complete an FE model. For a given geometry of a new design , Figure 4-9 indicates the time consumption for a smeared model and an “exact” FE model. The period “a” is used for calculating the smeared material parameters, “b” is for modifying the geometry, “c” is for generating the mesh, “d” is for setting up the model, and “e” is the computer time of the calculations. Period “a” and “b” apply only for the smeared model, and they usually take a few hours. Period “c” of the smeared model is shorter than the one of the “exact” model, because the meshing takes more time on the “exact” model with stiffeners. Period “c” can take from minutes to days depending on the complexity of the geometry. Period “d” is almost the same for both the smeared and the “exact” model. As mentioned period “e” of the smeared model takes less than half the time for the “exact” model. Period “e” will become shorter in the future according to the improvement of the computer technique. In all, if the model is very simple, it is not worth spending time on making the smeared model. It is obvious that the operator effort is larger than the computer time for a simple model. However, it is an advantage to use the smeared model, if the structure is complex and composed of several stiffened panels as is usually the case. To generate a mesh for a complex structure with stiffeners takes a long time. A smeared plate simplifies the geometry, and therefore, saves the operator effort. Moreover, the computer take days or even weeks to calculate the modal properties and response of a complex FE model. In this case, the use of the smeared model results in considerable time savings in period “e”. Furthermore, the entire mesh of a complex model could exceed the computer memory. If this

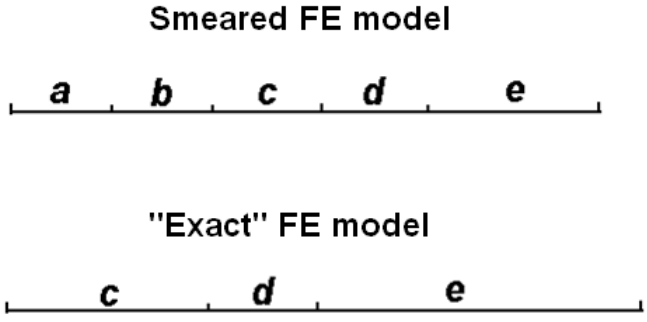

Figure 4-9. The time consumption for a smeared model and an ”exact” FE model. The period “a” is used for calculating the smeared material parameters, “b” is for modifying the geometry, “c” is for generating the mesh, “d” is for setting up the model, and “e” is the computer time of the calculations.

happens, the mesh size has to be enlarged to save computer memory, and the coarse mesh results in reduced accuracy, which is usually a serious problem, and this generally gives unreliable results. For such cases, it is certainly better to use smeared plates instead, since its estimated results are under control.

5 Conclusions and suggestions for future research

5.1 Summary and conclusions

An improved smearing technique for predicting the dynamic properties of cross-stiffened rectangular panels has been developed. In contrast to the ordinary smearing technique, this takes stiffeners in both the *x* and *y* directions into account in the calculation of the bending stiffness. Moreover, angled stiffeners are included in the improved technique. Furthermore, the technique has been extended for doubly curved panels. A number of models of cross-stiffened rectangular panels have been examined. With experimental results and "exact" FE calculations as references, the improved technique has been found to give good accuracies for determining the natural frequencies, mode shapes, mobilities, and mean square velocities of stiffened panels. Moreover, the developed technique has been employed for determining the equivalent material parameters of cross-stiffened panels. These parameters have then been used for modeling the smeared plate by means of a general type of orthotropic finite element. The estimated results using this technique are evaluated by comparison with vibration and sound radiation data obtained with "exact" FE models and measurements. For the cases considered it can be concluded that the smeared FE-plate model can estimate the panel vibration as well as the sound radiation very well up to the frequency limit of the smearing technique. The limitations due to the assumptions in the present technique have also been illustrated in this dissertation. Also discussed are the frequency limit of the smearing technique, the error in the fundamental frequency of a curved panel and the less accuracy with increasing stiffener angles. All in all, the improved technique has been shown to be very efficient for making coarse estimates in an early stage of a design of stiffened panels.

5.2 Suggestions for future research

The limitations mentioned in Section 3.3 give several directions for improving the smearing technique. The investigation demonstrates that it is difficult to predict the fundamental panel mode (1, 1) of highly curved panels accurately when using the Donell-Mushtari-Vlasor's shell equations. However, it is expected that it should be possible to improve the developed estimation method to a wider range of structures by adding a correction factor to these shell equations, as mentioned in Ref. [5]. Moreover, the smearing technique is derived from thin plate theory, and therefore, it cannot be expected to work well for thick panel or large stiffeners. In future works, it is worth to make a parameter study to investigate the working range of this technique with respect to the thickness of the panel and size of the stiffeners. Furthermore, the high sound pressure in a loudspeaker cabinet is important. This leads to a study how the high air pressure inside the closed cabinet affects the vibration of the cabinet when the loudspeaker unit is acting.[1] These problems are still the focus of the future research on estimating loudspeaker cabinet vibrations using a theoretical/numerical methodology.

[1] An investigation of the high pressure for an enclosed cabinet has been started and recorded in Appendix A.

Paper I

Y. Luan, M. Ohlrich and F. Jacobsen, "Improvements of the smearing technique for cross-stiffened thin rectangular plates," *Journal of Sound and Vibration*, 2011 (in press).

Improvements of the smearing technique for cross-stiffened thin rectangular plates

Yu Luan[a,b,*], Mogens Ohlrich[b], Finn Jacobsen[b]

[a]*Acoustic Department, Bang & Olufsen, Peter Bangs Vej 15, DK-7600, Struer, Denmark*
[b]*Acoustic Technology, Department of Electrical Engineering, Technical University of Denmark, Building 352, DK-2800 Kongens Lyngby, Denmark*

Abstract

New developments in the simplified smearing technique for modeling vibrations of cross-stiffened, thin rectangular plates are presented. The computationally efficient smearing technique has been known for many years, but so far the accuracy of , say, predicted natural frequencies has been inadequate. The reason is that only the stiffeners at a right angle to the axis of angular motion are taken into account when calculating the bending stiffness, whereas the stiffeners that are parallel to this axis of angular motion are neglected. To improve predictions, the parallel stiffeners are taken into account in this paper. The improved smearing technique results in better accuracy for predicted natural frequencies of flat stiffened plates, as demonstrated for both simply supported and clamped boundary conditions. The improved prediction accuracy is demonstrated by comparing results from a numerical model based on the current development with results from finite element (FE) simulations that include the exact cross-sectional geometries of the stiffened panel. In order to demonstrate applications of the improved smearing technique, the predicted forced response is compared with both experimental and FE results. Another improvement concerns the orientation of the stiffeners. The original smearing technique presupposes that the stiffeners are parallel to the edges of the plate, but simple considerations make it possible to relax this requirement. To test the validity of the resulting technique a series of plates are examined for stiffeners angled relative to the plate edges.

Keywords: smeared plate, stiffened plate, cross-stiffened, rectangular plate

1. Introduction

Stiffeners are efficient for enhancing the stiffness of a plate or shell without adding too much mass. Vibrations of stiffened plates have been extensively studied using various analytical and numerical techniques; a comprehensive review has recently been given by Xu et al. [1]. In addition, the work by Omid'varan and Delagarza on free vibration of grid-stiffened plates should also be mentioned [2, 3]. Moreover, the smearing technique, which treats the stiffened plate as an equivalent orthotropic plate by smearing the stiffeners into the plate, is one of the earlier techniques originally developed in 1970s [4]. This is very efficient, but obviously, the technique cannot be used for stress-strain analysis of the stiffeners. The smearing technique has been thoroughly summarized a few years ago by Szilard [5]; and it has recently been used for doubly curved cross-stiffened shells [6]. A related smearing technique for modeling multilayer structures has recently been proposed by Guyader *et al.* [7]. The present paper which deals with flexural vibration improves the smearing technique and investigates it as an approximate tool for fast prediction of the natural frequencies, forced vibrations of small amplitude and average mean square velocities of rectangular thin plates orthogonally reinforced by small stiffeners.

With the rapid progress of computer technologies, the FE methods have nowadays become a standard tool for the dynamic analyses of complex structures. However, determining and optimizing the vibrational properties of a designed stiffened structure may be very time-consuming if rigorous analyses are to be made. Engineers usually draw a new design structure with a three-dimensional program and later simulate its dynamic properties with an FE program. The drawing process and the FE calculations may take days or even weeks for a relatively simple structure. Moreover, it is often necessary to make modifications to the structure, which means that new FE calculations are required. All this can be very time-consuming. Even though computers become more and more powerful, the engineer’s working hours for making a drawing and developing an FE model have almost not changed. Thus, it is very useful if the panel geometry can be simplified, for example by employing a smearing technique, which is a coarse but fast and efficient technique that “smears” the stiffeners to the base plate or shell.

The accuracy of the predicted dynamic properties such as natural frequencies obtained with Szilard’s technique is not completely adequate for engineering purposes, especially for cast or molded plates with wide stiffeners. The reason is that only the stiffeners arranged at a right angle to the axis of angular motion are taken into account when the bending stiffness of the equivalent plate is calculated, whereas the stiffeners that are parallel to this axis of angular motion are neglected, since these stiffeners are assumed to have a negligible influence on the bending stiffness in question. Another limitation of Szilard’s technique is that it assumes that the stiffeners are parallel to the edges of the plate. Thus the purpose of this paper is to improve the smearing technique by including the parallel stiffeners in the analysis, and to extend the smearing technique to include modeling of panels with angled stiffeners.

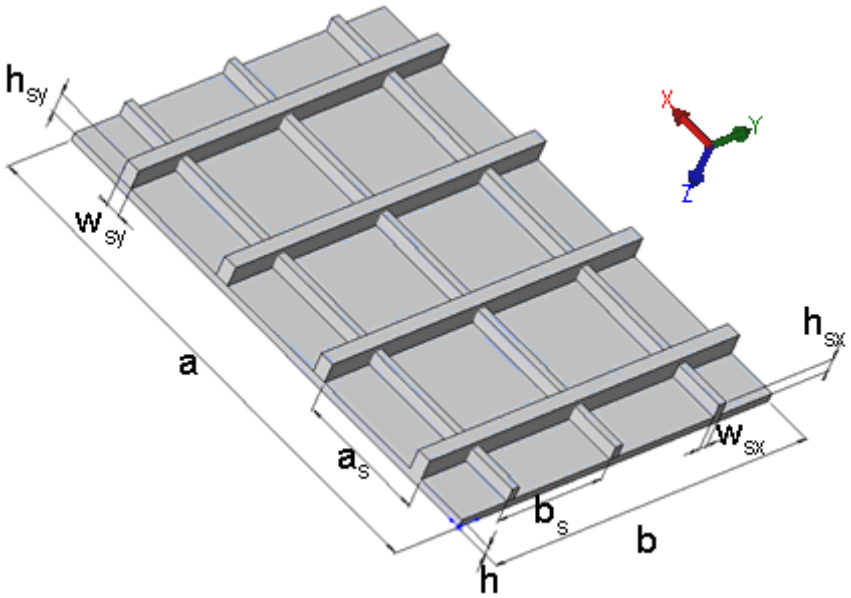

Fig. 1. Geometrical parameters of a cross-stiffened rectangular plate.

2. Smearing technique of stiffened plates

2.1. Outline of Szilard's technique

A cross-stiffened rectangular plate is considered with geometrical parameters as shown in Fig. 1. The overall length of the plate is a in the x direction and b in the y direction, and the plate thickness is h. In the x direction the stiffeners have the width w_{sx}, height h_{sx}, and spacing b_s, and in the y direction the corresponding values are w_{sy}, h_{sy}, and a_s.

The governing equation of flexural motion for an *equivalent smeared* plate of the actual stiffened plate structure has been derived by Szilard [5] by using the ordinary Kirchhoff bending theory, see for example [8]; for the transverse displacement $w(x,y,t)$ it is

$$D_x \frac{\partial^4 w(x,y,t)}{\partial x^4} + 2H \frac{\partial^4 w(x,y,t)}{\partial x^2 \partial y^2} + D_y \frac{\partial^4 w(x,y,t)}{\partial y^4} + \rho'' \frac{\partial^2 w(x,y,t)}{\partial t^2} = p(x,y,t), \qquad (1)$$

where D_x and D_y are the equivalent bending stiffness per unit width in the x and y direction, H is the effective torsional rigidity, and $\rho'' = \rho\, h_e$ represents the smeared average mass per unit area, ρ being the mass density of the material and h_e the equivalent thickness of the smeared plate. Finally, $p(x,y,t)$ is the external forcing of the structure.

In the following it is assumed that the base plate of the rib-stiffened structure is homogeneous and that the plate and the stiffeners are made of the same material. The bending stiffness of the structure, D_y, is determined by EI_y, where E is the Young's modulus of the material, and I_y is the area moment of inertia in the y direction. Szilard assumed that the stiffeners in the x direction have a negligible little effect on the bending stiffness in the y direction. Therefore, only stiffeners in the y direction were taken into account in his evaluation of I_y, which is given by

$$I_y = I_p + I_{sy}, \qquad (2)$$

where I_p and I_{sy} represent the area moment of inertia of plate and stiffeners [5]. The area moment of inertia of the plate with respect to the neutral axis of the system is

$$I_p = \frac{h^3}{12(1-\nu^2)} + (d_y - \frac{h}{2})^2 \cdot h, \tag{3}$$

in which v is the Poisson's ratio, and d_y denotes the distance between the bottom surface of the plate and the neutral axis of the stiffened plate for bending in the y direction. The area moment of inertia of the stiffeners with respect to the same neutral axis is [5]

$$I_{sy} = \frac{1}{a_s} \cdot [I_{sy0} + (h_{sy} + h - d_y - \frac{h_{sy}}{2})^2 \cdot (w_{sy} \cdot h_{sy})], \tag{4}$$

where

$$I_{sy0} = \frac{w_{sy} \cdot h_{sy}^3}{12} \tag{5}$$

represents the area moment of inertia of the y-going stiffener with respect to its own neutral axis. The bending stiffness in the x direction, $D_x = EI_x$, is obtained in a similar manner. The effective torsional rigidity is [5]

$$H = \frac{Eh^3}{12\left(1-\nu^2\right)} + 6G_{xy}\left(\frac{I_{sx0}\eta_x}{b_s} + \frac{I_{sy0}\eta_y}{a_s}\right), \tag{6}$$

where $G_{xy} = E/(2(1+\nu))$ is the shear modulus of the material and

$$I_{sx0} = \frac{w_{sx} \cdot h_{sx}^3}{12} \tag{7}$$

represents the area moment of inertia of the x stiffener with respect to its own neutral axis. The quantities η_x and η_y are numerical factors that depend on the ratios h_{sx}/w_{sx} and h_{sy}/w_{sy}, respectively. The values of η can be found on p. 512 of Ref. [5]. The corresponding equivalent thickness h_e is calculated as

$$h_e = h + \frac{h_{sx}w_{sx}}{b_s} + \frac{h_{sy}w_{sy}}{a_s} - \frac{\mathrm{Min}\{h_{sx}, h_{sy}\}w_{sx}w_{sy}}{a_s b_s}, \tag{8}$$

where $\mathrm{Min}\{h_{sx},h_{sy}\}$ represents the minimum value of the stiffener heights h_{sx} and h_{sy}.

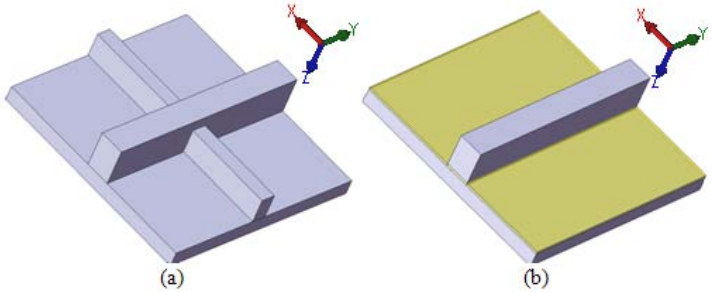

Fig. 2. (a) A repeating section; and (b) the repeating section with the *x* stiffener smeared.

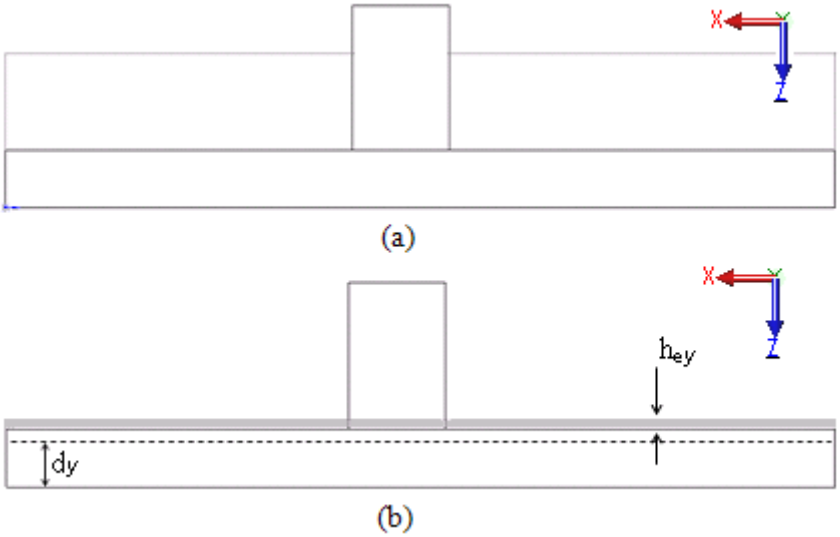

Fig. 3. (a) Side view of the repeating section; and (b) the **repeating** section with the *x* stiffener smeared. The dashed line shows the neutral axis for the direction in question.

2.2. Improved smearing technique

In order to improve the accuracy of the smearing technique, the influence of stiffeners in the *x* direction is also taken into account in the calculation of I_y. A repeating section of the stiffened plate is shown in Fig. 2(a), and Fig. 2(b) shows how the stiffener in the *x* direction is smeared to a thin layer attached to the top of the base plate. A side view of the geometry is shown in Fig. 3. Figure 3(a) shows the actual repeating section, whereas Fig. 3(b) shows the repeating section with the *x* stiffener smeared. This smearing of the rectangular shaped *x* stiffeners has two effects: the mass of the *x* stiffener changes the position of the neutral axis slightly and thus results in a new value of d_y, and the smearing increases the area moment of inertia because of the added layer.

First, d_y is redefined by finding the new neutral axis of the stiffened plate in the *y* direction (about the *x* axis). The mass of the plate and the *y* stiffener, as well as the new layer from the smeared *x* stiffener are taken into account. Besides, the overlapping parts of the *x* and *y* stiffeners are subtracted in the calculation. The minimum value of h_{sx} and h_{sy} is selected, and the volume of the overlapping part is obtained by multiplying this value with $w_{sx}w_{sy}$. Thus, the new distance to neutral axis becomes

$$d_y = \frac{N}{D}, \tag{9}$$

where the numerator is given by

$$N = \frac{1}{2}h^2 a_s b_s + a_s w_{sx} h_{sx}\left(h + \frac{h_{ey}}{2}\right) + b_s w_{sy} h_{sy}\left(h + \frac{h_{sy}}{2}\right) - w_{sx} w_{sy}\,\mathrm{Min}\{h_{sx}, h_{sy}\}(h + \frac{\mathrm{Min}\{h_{sx}, h_{sy}\}}{2}),$$

and the denominator by

$$D = h a_s b_s + a_s w_{sx} h_{sx} + b_s w_{sy} h_{sy} - w_{sx} w_{sy}\,\mathrm{Min}\{h_{sx}, h_{sy}\}.$$

Here, h_{ey} is the thickness of the added upper layer on the base plate resulting from the smeared *x* stiffener.

The area moment of inertia of the added plate layer with respect to the new neutral axis is now determined,

$$I_{sx} = \frac{h_{ey}^3}{12} + h_{ey}(\frac{h_{ey}}{2} + h - d_y)^2. \tag{10}$$

Adding this quantity to the expression in Eq. (2) gives a new improved result for the area moment of inertia:

$$I_y = I_p + I_{sy} + I_{sx}. \tag{11}$$

Thus, this results in an improved version of the bending stiffness $D_y = EI_y$. In a similar manner an improved value of I_x is obtained, and this results in a new value of $D_x = EI_x$. Substituting these updated values for D_x and D_y into Eq. (1) results in an improved equation of motion for the equivalently smeared plate.

In the development of the smeared properties of the cross-stiffened plate it has been tacitly assumed that the stiffeners are parallel to the edges of the plate. However, if the stiffeners are angled relative to the edge, one can include this angle in the calculation of bending stiffness and effective torsional rigidity. Also, as the stiffeners are angled they become longer with increasing added mass, which is taken into account in the calculation. However, apart from the changes in directional stiffness and added mass, the smearing technique necessarily assumes a main-axis symmetric modal pattern that is the same as in the case with stiffeners parallel to the edges of the plate.

Defining angles α and β as shown in Fig. 4 to be the angles from the *x* stiffeners to the *x* axis, and from the *y* stiffeners to the *y* axis, respectively. In the *x* direction, the stiffness of the angled *x* stiffener is weighted with $\cos(\alpha)$; and with $\sin(\beta)$ for the angled *y* stiffener. The stiffness in the *y* direction is obtained in a similar manner. Then the resulting bending stiffness in the *x* and *y* directions become

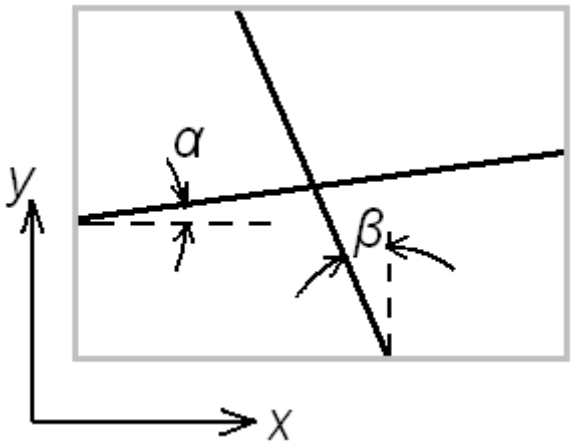

Fig. 4. A sketch of the repeating section of angled stiffeners.

$$D_{x,\text{angled}} = D_x \cos(\alpha) + D_y \sin(\beta) \tag{12}$$

and

$$D_{y,\text{angled}} = D_x \sin(\alpha) + D_y \cos(\beta), \tag{13}$$

where $D_x = EI_x$ and $D_y = EI_y$ are the previously defined bending stiffnesses for stiffeners parallel to the boundaries.

The effective torsional rigidity is also corrected with the new values of area moment of inertia of the *x* and *y* stiffeners. Equations (7) and (5) now become

$$I_{sx0,\text{angled}} = I_{sx0} \cos(\alpha) + I_{sy0} \sin(\beta) \tag{14}$$

and

$$I_{sy0,\text{angled}} = I_{sx0} \sin(\alpha) + I_{sy0} \cos(\beta), \tag{15}$$

where I_{sx0} and I_{sy0} are defined in Eqs. (7) and (5). By substituting Eqs. (14) and (15) into Eq. (6), the effective torsional rigidity is updated for panels with angled stiffeners. Furthermore, the mass per unit area is corrected to included the added mass. This is done with an updated equivalent thickness for angled stiffeners,

$$h_{e,\text{angled}} = h + \frac{h_{sx} w_{sx}}{b_s \cos(\alpha)} + \frac{h_{sy} w_{sy}}{a_s \cos(\beta)} - \frac{\text{Min}\{h_{sx}, h_{sy}\} w_{sx} w_{sy}}{a_s b_s}. \tag{16}$$

By replacing the rigidities and mass per unit area in Eq. (1) with the angled parameters presented in Eqs. (12) to (15) , the smearing technique is extended to include the influence of angled stiffeners.

2.3. Application of the smearing technique

For a thin cross-stiffened rectangular plate with all edges simply supported, the natural frequencies of the correspondingly equivalent smeared plate are [4]

$$f_{mn} = \frac{1}{2\pi}\sqrt{\frac{1}{\rho''}}\sqrt{D_x(\frac{m\pi}{a})^4 + 2H(\frac{m\pi}{a})^2(\frac{n\pi}{b})^2 + D_y(\frac{n\pi}{b})^4}\,, \tag{17}$$

where *m* and *n* are the mode numbers corresponding to the numbers of half-sinusoidals in the *x* and *y* directions, respectively.

Expressions for a cross-stiffened plate with all four edges clamped (CCCC) can be obtained with the technique recently presented by Xing and Liu for thin orthotropic rectangular plates with different boundary conditions [9] using the improved D_x and D_y. Two eigenvalue equations from Ref. [9] are solved iteratively using Newton's technique. Finally, the natural frequencies are obtained from the resulting eigenvalues.

The smearing technique can also be used for evaluating the forced harmonic vibration of a simply supported cross-stiffened thin rectangular plate. The external forcing in Eq. (1) can be expressed as a double sine series with terms of the form

$$p_{mn} = P_{mn}\sin\frac{m\pi x}{a}\sin\frac{n\pi y}{b}\,. \tag{18}$$

Here, the time variation $e^{i\omega t}$ with angular frequency ω is understood. By substituting Eq. (18) into Eq. (1), the total displacement at position (*x*, *y*) can be found after some algebra to be

$$w(x,y) = \sum_{m=0}^{\infty}\sum_{n=0}^{\infty}\frac{P_{mn}}{\rho h\left(\omega_{mn}^2 - \omega^2\right)}\sin\frac{m\pi x}{a}\sin\frac{n\pi y}{b}\,, \tag{19}$$

where ω_{mn} is the angular natural frequency of the plate.

For point force excitation of amplitude F_0 at panel position (x_0, y_0) it follows that $p(x,y) = F_0\delta(x-x_0)\cdot\delta(y-y_0)$, where δ is the Dirac delta function, from which the coefficients P_{mn} easily can be determined. The transfer mobility $Y(x,y;x_0,y_0)$ that relates the transverse velocity response at location (x,y) to a point force at (x_0,y_0) can therefore be determined from

$$Y(x,y;x_0,y_0) = \frac{i\omega\, w(x,y)}{F_0}\,. \tag{20}$$

The point (or direct) mobility is obtained simply by replacing the response location (*x*, *y*) by (x_0,y_0) in Eq. (20).

3. Comparison with Szilard's technique

The dynamics of a stiffened plate is studied in this section. The natural frequencies for the plate with different boundary conditions are calculated using the improved smearing technique and compared with Szilard's technique. The accuracy of these predicted results is evaluated against reference data obtained by FE calculations with the commercial software package ANSYS.

The structural model considered here is a rectangular, cross-stiffened plate with a base plate thickness of h = 6 mm. The main dimensions of the plate are a = 344 mm and b = 258 mm. The pattern of the cross-stiffening is chosen to be spatially periodic, such that a_s = 86 mm and b_s = 86 mm. With half end-spacing it follows that there are three stiffeners in the x direction and four stiffeners in the y direction. The plate is simply supported along all four edges (SSSS) for model #1, whereas the plate of model #2 is clamped on all edges (CCCC). Both models have small stiffeners in the x direction and larger stiffeners in the y direction. The size of the stiffeners in the x direction is h_{sx} = 6 mm, w_{sx} = 6 mm, and in the y direction h_{sy} = 9 mm and w_{sy} = 9 mm. The material properties are for hard PVC, which has $E = 3\text{x}10^9$ N/m^2, υ = 0.33, and ρ = 1360 kg/m^3.

In order to represent the bending vibration at a high frequency, say, 800 Hz, accurately the mesh size limit of the FE calculation is taken to be ten times smaller than the bending wavelength at that frequency. This means that more than ten elements are included per wavelength of motion at 800 Hz. The wavelength of a bending wave is $\lambda_b = \sqrt{1.8 c_L h / f}$, where $c_L = (E/\rho)^{1/2}$ is the wave speed of a longitudinal wave in the plate [8]. Substituting the above-mentioned values gives a wavelength of 155 mm at 800 Hz, and 15 mm is therefore chosen to be the maximum mesh size in the following FE models.

The panel mode numbers are defined as m "cells of equal phase" in the x direction and n in the y direction. For the present panel the range of (m, n) is limited to (3, 2), because the smearing technique is not expected to work when the frequency becomes so high that the spacing between the stiffeners is comparable to or larger than half a wavelength in the base plate.

Table 1. Natural frequencies of panel model #1 (SSSS) obtained with the improved technique and Szilard's technique, and their deviations compared with ANSYS results.

		FE	Improved technique		Szilard's technique	
m	n	Freq. [Hz]	Freq. [Hz]	Deviation	Freq. [Hz]	Deviation
1	1	144	138	-4%	135	-6%
2	1	263	258	-2%	244	-7%
3	1	458	468	2%	451	-2%
1	2	487	488	0%	462	-5%
2	2	561	552	-2%	541	-4%
3	2	561	552	-3%	541	-7%

Table 1 gives the natural frequencies of the simply supported model #1 obtained with the two techniques, and their deviations from the ANSYS benchmark results, also called FE results. In this case with simple supports m and n represent the number of "half-sinusoidals". In the table the deviation of natural frequency denotes the difference between the predicted analytical natural frequency ($f_{\text{analytical}}$) using the two smearing techniques, respectively, and the FE results (f_{FE}). Thus, this deviation in percentage is calculated as $100*(f_{\text{analytical}} - f_{\text{FE}})/f_{\text{FE}}$. It is apparent that the improved smearing technique gives smaller deviations in the predicted natural frequencies: about half the deviations as obtained by Szilard's technique.

The natural frequency of mode (3, 1) obtained with the improved technique is observed to be *overestimated* and is seen to deviate from the reference FE-value by 2%. The reason for this overestimation can be found by inspection of the corresponding mode shape shown in Fig. 5. This

shows that the two middle stiffeners in the *y* direction (the vertical direction in the figure) are very close to the nodal lines. Therefore, they do not contribute much to the stiffness in the *x* direction (horizontal in the figure). When the bending stiffness in the *x* direction is calculated using the improved smearing technique, the stiffeners in the *y* direction are thus taken into account in the calculation. This increases the bending stiffness and gives rise to an overestimation of the natural frequency.

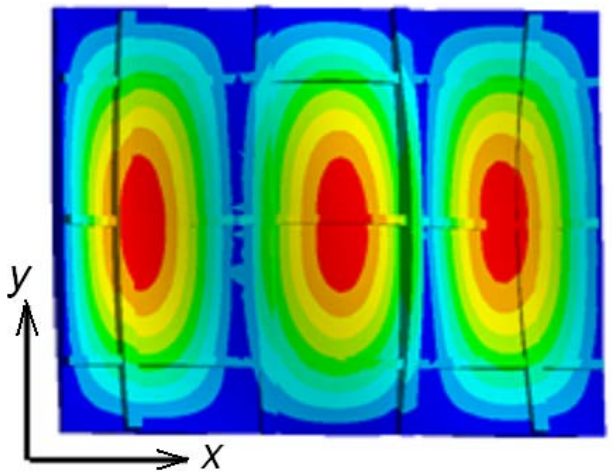

Fig. 5. Modal pattern of mode (3, 1) of an FE estimation of model #1.

Table 2. Natural frequencies of panel model #2 (CCCC) obtained with the improved technique and Szilard's technique, and their deviations compared with ANSYS results.

		FE	Improved technique		Szilard's technique	
m	n	Freq. [Hz]	Freq. [Hz]	Deviation	Freq. [Hz]	Deviation
1	1	298	284	-5%	277	-7%
2	1	432	419	-3%	397	-8%
3	1	686	678	-1%	628	-9%
1	2	751	722	-4%	712	-5%
2	2	857	815	-5%	797	-7%
3	2	1022	1012	-1%	961	-6%

Model #2 is the same structure as model #1 but with the boundary conditions changed to all four edges being fully clamped. Table 2 lists the natural frequencies of model #2 predicted with the improved technique and with Szilard's technique, and their deviations compared with FE results. As can be seen, the improved technique is generally more accurate than Szilard's technique. Again, the deviations are on average reduced by a factor of two.

4. Application of the improved smearing technique

4.1 Forced vibration

The improved smearing technique is readily applied for predicting the forced vibration of a cross-stiffened plate structure. An experimental investigation has also been conducted in an attempt

to validate the improved smearing prediction technique. In addition to this a comparison is made between this predicting technique and benchmark results by ANSYS calculation for the same cases of forced vibration.

4.1.1 Predictions and experimental results

The tested model #3 is a stiffened panel, fabricated (milled out) from a solid block of hard PVC material. The simply supported boundary condition was attempted accomplished by a machined groove around the plate perimeter; see the cut-out illustration in Fig. 6. This means that the plate was supported by a thin strip that was connected to an almost rigid supporting edge (not shown). Moreover, the supporting edge was mounted on a thick-walled hard-wood box, which was bolted to a steel stand of 300 kg. The main dimensions of the plate and the distribution of stiffeners were the same as those of model #1, but the size of the stiffeners was different. The stiffeners in both the x and y directions had the same height, $h_{sx} = h_{sy} = 10$ mm, and width, $w_{sx} = w_{sy} = 6$ mm. Again, $E = 3\text{x}10^9$ N/m^2, $\upsilon = 0.33$, and $\rho = 1360$ kg/m^3.

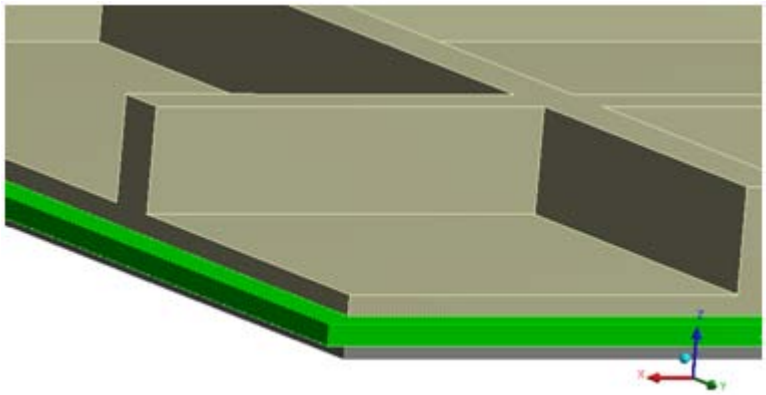

Fig. 6. Narrow plate-strip used as supporting edges of a stiffened plate model.

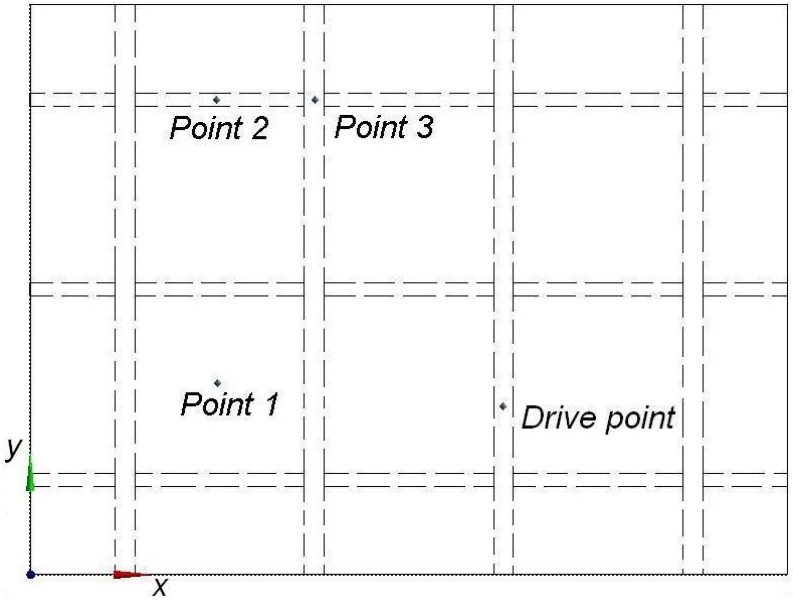

Fig. 7. A sketch of the cross-stiffened plate of model #3. The driving point and the three points for the transfer mobility are shown.

In the experiments the plate was driven by an electrodynamic exciter of type Brüel & Kjær 4810 (B&K, Nærum, Denmark) via a stringer at a stiffener; the coordinates of the drive point were $(x_0, y_0) = (0.215, 0.076)$, where the origin of the coordinate system is at the lower left-hand corner

of the plate, see Fig. 7. The input force was measured with a force transducer of type B&K 8200, and the response velocities were measured with a laser vibrometer of type Polytec PDV-100 (Waldbronn, Germany) at the driving point and at three points located, respectively, in a plate field, on a stiffener, and at the crossing of two stiffeners; the location of stiffeners can be seen from the dashed lines in Fig. 7 that indicate the (hidden) stiffeners on the rear side of the panel. The force and laser velocity signals were fed to charge amplifiers of type B&K Nexus 2692, and the frequency responses between force and velocities were measured using a B&K "PULSE" analyzer 3560, with a frequency resolution of 0.25 Hz.

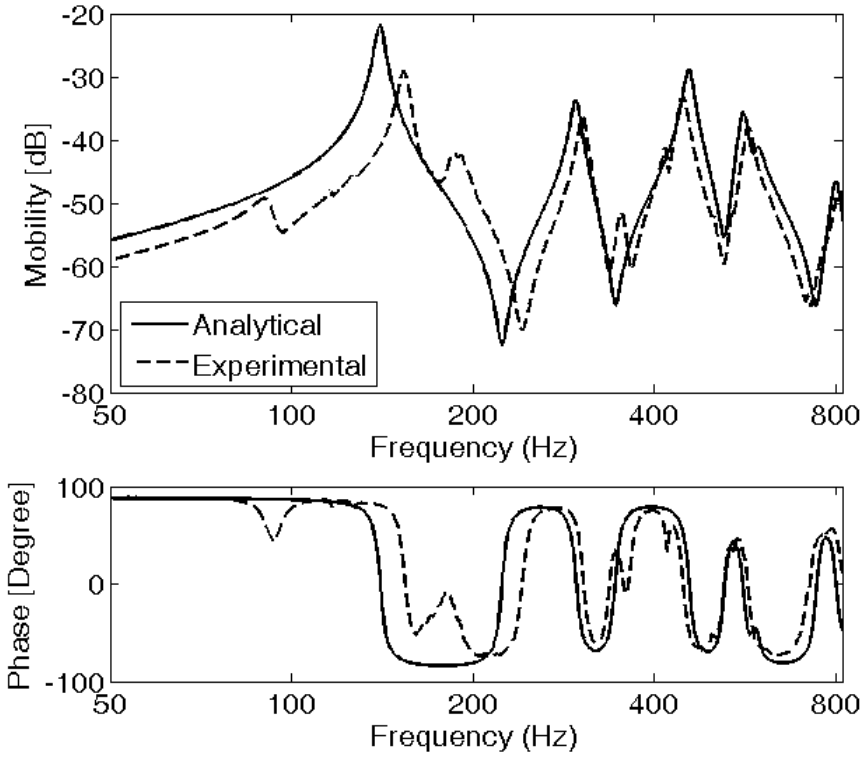

Fig. 8. Point mobility at the driving point of model #3. The upper figure is the mobility amplitude, while the lower figure presents the phase. Solid lines are the analytical estimations obtained using the improved smearing technique; the dashed lines represent the experimental results.

Figure 8 shows a comparison of the analytical point mobility as calculated by the improved smearing technique and the experimental result. The unexpected peaks at low frequencies are not panel modes but are caused by experimental difficulties with the test arrangement. These difficulties are due to the thin strip support and the supporting box system; the thin strip was assumed to behave as a simple support, but since this was not a perfect simple support, it allowed for small shear-related motion and moment constraint at the edges of the plate. It is probably because of these non-ideal conditions at the support that the first mode occurs at a higher frequency than the analytical result. However, the support had a negligible influence on the other modes, which are found to agree fairly well with the prediction.

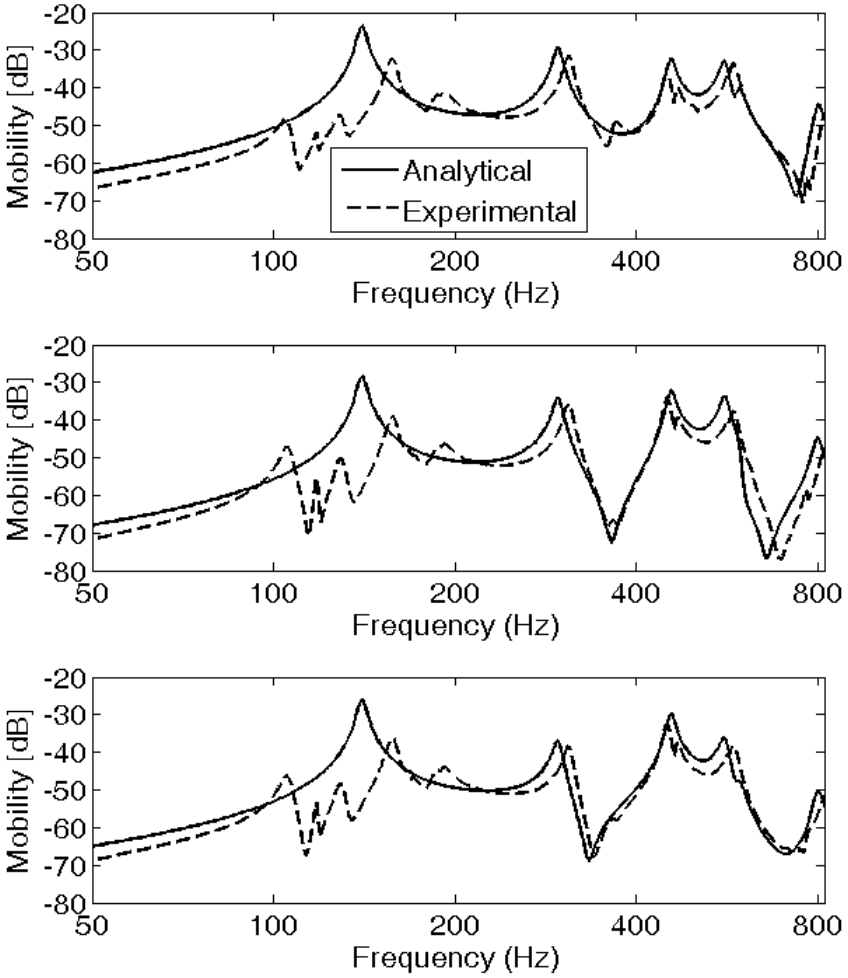

Fig. 9. Transfer mobilities at three panel points. Solid lines are the analytical estimations obtained using the improved smearing technique; the dashed lines present the experimental results. The upper figure is the transfer mobility at point no. 1; the mid figure is at point no. 2; the lower figure is at point no. 3.

In Fig. 9 the predicted transfer mobilities at the three points mentioned above are compared with the experimental data except for the lowest mode. The agreement is fairly good in all three cases, from which one may conclude that transfer mobilities in general can be predicted fairly well.

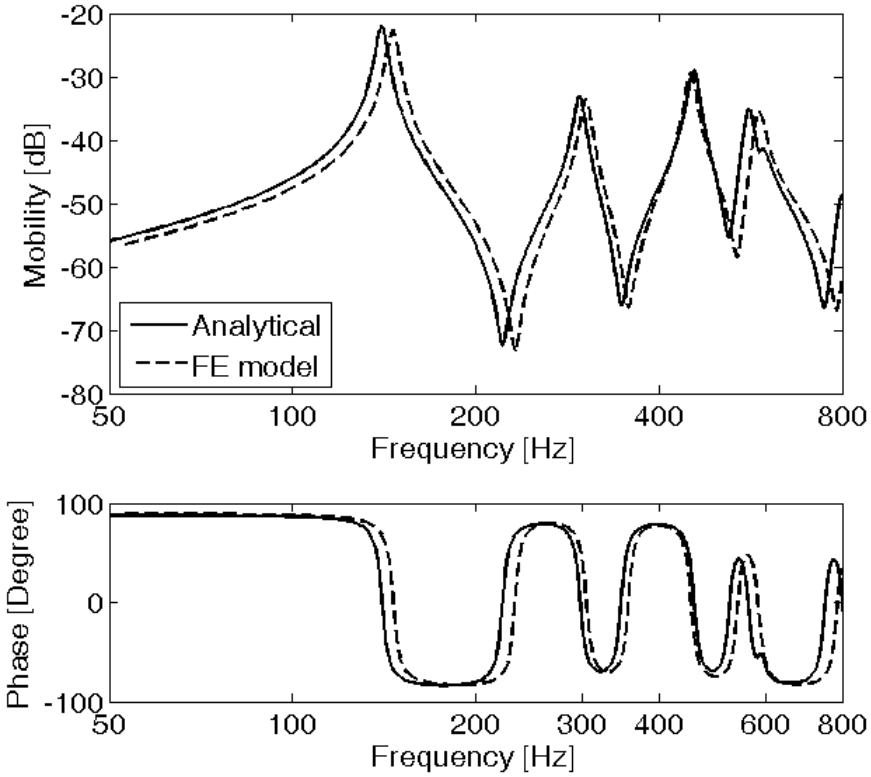

Fig. 10. Point mobility at the driving point of model #3. The upper figure is the mobility amplitude, while the lower figure presents the phase. Solid lines are the analytical estimations obtained using the improved smearing technique; the dashed lines present the FE results.

4.1.2 Finite element model

An FE model was made for model #3. This was to be used as a reference, and especially for validating the prediction of the mobilities around the natural frequency of the first mode. The element size limit was again chosen to be 15 mm. The analytically predicted point mobility, which was obtained by the improved smearing technique, is compared with the FE result in Fig. 10. Good agreement is reached both in the amplitude and phase; the level of the analytical point mobility is almost the same as the FE data, although a small shift of natural frequencies of a few percent can be seen. In Fig. 11 the analytical transfer mobilities at the three response points are compared with FE data, and good agreement is found for all three response points.

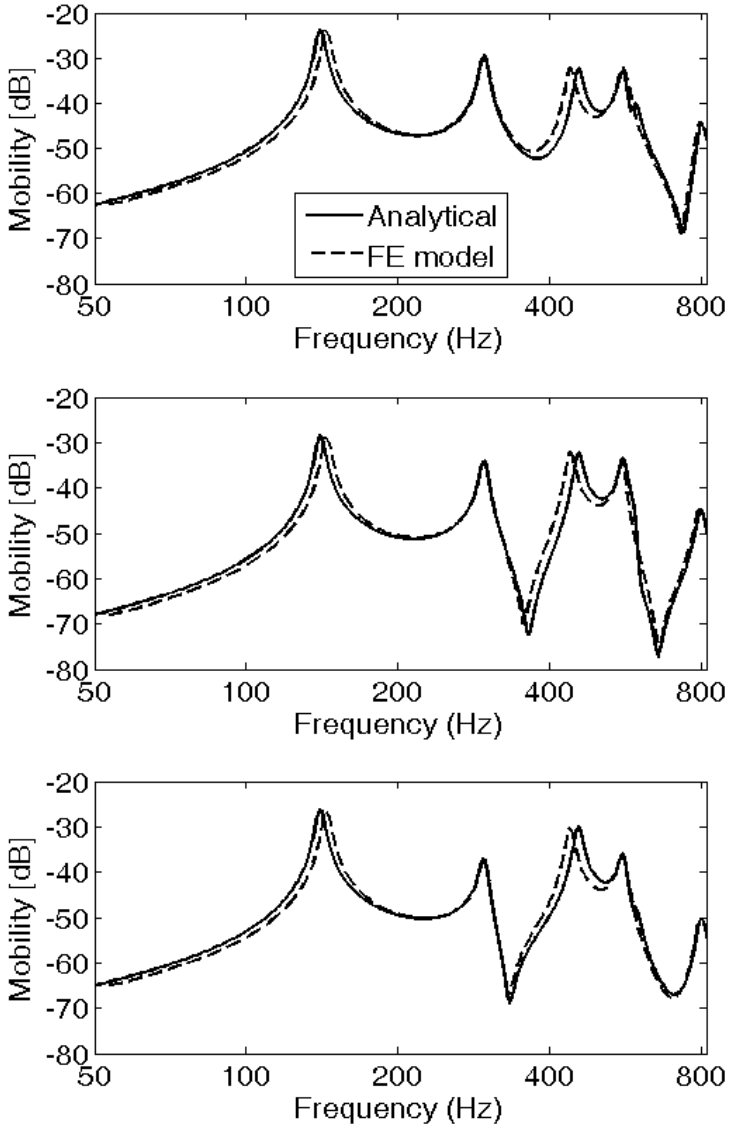

Fig. 11. Transfer mobilities at three points. Solid lines are the analytical estimations obtained using the improved smearing technique; the dashed lines present the FE results. The upper figure is the transfer mobility at point no. 1; the mid figure is at point no. 2; the lower figure is at point no. 3.

4.2 Plates with angled stiffeners

4.2.1 Natural frequencies

This section presents results for the natural frequencies of plates with stiffeners that are angled relative to the edges of the plate. The natural frequencies calculated using Eqs. (12) to (17) are compared with FE results, determined with all the details of the angled stiffeners taken into account. The deviations in natural frequencies reveal a reduced accuracy of the smearing technique for plates with angled stiffeners.

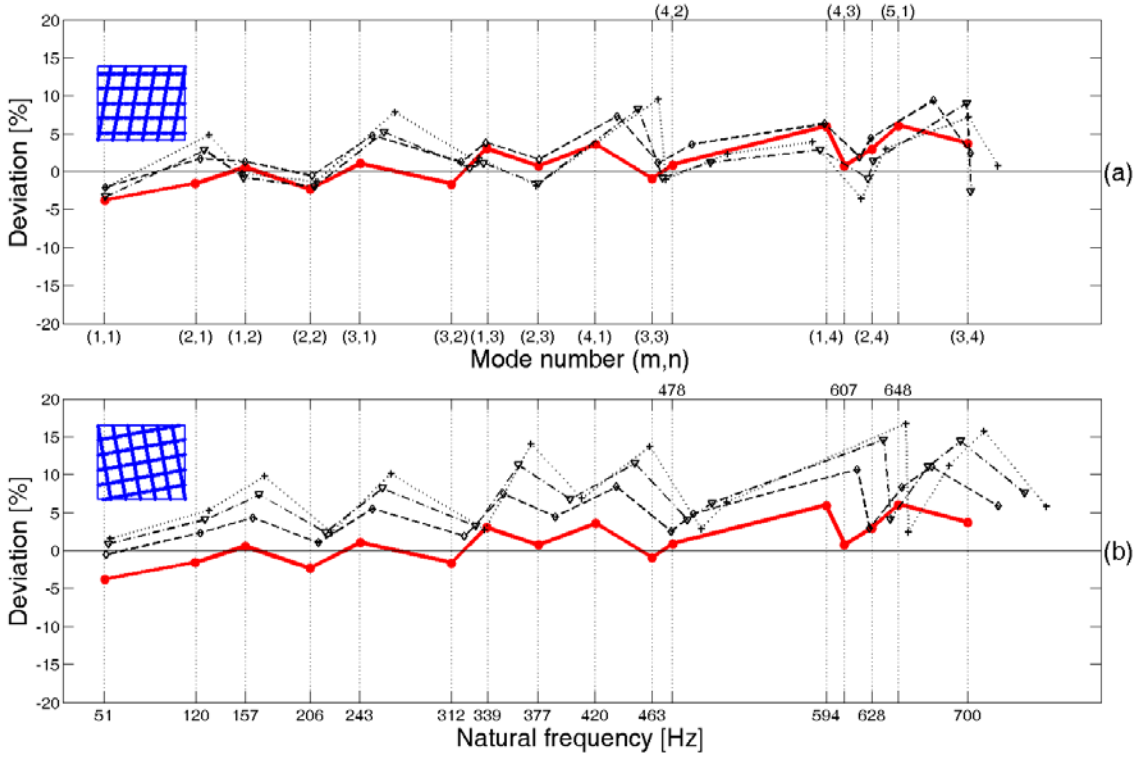

Fig. 12. Deviations between predicted natural frequencies and FE results for panels with angled stiffeners. (a) Panel models with only *y* stiffener angled with β = 0, 5, 10, 15 degrees; (b) panel models with both *x* and *y* stiffeners angled with α = β = 0, 5, 10, 15 degrees. The small sketches in both the upper and lower figures illustrate the geometry and arrangement of stiffeners. Solid lines with point marks are for 0 degrees (the original prototype); dashed lines with diamond marks are for 5 degrees; dash-dotted lines with downward-pointing triangles are for 10 degrees; dotted lines with plus signs are for 15 degrees.

In this study a somewhat larger panel is considered. The first panel model, called the original prototype, has 6x5 stiffeners and overall dimensions of a = 516 mm and b = 430 mm, and the stiffener angles α and β are zero, which means that the stiffeners in the original prototype are parallel to the plate edges. The four edges of the plate are assumed to be simply supported. The other dimensions of this cross-stiffened plate are h = 6 mm, a_s = 86 mm, b_s = 86 mm, $h_{sx} = h_{sy}$ = 9 mm, and $w_{sx} = w_{sy}$ = 6 mm, and the material properties are as previous mentioned. Two series of panel models are investigated. The first series is for α = 0 and β=5, 10, 15 degrees, respectively; while the second series is for $\alpha = \beta$ = 5, $\alpha = \beta$ = 10, $\alpha = \beta$ = 15 degrees, respectively.

The deviations of the predicted natural frequencies of these models are shown in Fig. 12. Both the original prototype mode numbers and natural frequencies are indicated in the figure. The upper figure is for the first series with only angled *y* stiffeners. This arrangement is illustrated by the small sketch in the left-hand side of the figure. The deviations are seen to become larger with increasing angle. In Section 2.1, it has been assumed that the modal pattern for plates with angled stiffeners is the same as a for plate with edge-parallel stiffeners. This is not exactly the case when the angle of stiffeners become large. Figure 13 shows as an example modal pattern of mode (3,2) of a panel model with β = 15 degrees. Obviously, the modal pattern is tilted by the angled stiffeners so that nodal lines tend to follow the stiffeners. Deviations in natural frequencies therefore occur. Nevertheless, the range of stiffener angle β can be taken up to approximate 15 degrees if deviations in natural frequencies up to 10% can be accepted. The lower figure of Fig. 12 shows the deviations for the second series, that is, parallel models with angled *x* and *y* stiffeners. The deviations are larger than for the first series because the stiffeners in both the *x* and *y* directions are angled, and therefore the modal pattern is changed more than in the first series with only the stiffeners in the *y*

direction angled. With such a tilted modal pattern, the apparent wavelength is longer than the corresponding wavelength of the un-tilted modal pattern, which is assumed in the calculation. Therefore, the FE results have lower natural frequencies than the estimated ones obtained using smearing technique, and thus the deviations are generally positive.

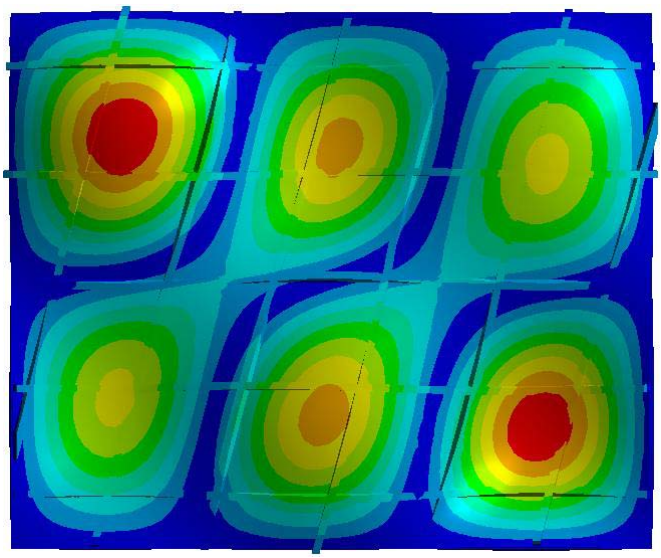

Fig. 13. Modal pattern of mode (3, 2) of the FE estimation of the model with angled *y* stiffeners.

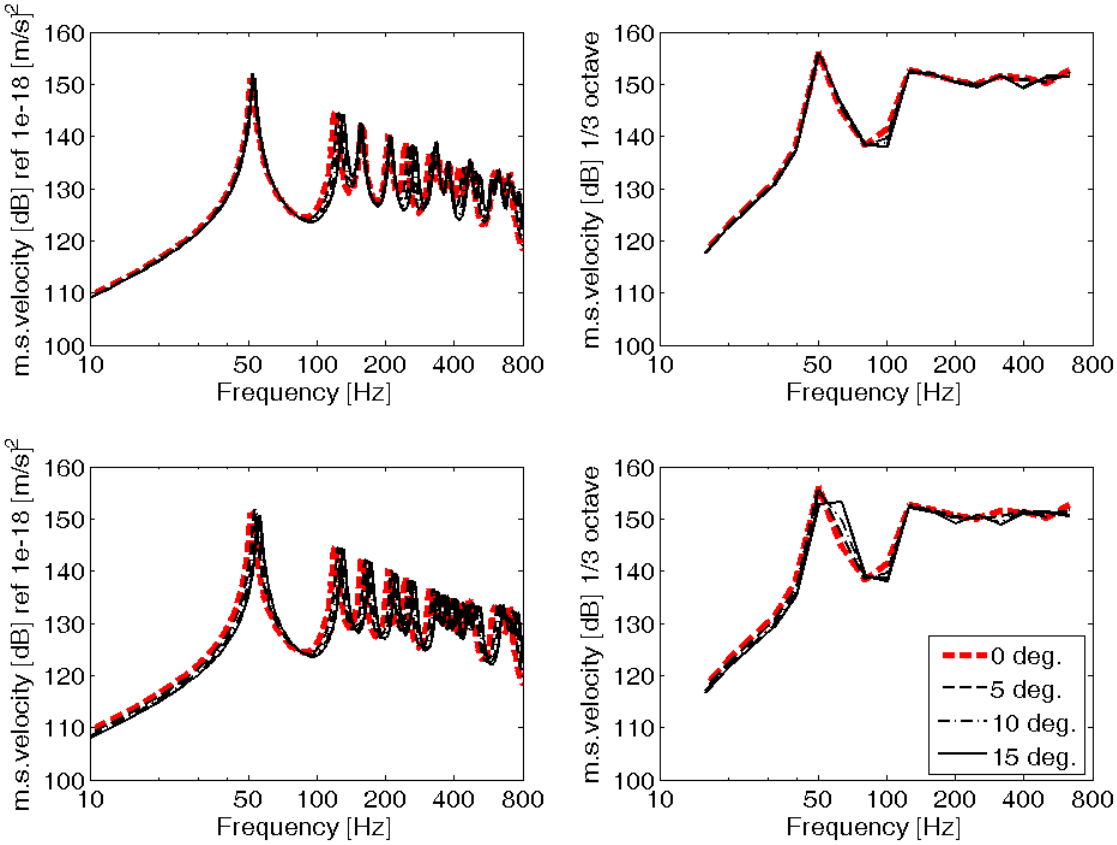

Fig. 14. Frequency variation of mean square velocities per squared unit force of the panel models with angled stiffeners. The left-hand figures show the narrow-band frequency variation, and the right-hand figures present corresponding results as one-third octave band levels. The upper figures are for models with only *y* stiffener angled with $\beta = 0, 5, 10, 15$ degrees; the lower figures are for models with both *x* and *y* stiffeners angled with $\alpha = \beta = 0, 5, 10, 15$ degrees.

4.2.2 Mean square vibration velocity

Some structural acoustic designers might not be solely interested in very accurate predictions of natural frequencies but may favor knowledge of band-averaged velocity levels of a vibrating plate for noise control measures. It is therefore of interest to investigate, for example, the mean square velocity averaged over the surface of the plate. By using the smearing technique, the stiffened plate can be smeared into an equivalent orthotropic plate with smeared equivalent properties. Well-known expressions for calculating the vibration of a simple plate [8] can therefore be used to obtain the mean square velocity with the given equivalent parameters. The same two series of models with angled stiffeners are now considered. For each model the spatially averaged mean square velocity of the panel is calculated for each of a large number of individual point force excitations, and these results are finally averaged. In this way the mean square velocity becomes independent of the mode shapes of the panel [8]. Figure 14 illustrates the frequency variation of the mean square velocity obtained in this way for the different models when it is assumed that the excitation force has a squared amplitude of 1 N^2 at each frequency. The upper figures are for the first series, and the lower figures are for the second series. The validity of the smearing technique for such predictions is established for stiffeners parallel to the boundaries [5], and it is apparent that angling the stiffeners by up to 15 degrees has a very limited influence on the narrow band mean square velocity and practically no influence on one-third octave band levels of the mean square velocity.

5. Conclusions

An improved smearing technique for predicting the natural frequencies of cross-stiffened rectangular plates has been developed. In contrast to Szilard's technique, this takes stiffeners in both the *x* and *y* directions into account in the bending stiffness calculation. Moreover, angled stiffeners are included in the improved technique. Two models of cross-stiffened rectangular flat plates with different boundary conditions have been examined. With FE calculations as references, the new technique has been found to give an improved accuracy for the natural frequencies compared with Szilard's technique; the prediction errors are approximately halved for the cases examined in this study. It has also been found that the improved technique can be applied for forced vibration. Good agreements have been obtained in the mobility comparison between the analytical data and the experimental or FE results. Furthermore, the smearing technique has been evaluated with angled stiffeners. Although the deviations in natural frequencies becomes larger with increasing stiffener angles, the mean square velocity level can still be estimated with a good accuracy. All in all, the improved technique is very efficient for making coarse estimates in an early stage of a design of stiffened plates.

References

[1] H. Xu, J. Du, W.L. Li, Vibrations of rectangular plates reinforced by any number of beams of arbitrary lengths and placement angles, *Journal of Sound and Vibration* 329 (2010) 3759-3779.

[2] C. Omid'varan, Free vibration of grid-stiffened plates, *Journal of Sound and Vibration* 19 (1971) 463-472.

[3] C. Omid'varan, W. Delagarza, Vibration of monolithic grid-stiffened plates, *Journal of Sound and Vibration* 26 (1973) 21-28.

[4] M.S. Troitsky, *Stiffened Plates*, Elsevier, Amsterdam, 1976.

[5] R. Szilard, *Theories and Applications of Plate Analysis*, John Wiley & Sons, Hoboken, New Jersey, 2004.

[6] Y. Luan, M. Ohlrich, F. Jacobsen, Smearing technique for vibration analysis of simply supported cross-stiffened and doubly curved thin rectangular shells, *Journal of the Acoustical Society of America* 129 (2011) 707-716.

[7] J.-L. Guyader, C. Cacciolati, E. Guyader, Prediction of vibroacoustic behaviour of multilayered structures using equivalent materials, *Proceedings of 17th International Congress on Sound and Vibration*, Cairo, Egypt, 2010.

[8] L. Cremer, M. Heckl, B.A.T. Petersson, *Structure-Borne Sound*, third ed., Springer-Verlag, Berlin, 2005, pp. 55, 123, 298-300.

[9] Y.F. Xing, B. Liu, New exact solutions for free vibrations of thin orthotropic rectangular plates, *Composite Structures* 89 (2009) 567-574.

Paper II

Y. Luan, M. Ohlrich, and F. Jacobsen, "Smearing technique for vibration analysis of simply supported cross-stiffened and doubly curved thin rectangular shells," ***Journal of Acoustical Society of America*** 129 **(2), 707-716, 2011.**

Smearing technique for vibration analysis of simply supported cross-stiffened and doubly curved thin rectangular shells[a)]

Yu Luan[b)]
Acoustic Department, Bang & Olufsen, Peter Bangs Vej 15, DK-7600, Struer, Denmark

Mogens Ohlrich and Finn Jacobsen
Acoustic Technology, Department of Electrical Engineering, Technical University of Denmark, Building 352, DK-2800 Kongens Lyngby, Denmark

(Received 13 November 2009; revised 28 October 2010; accepted 7 November 2010)

Plates stiffened with ribs can be modeled as equivalent homogeneous isotropic or orthotropic plates. Modeling such an equivalent *smeared* plate numerically, say, with the finite element method requires far less computer resources than modeling the complete stiffened plate. This may be important when a number of stiffened plates are combined in a complicated assembly composed of many plate panels. However, whereas the equivalent smeared plate technique is well established and recently improved for flat panels, there is no similar established technique for doubly curved stiffened shells. In this paper the improved smeared plate technique is combined with the equation of motion for a doubly curved thin rectangular shell, and a solution is offered for using the smearing technique for stiffened shell structures. The developed prediction technique is validated by comparing natural frequencies and mode shapes as well as forced responses from simulations based on the smeared theory with results from experiments with a doubly curved cross-stiffened shell. Moreover, natural frequencies of cross-stiffened panels determined by finite element simulations that include the exact cross-sectional geometries of panels with cross-stiffeners are compared with predictions based on the smeared theory for a range of different panel curvatures. Good agreement is found.
 [DOI: 10.1121/1.3523305]

PACS number(s): 43.40.Ey, 43.40.Dx [JHG] Pages: 707–716

I. INTRODUCTION

Stiffeners are efficient for enhancing the stiffness of a plate or shell structure without adding unnecessary amounts of mass as a simple increase of plate thickness would do. However, the increased complexity of plates with added stiffeners normally requires much longer computing time for finding the structural acoustic properties of a stiffened structure in a design process. To reduce the computational effort, a coarse but efficient method is to *smear* the stiffeners to the base plate or shell. This technique of smeared stiffened plates with an effective torsional rigidity was developed by Lampert in the 1970s[1] and summarized by Szilard in 2004.[2] The accuracy of this technique for flat plates has recently been improved.[3] However, there is no similar established theory for doubly curved stiffened shells, and this is the subject of the present paper.

In the last 40 years researchers have paid a great deal of attention to the dynamic behavior of stiffened shells. Works have been done on cylindrical shells[4–29] and on conical shells.[30,31] Since doubly curved shells need more degrees of freedom for analysis researchers mostly use the finite element method (FEM) to deal with such cases. The application of FEM to the vibration analysis of a stiffened shell makes it possible to model discrete stiffeners, variable curvature, and irregular geometry. However, FEM calculations based on the detailed geometries of such panels have been found to be very time-consuming.

Nowadays, engineers usually draw a new design structure with a three-dimensional program and later simulate its dynamic properties with an FEM program. The drawing process and the FEM calculations may take days or even weeks for a relatively simple structure. Furthermore, it is often necessary to make modifications to the structure and for that new FEM calculations are required. All this can be very time-consuming. Even though computers become more and more powerful, the engineer's working hours for making a drawing and developing an FEM model have almost not changed. Thus, it is very useful if the geometry can be simplified, for example, by the smearing technique.

The purpose of this paper is to present a smearing technique for determining the natural frequencies and mode shapes of a simply supported doubly curved thin rectangular shell with periodically arranged small stiffeners. The smearing technique becomes unreliable at high frequencies, where half of the bending wavelength in the base plate becomes comparable to—or smaller than—the stiffener spacing. However, the proposed technique is useful for making a fast estimate, although its application is limited to the lower number of vibrational modes.

The expressions to be derived in the following for stiffened shells are based fundamentally on smeared properties of

[a)]Portions of this work were presented in "The structural acoustic properties of stiffened shells," Proceedings of Acoustics'08, Paris, France, 2008.

[b)]Author to whom correspondence should be addressed. Current address: Acoustic Technology, Department of Electrical Engineering, Technical University of Denmark. Electronic mail: yl@elektro.dtu.dk

equivalent flat plates with stiffeners. Such properties of flat stiffened plates are therefore summarized in Sec. II. These results are then utilized, in Sec. III, for developing the smearing technique for curved cross-stiffened panels. In Sec. IV predictions using the developed smearing technique are validated experimentally for a weakly doubly curved and cross-stiffened panel. It is demonstrated that good agreement is achieved between predicted and measured values of natural frequencies and mode shapes as well as forced responses in terms of point and transfer mobilities. With the smearing technique experimentally validated for the test panel, this technique is then used for predicting the modal properties of cross-stiffened panels for a range of different curvatures. These predicted results are compared with finite element (FE) calculations (using ANSYS) in which all stiffener details are modeled; these time-extensive FE calculations are used as reference for evaluating the predicted results.

II. SMEARED STIFFENED PLATE

It has long been recognized that the lower modes of vibration of stiffened plates may be estimated by "smearing" the mass and stiffening effects of the stiffeners over the surface of the plate. The results in this section are based on existing theory.[2,3]

In the following, the natural frequencies of a thin rectangular plate with cross-stiffeners are determined. The plate is simply supported along all four edges. The geometrical parameters of the plate are shown in Fig. 1; the length of the plate is a in the x direction and b in the y direction, and its thickness is h. The stiffeners in the x direction have the width w_{sx}, height h_{sx}, and spacing b_s and in the y direction the corresponding values are w_{sy}, h_{sy}, and a_s.

The governing equation of motion for an equivalent smeared plate of the stiffened plate has been derived by Szilard;[2] for the transverse displacement $w(x,y,t)$ this yields

$$D_x\frac{\partial^4 w(x,y,t)}{\partial x^4}+2H\frac{\partial^4 w(x,y,t)}{\partial x^2\partial y^2}+D_y\frac{\partial^4 w(x,y,t)}{\partial y^4}+\rho h_e\frac{\partial^2 w(x,y,t)}{\partial t^2}=p, \quad (1)$$

where D_x and D_y are the equivalent bending stiffness per unit width in the x and y directions, H is the effective torsional rigidity, ρ is the mass density of the material, h_e is the thickness of the equivalent smeared plate, and p is the external forcing. The development of the improved D_x and D_y can be found in Ref. 3, but for ease of reference some details are also given in the Appendix. With the stiffeners smeared and spread on top of the plate, the thickness of the equivalent smeared plate becomes

$$h_e=h+h_s w_s\left(\frac{1}{a_s}+\frac{1}{b_s}\right)-\frac{h_s w_s^2}{a_s b_s}. \quad (2)$$

For a thin cross-stiffened rectangular plate with all edges simply supported, the natural frequencies of the corresponding smeared plate are[32]

$$f_{mn,\mathrm{flat,stiff}}=\frac{1}{2\pi}\sqrt{\frac{1}{\rho''}}\sqrt{D_x\left(\frac{m\pi}{a}\right)^4+2H\left(\frac{m\pi}{a}\right)^2\left(\frac{n\pi}{b}\right)^2+D_y\left(\frac{n\pi}{b}\right)^4}, \quad (3)$$

where $\rho''=\rho h_e$ is the smeared average mass per unit area, and the integers m and n are the mode numbers corresponding to the x and y directions.

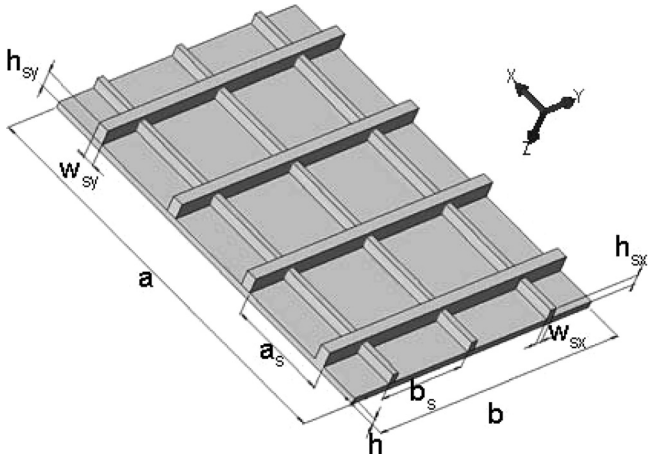

FIG. 1. Geometrical parameters of a cross-stiffened flat rectangular plate.

III. SMEARED STIFFENED SHELL

In this section, an equation for the natural frequencies of a simply supported doubly curved and cross-stiffened rectangular shell is presented together with an expression for the forced response. First, the unstiffened rectangular shell is considered.

A. Natural frequencies of a doubly curved thin rectangular shell

Soedel studied a simply supported doubly curved rectangular shell.[33] Here, the shell has a constant radius of curvature R_x in the x direction, and a constant radius of curvature R_y in the y direction. The x–y coordinate system is selected on the imagined flat base plate. The curved edge lengths of the shell are a in the x–z plane, and b in the y–z plane, and the thickness of the shell is h. In what follows E is the Young's modulus, ν is the Poisson's ratio, and ρ is the density.

Assumptions such as Donell–Mushtari–Vlasor's simplification and the infinitesimal distance assumption are used in

Soedel's derivation. The first basic assumption of Donell–Mushtari–Vlasor's simplification is that contributions of in-plane deflections can be neglected in the bending strain expressions but not in the membrane strain expressions. The second assumption is that the influence of inertia in the in-plane direction can be neglected. Third, the infinitesimal distance assumption is

$$(ds)^2 \cong (dx)^2 + (dy)^2, \tag{4}$$

where ds is the magnitude of the differential change.[33] Both assumptions introduce a considerable error in the estimation of the fundamental natural frequency.[11]

With these assumptions, the equation of motion for free transverse vibration $w(x,y,t) = U_3 e^{iwt}$ of a homogenous shell becomes[33]

$$D\nabla^8 U_3 + Eh\nabla_k^4 U_3 - \rho'' \omega^2 \nabla^4 U_3 = 0, \tag{5}$$

where

$$D = \frac{Eh^3}{12(1-\nu^2)}, \tag{6}$$

$$\nabla^2(\cdot) = \frac{\partial^2(\cdot)}{\partial x^2} + \frac{\partial^2(\cdot)}{\partial y^2}, \tag{7}$$

$$\nabla_k^2(\cdot) = \frac{1}{R_x}\frac{\partial^2(\cdot)}{\partial x^2} + \frac{1}{R_y}\frac{\partial^2(\cdot)}{\partial y^2}, \tag{8}$$

in which $\rho'' = \rho h$ is the mass per unit area, and D is the bending stiffness. For the doubly curved, simply supported rectangular shell, the transverse displacement is expressed by a double sine series with terms of the form

$$U_{3,mn} = A_{mn} \sin\frac{m\pi x}{a} \sin\frac{n\pi y}{b}. \tag{9}$$

Substituting Eq. (9) into Eq. (5) gives

$$D\left[\left(\frac{m\pi}{a}\right)^2 + \left(\frac{n\pi}{b}\right)^2\right]^4 + Eh\left[\frac{1}{R_x}\left(\frac{m\pi}{a}\right)^2 + \frac{1}{R_y}\left(\frac{n\pi}{b}\right)^2\right]^2 - \rho''\omega^2\left[\left(\frac{m\pi}{a}\right)^2 + \left(\frac{n\pi}{b}\right)^2\right]^2 = 0. \tag{10}$$

The natural frequencies are therefore

$$f_{mn,\text{curve}}^2 = \frac{1}{4\pi^2}\left[\left(\frac{m\pi}{a}\right)^2 + \left(\frac{n\pi}{b}\right)^2\right]^2 \frac{D}{\rho''} + \frac{\left[\frac{1}{R_x}\left(\frac{m\pi}{a}\right)^2 + \frac{1}{R_y}\left(\frac{n\pi}{b}\right)^2\right]^2}{4\pi^2\left[\left(\frac{m\pi}{a}\right)^2 + \left(\frac{n\pi}{b}\right)^2\right]^2} \cdot \frac{E}{\rho}. \tag{11}$$

It is well known that the natural frequencies of a thin rectangular flat plate are

$$f_{mn,\text{flat}} = \frac{1}{2\pi}\sqrt{\left[\left(\frac{m\pi}{a}\right)^2 + \left(\frac{n\pi}{b}\right)^2\right]^2 \frac{D}{\rho''}}$$

$$\Rightarrow f_{mn,\text{flat}}^2 = \frac{1}{4\pi^2}\left[\left(\frac{m\pi}{a}\right)^2 + \left(\frac{n\pi}{b}\right)^2\right]^2 \frac{D}{\rho''}, \tag{12}$$

where the geometrical and material parameters of the flat plate are the same as those of the curved shell except for the curvatures. Therefore, Eq. (11) can be rewritten,

$$f_{mn,\text{curve}}^2 = f_{mn,\text{flat}}^2 + \frac{\left[\frac{1}{R_x}\left(\frac{m\pi}{a}\right)^2 + \frac{1}{R_y}\left(\frac{n\pi}{b}\right)^2\right]^2}{4\pi^2\left[\left(\frac{m\pi}{a}\right)^2 + \left(\frac{n\pi}{b}\right)^2\right]^2} \cdot \frac{E}{\rho}. \tag{13}$$

All in all, the formula for the natural frequencies of a simply supported, doubly curved, thin rectangular shell can be seen to be the sum of two terms. The first term relates to a flat plate that has the same geometrical and material parameters as the curved shell except for the curvatures; the second term is accounting for the curvature. In other words, in parts a doubly curved rectangular shell has properties similar to a flat rectangular plate for which the shell is pressed and extended into a flat surface. The thickness does not change during this process. The edge lengths of the flat plate are equal to the curved edge lengths of the shell, which are still a and b. Thus, the natural frequencies of the doubly curved shell can be obtained by finding the natural frequencies of the related flat plate and adding the curvature term; see Eq. (13).

B. Natural frequencies of a simply supported, doubly curved, and cross-stiffened thin rectangular shell

This section presents the natural frequencies of a simply supported, doubly curved, and cross-stiffened thin rectangular shell. Both a physical explanation and an analytical derivation are offered.

Equation (13) indicates a possible way of finding the natural frequencies even for a doubly curved *cross-stiffened* shell. If these stiffeners are smeared on the surface of the shell, the resulting structure can be regarded as an equivalent smeared shell. The smeared shell also has its related plate, which is the shell pressed and extended into a flat surface. The related smeared plate has its equivalent bending stiffness in the x and y direction, D_x and D_y, torsional rigidity, H, and equivalent thickness, h_e. None of these parameters appears in the curvature term in Eq. (13), which means that this term is independent of the smearing technique. The two terms in Eq. (13) can thus be obtained individually. Equation (3) yields the natural frequencies of the related plate, whereas the curvature term of Eq. (13) can be obtained from the base shell properties. Following these arguments this results in the natural frequencies of a simply supported, doubly curved, and cross-stiffened thin rectangular shell

$$f_{mn,\text{curve,stiff}}^2 = f_{mn,\text{flat,stiff}}^2 + \frac{\left[\frac{1}{R_x}\left(\frac{m\pi}{a}\right)^2 + \frac{1}{R_y}\left(\frac{n\pi}{b}\right)^2\right]^2}{4\pi^2\left[\left(\frac{m\pi}{a}\right)^2 + \left(\frac{n\pi}{b}\right)^2\right]^2} \cdot \frac{E}{\rho}. \tag{14}$$

An analytical derivation of Eq. (14) can be developed by using the equation of motion for the shell. Equation (5) can represent an equation of motion for a stiffened shell, provided that the parameters D, h, and $\rho'' = \rho h$ are replaced by the corresponding properties of an equivalent *smeared* shell, that is, by D_e, h_e, and $\rho'' = \rho h_e$. The equation of motion of the equivalent smeared shell therefore becomes

$$D_e \nabla^8 U_3 + E h_e \nabla_k^4 U_3 - \rho'' \omega^2 \nabla^4 U_3 = 0, \tag{15}$$

As can be seen from Eq. (6), the bending stiffness D of a shell is independent of the curvature. Therefore D can be obtained from a structure where the radii of the shell go to infinity, in other words, a corresponding flat plate. Similarly, the equivalent bending stiffness D_e can also be calculated for an equivalent smeared flat plate, which is the smeared shell pressed and extended into a flat surface.

It was shown in Sec. II that the equivalent smeared plate has its equivalent bending stiffnesses D_x and D_y and torsional rigidity H. In order to use Eq. (15), D_x, D_y, and H should be combined into one parameter, D_e. The challenge now is to find an expression for D_e, which should include the orthotropic behavior of the equivalent smeared plate.

It can be assumed that an equivalent "isotropic" plate, which has the same geometrical properties of the previous equivalent smeared plate, exists. Also, the "isotropic" plate has an equivalent bending stiffness, D_e, and its mechanical properties are the same as those of the mentioned equivalent smeared plate. The equation of motion of an isotropic plate is[33]

$$D\left(\frac{\partial^4 w(x,y,t)}{\partial x^4} + 2\frac{\partial^4 w(x,y,t)}{\partial x^2 \partial y^2} + \frac{\partial^4 w(x,y,t)}{\partial y^4}\right) + \rho h \frac{\partial^2 w(x,y,t)}{\partial t^2} = p. \tag{16}$$

By replacing D with D_e and h with h_e, one can use Eq. (16) as the equation of motion for the equivalent "isotropic" plate. With the simply supported boundary condition, the natural frequencies of this plate can now be obtained,

$$f_{mn,\mathrm{iso}} = \frac{1}{2\pi}\left[\left(\frac{m\pi}{a}\right)^2 + \left(\frac{n\pi}{b}\right)^2\right]\sqrt{\frac{D_e}{\rho h_e}}. \tag{17}$$

Since the "isotropic" plate has the same mechanical properties as the equivalent smeared plate, their natural frequencies should also be identical. They are

$$f_{mn,\mathrm{iso}} = f_{mn,\mathrm{flat,stiff}}. \tag{18}$$

Substituting Eqs. (3) and (17) into Eq. (18) gives an expression for the bending stiffness of the assumed "isotropic" equivalent plate,

$$D_e = \frac{D_x\left(\frac{m\pi}{a}\right)^4 + 2H\left(\frac{m\pi}{a}\right)^2\left(\frac{n\pi}{b}\right)^2 + D_y\left(\frac{n\pi}{b}\right)^4}{\left[\left(\frac{m\pi}{a}\right)^2 + \left(\frac{n\pi}{b}\right)^2\right]}. \tag{19}$$

This yields the wanted bending stiffness. Now, by substituting Eq. (19) into Eq. (15), one can obtain the natural frequencies of the simply supported, doubly curved, and cross-stiffened thin rectangular shell,

$$\begin{aligned} f_{mn,\mathrm{curve,stiff}}^2 &= \frac{1}{4\pi^2}\frac{1}{\rho''} \\ &= \left[D_x\left(\frac{m\pi}{a}\right)^4 + 2H\left(\frac{m\pi}{a}\right)^2\left(\frac{n\pi}{b}\right)^2 + D_y\left(\frac{n\pi}{b}\right)^4\right] \\ &\quad + \frac{\left[\frac{1}{R_x}\left(\frac{m\pi}{a}\right)^2 + \frac{1}{R_y}\left(\frac{n\pi}{b}\right)^2\right]^2}{4\pi^2\left[\left(\frac{m\pi}{a}\right)^2 + \left(\frac{n\pi}{b}\right)^2\right]^2}\cdot\frac{E}{\rho}. \end{aligned} \tag{20}$$

Note that the first term equals $f_{mn,\mathrm{flat,stiff}}^2$ in Eq. (3). It can therefore be seen that Eq. (20) is identical with Eq. (14).

C. Forced vibration of a simply supported, doubly curved, and cross-stiffened thin rectangular shell

The smearing technique can also be used for evaluation of forced vibration of a simply supported, doubly curved, and cross-stiffened thin rectangular shell. If a pressure $p = p(x,y)$ is applied on the panel in its normal direction, it can be inserted in Eq. (15), and with Eq. (19) also substituted, the equation of motion becomes

$$D_e \nabla^8 U_3 + E h_e \nabla_k^4 U_3 - \rho'' \omega^2 \nabla^4 U_3 = \nabla^4 p, \tag{21}$$

where the pressure can be expressed by a double sine series with terms of the form

$$p_{mn} = P_{mn} \sin\frac{m\pi x}{a}\sin\frac{n\pi y}{b}. \tag{22}$$

By substituting Eqs. (9) and (22) into Eq. (21), the total displacement at position (x,y) can be found after some algebra to be

$$U_3(x,y) = \sum_{m=0}^{\infty}\sum_{n=0}^{\infty} A_{mn} \sin\frac{m\pi x}{a}\sin\frac{n\pi y}{b}, \tag{23}$$

where

$$A_{mn} = P_{mn}\frac{\left[\left(\frac{m\pi}{a}\right)^2 + \left(\frac{n\pi}{b}\right)^2\right]^2}{D_e\left[\left(\frac{m\pi}{a}\right)^2 + \left(\frac{n\pi}{b}\right)^2\right]^4 + E h_e\left[\frac{1}{R_x}\left(\frac{m\pi}{a}\right)^2 + \frac{1}{R_y}\left(\frac{n\pi}{b}\right)^2\right]^2 - \rho h_e \omega^2\left[\left(\frac{m\pi}{a}\right)^2 + \left(\frac{n\pi}{b}\right)^2\right]^2}. \tag{24}$$

For point force excitation of amplitude F_0 at panel position (x_0, y_0) it follows that $P_{mn} = F_0\delta(x - x_0) \cdot \delta(y - y_0)$, where δ is the Dirac delta function. The transfer mobility $Y(x, y; x_0, y_0)$ that relates the transverse velocity response at location (x, y) to a point force at (x_0, y_0) can therefore be determined from

$$Y(x, y; x_0, y_0) = \frac{i\omega U_3(x, y)}{F_0}. \tag{25}$$

The point (or direct) mobility is obtained simply by replacing the response location (x, y) by (x_0, y_0) in Eq. (25).

IV. COMPARISON OF RESULTS

A. Experiments with a curved stiffened panel

A physical model has been used to test the equation obtained by the presented smearing technique. The model is a doubly curved cross-stiffened thin rectangular shell, which is fabricated (milled out) from a solid block of polyvinyl chloride (PVC). The experimental arrangement is shown in Fig. 2, where it is seen that the solid edge block of the machined panel is screwed into a thick-walled hard-wood box, which is bolted to a 300 kg steel stand. The simply supported boundary condition of the panel was attempted accomplished by a machined narrow groove around the panel perimeter, see Fig. 2. This means that the panel was supported by a thin narrow strip that is connected to an almost rigid supporting edge. The material properties are $E = 3 \times 10^9$ N/m^2, $\nu = 0.33$, and $\rho = 1360$ kg/m^3. The dimensions of the shell are $a = 344$ mm, $b = 258$ mm, $h = 6$ mm, $R_x = 2$ m, and $R_y = 1.5$ m. The pattern of the cross-stiffening is chosen to be spatially periodic, such that $a_s = 86$ mm and $b_s = 86$ mm. With half end-spacing it follows that there are three stiffeners in the x direction and four stiffeners in the y direction. Stiffeners in both the x and y directions had the same height, $h_{sx} = h_{sy} = 10$ mm, and same width, $w_{sx} = w_{sy} = 6$ mm.

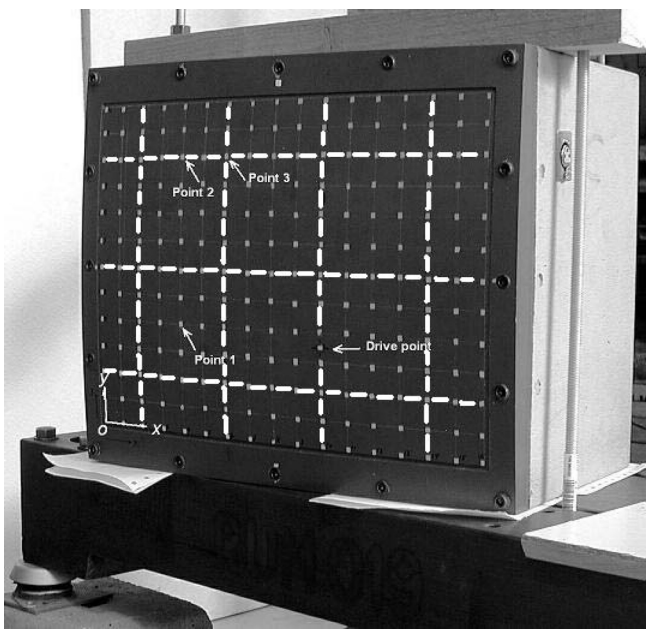

FIG. 2. Experimental arrangement with a doubly curved cross-stiffened panel. White dashed lines on the panel face show the positions of the hidden stiffeners on the rear side.

The curved cross-stiffened panel was driven via a stringer at a stiffener by an electrodynamic exciter of type Brüel & Kjær (B&K, Nærum, Denmark) 4810; the coordinates of the drive point were $(x_0, y_0) = (0.213, 0.076)$, where the origin of the coordinate system is at the lower left-hand corner of the curved panel in Fig. 2. The input force was measured with a force transducer of type B&K 8200, and the response velocities were measured with a laser vibrometer of type Polytec (Waldbronn, Germany) PDV-100 at 192 points evenly spread over the panel. The force and velocity signals were fed to charge amplifiers of type B&K Nexus 2692, and the frequency response functions between velocities and excitation force were measured using a B&K "PULSE" Analyzer 3560 with a frequency resolution of 0.25 Hz.

The natural frequencies and mode shapes of the panel were obtained from the measured mobilities. In Table I the natural frequencies predicted by Eq. (20) are compared with the experimentally measured data. The mode numbers are defined as m in the x direction and n in the y direction. In the table the deviation of natural frequency denotes the difference between the predicted analytical natural frequency ($f_{\text{analytical}}$) and the experimental data (f_{Ex}). Thus, this deviation in percentage is calculated as $100^*(f_{\text{analytical}} - f_{\text{Ex}})/f_{\text{Ex}}$ Generally a very good agreement is found with deviations within 4%, except for the fundamental natural frequency; this was found to deviate from the measured value by −7%, but this mode is left out of the table. The reason for this difficulty in accurately predicting the fundamental frequency is the assumptions used in the equation of motion of the shell, Eq. (5); these assumptions introduce a considerable error in the estimation of the fundamental natural frequency.[34] Such deviation for the fundamental natural frequency can be up to −30% if the panel is strongly curved as is the case for some of the simulated cases that will be shown in Sec. IV B. With the chosen dimensions of the stiffened panel the range of modes (m, n) is limited to mode (3, 2) for the case considered, because the smearing method is not expected to work well when the frequency becomes so high that the spacing between the stiffeners is comparable to—or larger than—half a flexural wavelength in the base plate.

The mobilities of the panel are predicted from Eq. (25), where the numerator is obtained as the product of $i\omega$ and the displacement U_3, which is given by Eq. (23). The damping value used in the predictions is taken to be the average value

TABLE I. Predicted and measured natural frequencies for the experimental panel model. The deviation for each mode is calculated as the difference between the analytical natural frequency ($f_{\text{analytical}}$) and the experimental data (f_{Ex}). Thus, the deviations are calculated as $100^*(f_{\text{analytical}} - f_{\text{Ex}})/f_{\text{Ex}}$.

m	N	Experiment frequency (Hz)	Analysis frequency (Hz)	Deviation (%)
2	1	327	329	0.6
1	2	453	471	4.0
2	2	573	574	0.2
3	3	611	612	0.2
3	2	800	810	1.3

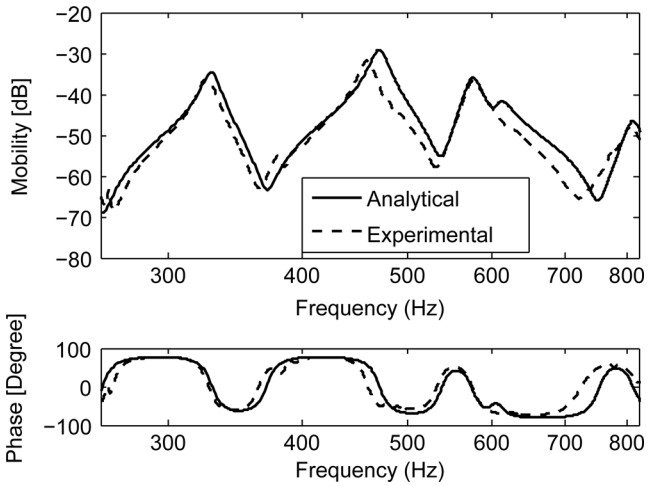

FIG. 3. Point mobility of the curved stiffened panel. Solid line, analytical result; dashed line, experimental result.

of the measured damping loss factors of the panel modes, 0.035. Figure 3 shows a comparison of the analytical and the measured point mobility. The solid curve is the predicted result using the smearing technique, and the dashed curve is the experimental result. Overall, a fairly good agreement can be seen, and the small deviations in mobility magnitude and phase reflect the deviations that were observed in the natural frequencies; this is especially the case for the 4% shift in the natural frequency of mode (1, 2) that results in about 5 dB deviation in the "mass-slope-region" of the mobility magnitude. From Fig. 3, it can also be observed that the weakly excited mode (3, 1) at 611 Hz is hardly visible in the measured result. This is because the drive point was relatively close to a nodal line of this mode; however, from an analysis of all measured data both its natural frequency and mode shape could be determined. Moreover, comparisons of predicted and measured responses at other positions also show a fairly good agreement with similar small deviations corresponding to those in the point mobility. This is seen in Fig. 4, which shows three examples of predicted and measured transfer mobilities for the response positions denoted as points 1–3 in Fig. 2. These points are located, respectively, in a plate field, on a stiffener, and at the crossing of two stiffeners; the location of stiffeners can be seen from the dashed lines in Fig. 2 that indicate the positions of the (hidden) stiffeners on the rear side of the panel.

An example of an experimentally determined modal pattern is shown in Fig. 5 in the form of a two-dimensional surface plot. The result shown is for mode (2, 1) at 327 Hz, and this clearly illustrates a modal pattern with two "half-sinusoidal" in the x direction and one half-sinusoidal in the y direction. This and the other mode shapes have been obtained from the real parts of the transfer mobilities measured at 192 positions, and the modal data have been normalized by the maximum amplitude value.

Two-dimensional plots are not suitable for comparing measured and predicted results. All the examined mode shapes are therefore shown in Fig. 6 by their detailed modal patterns in the x and y directions, respectively. The mode shapes predicted by the smearing technique are plotted as

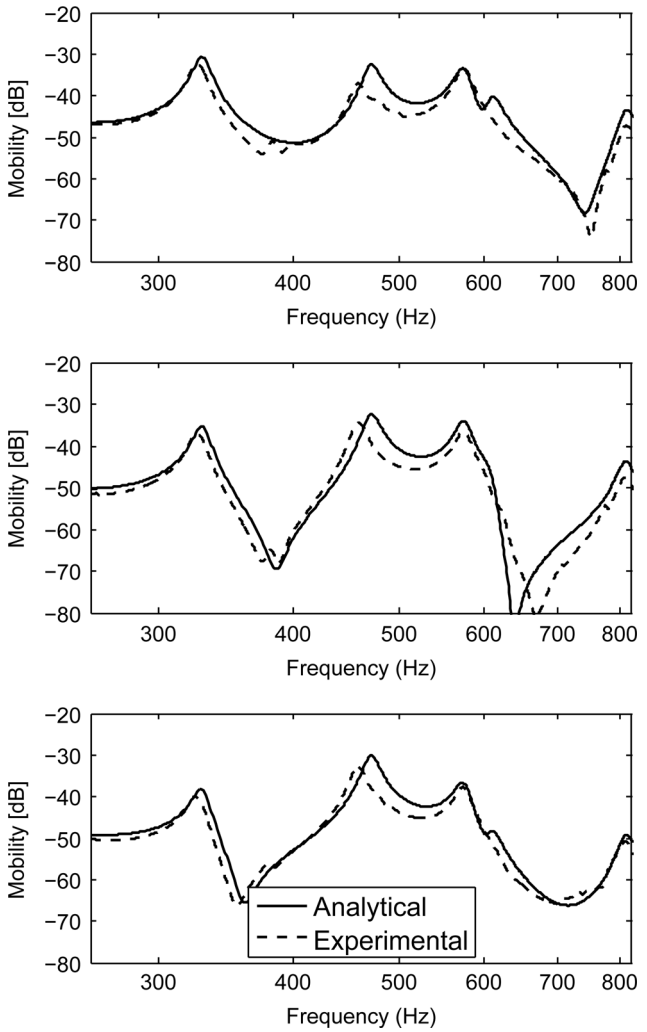

FIG. 4. Transfer mobility of the curved stiffened panel. Solid line, analytical result; dashed line, experimental result. The upper figure is the transfer mobility at point 1 in a plate field (see Fig. 2); the middle figure is at point 2 on a stiffener; the lower figure is at point 3 at the crossing of two stiffeners.

solid lines, whereas the experimentally determined mode shapes are presented as circles located at the actual measurement points; the dashed line represents the corresponding un-deformed panel surface-line. Overall the agreement is seen to be good between the predicted and measured results. A close inspection, however, reveals that there are small deviations. First, it is observed from the x-wise modal pattern of mode (2, 1) that there are small displacements at each end of the panel, and that these are in anti-phase. Similar observations can be made for modes (3, 1) and (3, 2). This is apparently caused by small shear deformations (displacements) at the experimental simple support, or by small motion of the whole experimental arrangement. Additional tests showed that the vibration level of the "rigid" frame were lower than the panel vibration by more than 25 dB at these modes. Thus, the edge-deviation is most likely caused by shear deformation at the narrow-strip support, which cannot fully accomplish an ideal simple line support. Second, it is observed that the measured modal patterns are not exactly sinusoidal as is the case for the predicted mode shapes; this applies in particular to mode (2, 2), both in the x and y

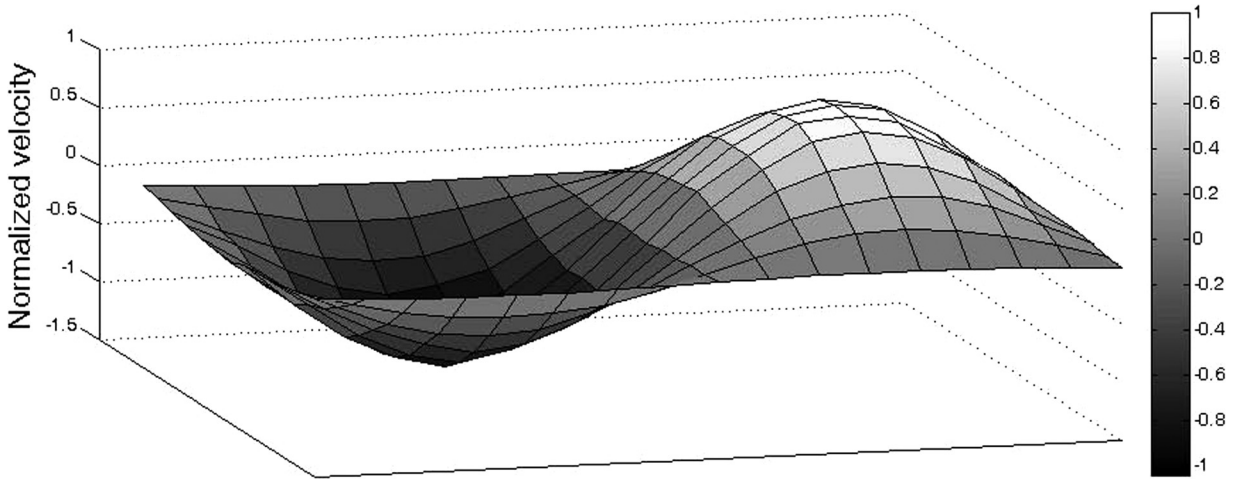

FIG. 5. Mode shape of mode (2, 1) obtained from experiment.

directions, and this causes the nodal lines to shift slightly from the predicted center positions of the zero-crossings. A possible explanation for this could be boundary vibration (albeit lower by 30 dB for this mode) of the supporting "rigid" frame and box structure or manufacturing inaccuracies in the curved stiffened panel; this was measured globally to be of the order of 1.5% for the thickness of the base panel, and this may have a small influence on the modal symmetry. The other modes, on the other hand, have mostly a fine match with the predicted modal patterns.

To sum up, the practically useable frequency range of the presented smearing technique is limited by the frequency at which half a bending wavelength in the base plate becomes comparable to—or smaller than—the stiffener spacing. This has been validated by the experiments reported herein, which have demonstrated that the prediction technique is reliable with an acceptable accuracy up to this frequency; at higher frequencies the technique may have a small influence on accurately replicating the actual mode shapes with beginning local deformation in base panel areas between adjacent stiffeners. However, this is outside the frequency range considered in this study. All in all, the prediction and the experiments have been found to be in good agreement, despite the minor experimental difficulties that give rise to small unpredictable errors.

B. Radius study by numerical simulations

In Sec. IV A a weakly curved cross-stiffened panel was considered with curvature radii of $R_x = 2$ and $R_y = 1.5$ m. With the smearing technique experimentally validated for the considered modal range this section examines a new series of panels that are basically similar to the experimental structure but with different values of curvature radii R_x. In this simulation study the panel radius R_x takes values of 2.0, 1.5, 1.0, 0.6, and 0.2 m, whereas the other geometrical parameters are unchanged. Figure 7 shows the geometry of four of these models. In the lower part of the figure the panel is shown rotated so it is easier to see the arrangement of the stiffeners.

The natural frequencies of this series of curved cross-stiffened panels were computed analytically by the use of the smearing technique and, as a reference, corresponding detailed numerical FE analyses were carried out using the software package ANSYS. The element size used in the FE computations was set to be 10 mm, and the boundary conditions of the

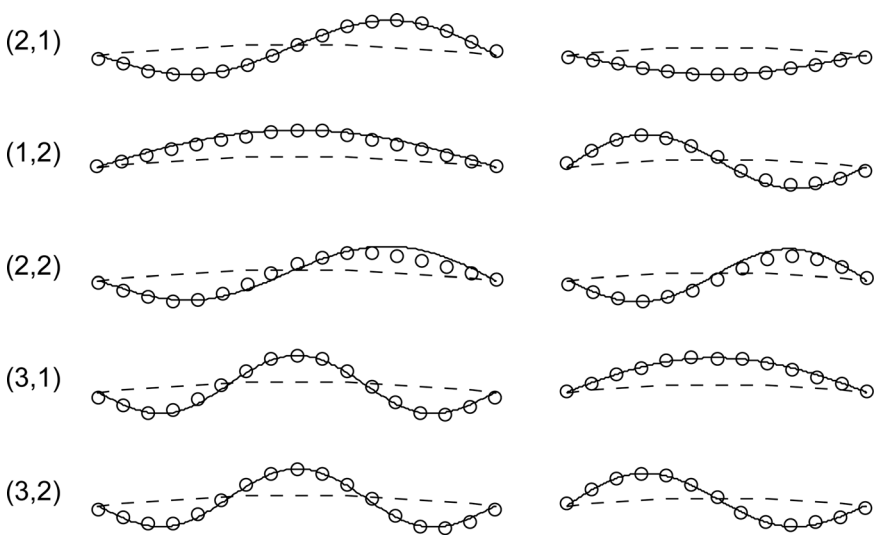

FIG. 6. Mode shape evaluation. The left-hand figures show the mode shapes in the x direction, while the right-hand figures are the mode shapes in the y direction. The corresponding mode numbers are shown to the left. Solid lines represent the theoretically determined mode shapes; the circles represent the experimentally determined mode shapes; and the dashed lines show the neutral positions of the curved base plate.

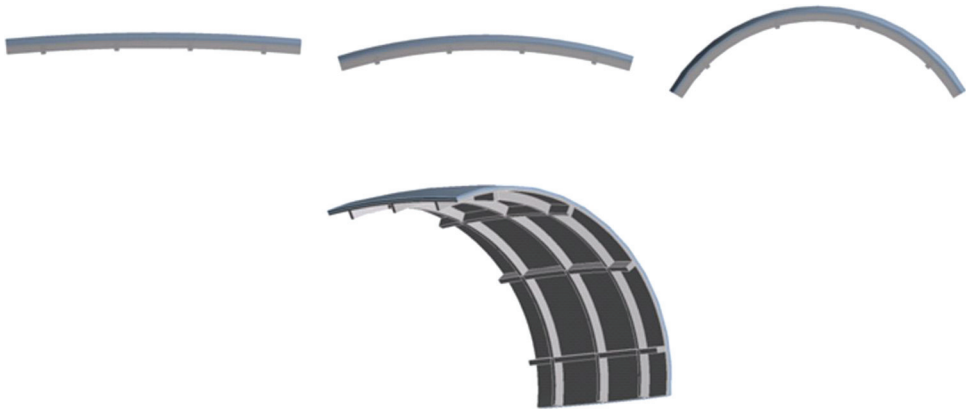

FIG. 7. (Color online) Geometries of four panel models. The upper models from left to right have a curvature radius R_x of 2.0, 1.0, and 0.6 m, respectively, while the lower model has a radius of $R_x = 0.2$ m.

models were again taken to be simply supported along the four panel edges.

The natural frequencies predicted with the analytical smearing technique ($f_{\text{analytical}}$) are compared with the results computed with the FE model (f_{FE}); the FE model contains all details of the structure and it is therefore considered to be the reference for evaluation of the prediction accuracy, as mentioned above. The deviation in predicted natural frequency is thus calculated as $100^*(f_{\text{analytical}} - f_{\text{FE}})/f_{\text{FE}}$, and the results for all modes are shown in Fig. 8. For each mode number n of an (m, n) mode the m values are connected by lines so that one can see how the error changes for different mode numbers m. It is observed that the deviations for all the modes shown are within -1% and $+4\%$ for curvature radii down to 0.6 m, and that the deviations become larger for the last model with smaller radius. Note that the fundamental mode (1, 1) is not included in this figure, since it is inaccurately predicted as mentioned in Sec. IV A. As an example, Fig. 9 shows the modal pattern of mode (2, 2) which is obtained from an FE simulation of the panel with $R_x = 0.2$ m. It is obvious that the modal pattern is not sinusoidal but compressed by the two stiffeners close to the edges in the strongly curved direction. The developed method assumes that the mode shape is sinusoidal and therefore gives a large deviation for this mode as shown in Fig. 8. It indicates that the smearing technique for curved plate cannot be used for predicting accurate results for strongly curved plates. It can also be seen that the stiffeners are twisted by the base plate. Such local twisting cannot be predicted by the smearing theory since the stiffeners are smeared. All in all it may be summarized that for the current series of simulations, the natural frequencies are well predicted with the smearing technique even for panels of a relatively small radius of say 0.6 m.

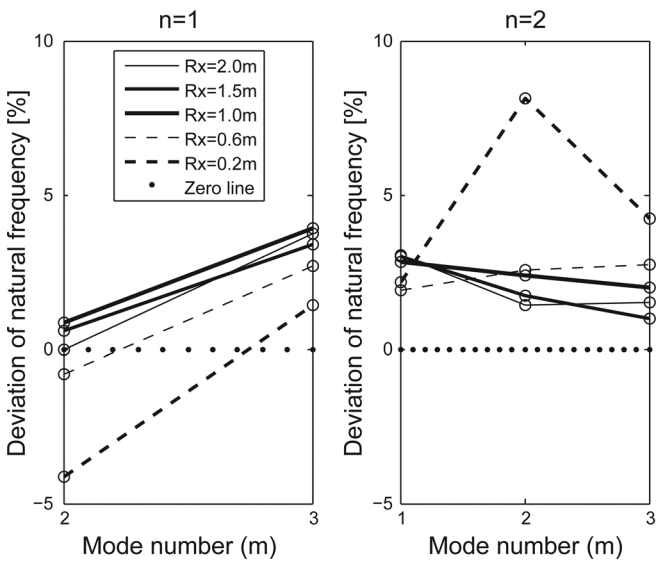

FIG. 8. Deviations of predicted natural frequencies for panels with different curvatures of radii of R_x. Natural frequencies obtained with the smearing technique ($f_{\text{analytical}}$) are compared with calculated results from the FE analysis (f_{FE}), which is considered as the reference. The deviation is calculated as $100^*(f_{\text{analytical}} - f_{\text{FE}})/f_{\text{FE}}$. The left-hand figure shows results for modes (2, 1) and (3, 1), while the right-hand figure is for modes (1, 2), (2, 2), and (3, 2).

V. CONCLUSIONS

A simple smearing method has been presented for calculating the natural frequencies, mode shapes, and forced vibrations of simply supported doubly curved and cross-stiffened thin rectangular shells. This developed smearing technique has been validated by experiments with a weakly doubly

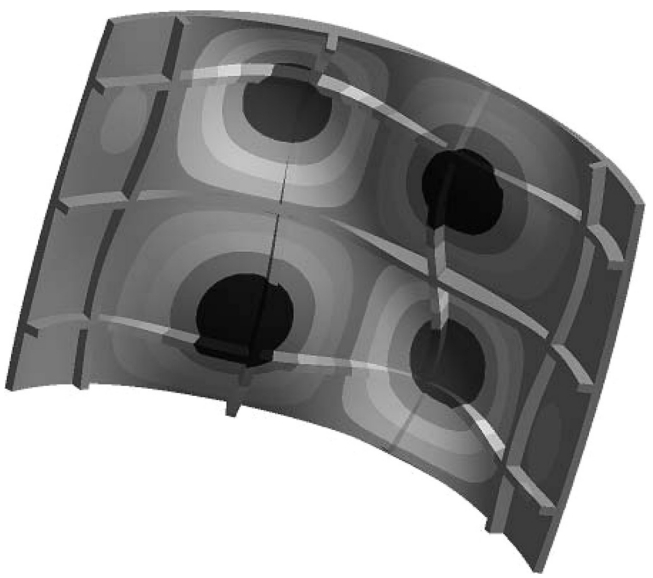

FIG. 9. Two-dimensional mode shape of mode (2, 2) obtained by the FE analysis for the panel with a curvature radius of $R_x = 0.2$ m and $R_y = 1.5$ m.

curved and cross-stiffened panel fabricated from a block of PVC-material. Comparison of the predicted and experimental results revealed a good agreement for the modal properties as well as for the forced panel responses. Simulation studies were also carried out for more curved panels by using the smearing technique and detailed FE analyses. For the cases examined herein, the results show that a reasonably good engineering accuracy can be obtained with limited computational effort for such doubly curved panels with moderate size cross-stiffeners.

This investigation also demonstrates that it is difficult to predict the fundamental panel mode (1, 1) of highly curved panels accurately when using the Donell–Mushtari–Vlasor's shell equations. However, it is expected that it should be possible to improve the developed estimation method to a wider range of structures by adding a correction factor to these shell equations, as mentioned in Ref. 34.

APPENDIX: A BRIEF DESCRIPTION OF THE SMEARING TECHNIQUE FOR CROSS-STIFFENED THIN RECTANGULAR PLATE[2,3]

The bending stiffness D_y can be calculated as the product of Young's modulus of the material, E, and the area moment of inertia in the y direction, I_y, which is

$$I_y = I_p + I_{sy} + I_{sx}, \tag{A1}$$

where the area moment of inertia of the plate with respect to the neutral axis of the system is

$$I_p = \frac{h^3}{12(1-\nu^2)} + \left(d_y - \frac{h}{2}\right)^2 \cdot h, \tag{A2}$$

in which ν is the Poisson's ratio, and d_y denotes the distance between the plate's bottom surface and the neutral axis of the stiffened plate in the y direction. The area moment of inertia of the stiffeners with respect to the same neutral axis is

$$I_{sy} = \frac{1}{a_s} \cdot \left[\frac{w_{sy} \cdot h_{sy}^3}{12} + \left(h_{sy} + h - d_y - \frac{h_{sy}}{2}\right)^2 \cdot (w_{sy} \cdot h_{sy})\right], \tag{A3}$$

and, in the x direction,

$$I_{sx} = \frac{h_{ey}^3}{12} + h_{ey}\left(\frac{h_{ey}}{2} + h - d_y\right)^2. \tag{A4}$$

The neutral axis $d_y$is

$$d_y = \frac{N}{D}, \tag{A5}$$

with the numerator

$$N = \frac{1}{2}h^2 a_s b_s + a_s w_{sx} h_{sx}\left(h + \frac{h_{ey}}{2}\right) + b_s w_{sy} h_{sy}\left(h + \frac{h_{sy}}{2}\right) - w_{sx} w_{sy} Min\{h_{sx}, h_{sy}\}\left(h + \frac{Min\{h_{sx}, h_{sy}\}}{2}\right)$$

and the denominator

$$D = h a_s b_s + a_s w_{sx} h_{sx} + b_s w_{sy} h_{sy} - w_{sx} w_{sy} Min\{h_{sx}, h_{sy}\},$$

in which h_{ey} is the thickness of the added upper layer on the plate resulting from the smeared x stiffener. Note that the other geometrical parameters are defined in Fig. 1 in the main body of the paper.

The bending stiffness in the x direction, D_x, is obtained in a similar manner.

[1]P. Lampert, "Postcracking stiffness of reinforced concrete beams in torsion and bending," in *Analysis of Structural Systems for Torsion, ACI SP-35*, edited by R. Szilard, P. Zia, and G. Fisher (American Concrete Institute, Detroit, MI, 1973).
[2]R. Szilard, *Theories and Applications of Plate Analysis* (Wiley, Hoboken, NJ, 2004), Chap. 10.
[3]Y. Luan and M. Ohlrich, "An improvement of the smeared theory for stiffened plates," in *Proceedings of Noise and Vibration: Emerging Methods 2009*, Oxford, England (2009).
[4]W. H. Hoppmann II, "Some characteristics of the flexural vibrations of orthogonally stiffened cylindrical shells," J. Acoust. Soc. Am. **30**, 77–82 (1958).
[5]J. E. Manning, and G. Maidanik, "Radiation properties of cylindrical shells," J. Acoust. Soc. Am. **36**, 1691–1698 (1964).
[6]S. A. Rinehart and J. T. S. Wang, "Vibration of simply supported cylindrical shells with longitudinal stiffeners," J. Sound Vib. **24**, 151–163 (1972).
[7]D. J. Mead and N. S. Bardell, "Free vibration of a thin cylindrical shell with discrete axial stiffeners," J. Sound Vib. **111**, 229–250 (1986).
[8]D. J. Mead and N. S. Bardell, "Free vibration of a thin cylindrical shell with periodic circumferential stiffeners," J. Sound Vib. **115**, 499–520 (1987).
[9]B. A. J. Mustafa and R. Ali, "Prediction of natural frequency of vibration of stiffened cylindrical shells and orthogonally stiffened curved panels," J. Sound Vib. **113**, 317–327 (1987).
[10]B. A. J. Mustafa and R. Ali, "Free vibration analysis of multi-symmetric stiffened shells," Comput. Struct. **27**, 803–810 (1987).
[11]N. S. Bardell and D. J. Mead, "Free vibration of an orthogonally stiffened cylindrical shell, part I: Discrete line simple supports," J. Sound Vib. **134**, 29–54 (1989).
[12]N. S. Bardell and D. J. Mead, "Free vibration of an orthogonally stiffened cylindrical shell, part II: Discrete general stiffeners," J. Sound Vib. **134**, 55–72 (1989).
[13]Z. Mecitoglu and M. C. Dokmeci, "Forced vibrations of stiffened cylindrical elastic panels (A)," J. Acoust. Soc. Am. **85**, S118 (1989).
[14]S. P. Cheng and C. Dade, "Dynamic analysis of stiffened plates and shells using spline Gauss collocation method," Comput. Struct. **36**, 623–629 (1990).
[15]M. L. Accorsi and M. S. Bennett, "A finite element based method for the analysis of free wave propagation in stiffened cylinders," J. Sound Vib. **148**, 279–292 (1991).
[16]Z. Mecitoglu and M. C. Dokmeci, "Free vibrations of a thin, stiffened, cylindrical shallow shell," AIAA J. **30**, 848–850 (1991).
[17]R. S. Langley, "A dynamic stiffness technique for the vibration analysis of stiffened shell structures," J. Sound Vib. **156**, 521–540 (1992).
[18]M. Conti and I. Dyer, "The influence of internal structures on bistatic scatter from finite cylindrical shells near axial incidence (A)," J. Acoust. Soc. Am. **94**, 1878 (1993).
[19]D. M. Photiadis, J. A. Bucaro, and B. H. Houston, "Scattering from flexural waves on a ribbed cylindrical shell," J. Acoust. Soc. Am. **96**, 2785–2790 (1994).
[20]G. Maze, D. Décultot, A. Klauson, and J. Metsaveer, "Acoustic scattering by immersed circular cylindrical shell stiffened by internal lengthwise rib (A)," J. Acoust. Soc. Am. **95**, 2868 (1994).
[21]A. Klauson, G. Maze, and J. Metsaveer, "Acoustic scattering by submerged cylindrical shell stiffened by an internal lengthwise rib," J. Acoust. Soc. Am. **96**, 1575–1581 (1994).
[22]A. Klauson, J. Metsaveer, D. Décultot, G. Maze, and J. Ripoche, "Identification of the resonances of a cylindrical shell stiffened by an internal lengthwise rib," J. Acoust. Soc. Am. **100**, 3135–3143 (1996).
[23]A. J. Stanley and N. Ganesan, "Free vibration characteristics of stiffened cylindrical shells," Comput. Struct. **65**, 33–45 (1997).
[24]D. M. Photiadis and B. H. Houston, "Anderson localization of vibration on a framed cylindrical shell," J. Acoust. Soc. Am. **106**, 1377–1391 (1999).

[25]M. H. Marcus, B. H. Houston, and D. M. Photiadis, "Wave localization on a submerged cylindrical shell with rib aperiodicity," J. Acoust. Soc. Am. **109**, 865–869 (2001).
[26]M. Tran-Van-Nhieu, "Scattering from a ribbed finite cylindrical shell," J. Acoust. Soc. Am. **110**, 2858–2866(2001).
[27]R. Liétard, D. Décultot, G. Maze, and M. Tran-Van-Nhieu, "Acoustic scattering from a finite cylindrical shell with evenly spaced stiffeners: Experimental investigation," J. Acoust. Soc. Am. **118**, 2142–2146 (2005).
[28]D. G. Karczub, "Expressions for direct evaluation of wave number in cylindrical shell vibration studies using the Flügge equations of motion," J. Acoust. Soc. Am. **119**, 3553–3557 (2006).
[29]M. Caresta and N. J. Kessissoglou, "Structural and acoustic responses of a fluid loaded cylindrical hill with structural discontinuities," Appl. Acoust. **70**, 954–963 (2009).
[30]Z. Mecitoğlu, "Vibration characteristics of a stiffened conical shell," J. Sound Vib. **197**, 191–206 (1992).
[31]A. N. Nayak and J. N. Bandyopadhyay, "Dynamic response analysis of stiffened conoidal shells," J. Sound Vib. **291**, 1288–1297 (2006).
[32]M. S. Troitsky, *Stiffened Plates* (Elsevier, Amsterdam, 1976), Chap. 8.
[33]W. Soedel, *Vibrations of Shells and Plates*, 3rd ed. (Marcel Dekker, Inc.. New York, 1993), Chap. 6.
[34]L. Cremer, M. Heckl, and E. E. Ungar, *Structure-Borne Sound*, (Springer-Verlag, Berlin, 1988), Chap. 8, p. 186.

Paper III

Y. Luan, M. Ohlrich and F. Jacobsen, "Applying a smearing technique for cross-stiffened rectangular plates for developing a general type of smeared finite element," *Journal of Acoustical Society of America* , 2011 (Submitted).

Applying a smearing technique for cross-stiffened rectangular plates for developing a general type of smeared finite element

Yu Luan[a)]
Acoustic Department, Bang & Olufsen, DK-7600, Struer, Denmark

Mogens Ohlrich and Finn Jacobsen
Acoustic Technology, Department of Electrical Engineering, Technical University of Denmark, Building 352, DK-2800 Kongens Lyngby, Denmark

Letter to the Editor

[a)] Current address: Acoustic Technology, Department of Electrical Engineering, Technical University of Denmark. Author to whom correspondence should be addressed. Electronic mail: yl@elektro.dtu.dk

Abstract
This paper presents an application of the smearing technique for cross-stiffened thin rectangular plates in a general type of finite element (FE). The vibration of cross-stiffened plates can be estimated by equivalent homogeneous orthotropic plates using a smearing technique. Equivalent stiffness properties of flat cross-stiffened plates are calculated as outlined in a recent paper by Luan *et al.* [J. Acoust. Soc. Am. **129** (2), 707-716]. From the general expressions of these properties *equivalent values* of the material properties are derived which are then used in an FE model of a corresponding smeared panel with a standard type of solid/shell element. In other words, a general orthotropic plate model can be used to model a cross-stiffened plate with the obtained equivalent material parameters. The results of FE models using the smeared plate are compared both with detailed FE results without using the smearing technique and with experimental data for vibration and sound radiation. Good agreement is found.

PACS number: 43.40.Dx, 43.40.Rj

I. INTRODUCTION

Rib-stiffened plates are widely used in engineering structures. However, in a design process the increased complexity due to the added stiffeners usually requires long computing time for finding the structural acoustic properties. One way of reducing the computational effort is to use a relatively coarse but efficient method, *the smearing technique*, in which properties of the stiffeners are smeared to the base plate so that the stiffened plate is characterized by an equivalent smeared plate. This technique of smeared stiffened plates with an effective torsional rigidity was developed by Lampert in the 1970s,[1] and summarized by Szilard in 2004.[2] The prediction accuracy of this technique for flat stiffened plates has recently been improved,[3] and the method has also been used for doubly curved cross-stiffened shells.[4] So far, there has been no simple way of implementing this smearing technique in standard FE modeling. In order to implement an equivalent technique, the general procedure is to calculate the property matrices. In this way, Rao *et al.* have studied free flexural vibration of stiffened plates,[5] and Berry *et al.* have predicted the sound radiation from rectangular baffled plates with arbitrary boundary conditions.[6] Berry and Locqueteau have also computed the vibration and sound radiation of fluid-loaded stiffened plates with consideration of in-plane deformation using a Ritz method.[7] However, these methods are not suitable for coarse estimation, since one has to write computer codes in order to use these techniques in an FE model. The purpose of this letter is to suggest and examine an effective method for coarse estimation of the vibration and sound radiation of rib cross-stiffened plates.

Instead of writing the computer code for an FE model, the present paper develops a simple way of applying the smearing technique in a general type of FE that is used for orthotropic thin flat plates, in the same way as the element of type Hex08.[8] (The Hex08 element is a very general type of solid/shell element, which is used for structural modeling in commercial FE software packages such as ACTRAN[8] and ANSYS.[9]) By using the smearing technique one can calculate the corresponding bending stiffnesses, effective torsional rigidity, and equivalent thickness of an equivalent smeared plate. From these results, the *equivalent material parameters* are determined, that is, the equivalent values of Young's modulus, shear modulus, etc. With these equivalent material parameters, the smeared orthotropic plate can be used to replace the cross-stiffened plate in an FE model by using an existing, conventional element type for orthotropic plates.

II. THE MATERIAL PARAMETERS

A. Properties of an orthotropic plate

This section summarizes the general stiffness properties for an orthotropic flat plate. These formulae will be used in Section II. B for calculating the *equivalent* material parameters of a smeared plate.

The bending stiffness per unit width in the x and y direction are[2]

$$D_i = \frac{E_i h^3}{12\left(1-\nu_x \nu_y\right)}, \qquad i = x, y, \tag{1}$$

where E_x, E_y are Young's modulus in the x and y direction, ν_x, ν_y are the corresponding Poisson's ratios, and h is the plate thickness. The effective torsional rigidity is[2]

$$H = \frac{1}{2}\left(\nu_y D_x + \nu_x D_y + G_{xy}\frac{h^3}{3}\right), \tag{2}$$

where G_{xy} is the shear modulus in the *x-y* plane. This quantity and the shear modulus in the *x-z* plane and *y-z* plane are[2]

$$G_{xj} = \frac{\sqrt{E_x E_j}}{2(1+\sqrt{\nu_x \nu_j})}, \qquad j = y, z, \tag{3}$$

$$G_{yz} = \frac{\sqrt{E_y E_z}}{2(1+\sqrt{\nu_y \nu_z})}. \tag{4}$$

B. The equivalent material parameters

In a general type of element for orthotropic plates a number of material parameters are required; these are the different Young's moduli, E_x, E_y, E_z, shear moduli, G_{xy}, G_{zx}, G_{yz}, Poisson's ratios, ν_x, ν_y, ν_z, and the material density, ρ. In order to model the smeared orthotropic plate with a plate thickness of h_e, these parameters should be replaced by *equivalent* material parameters denoted by $E_{x,e}$, $E_{y,e}$, $E_{z,e}$, $G_{xy,e}$, $G_{zx,e}$, $G_{yz,e}$, together with assumptions of $\nu_e = \nu_x = \nu_y = \nu_z$ and $\rho_e = \rho$.

The equivalent bending stiffnesses, $D_{x,e}$ and $D_{y,e}$, the effective torsional rigidity, H_e, and the equivalent thickness, h_e, can be calculated as outlined in the Appendix of Ref. 4. By substituting these smeared properties into Eqs. (1) to (4), the equivalent material parameters are obtained. The equivalent Young's modulus is obtained from Eq. (1) as

$$E_{i,e} = D_{x,e} \frac{12\left(1-\nu_e^2\right)}{h_e^3}, \qquad i = x, y. \tag{5}$$

It is assumed that there is no change in Young's modulus in the normal direction of the plate after smearing, and therefore,

$$E_{z,e} = E, \tag{6}$$

where E is the original Young's modulus of the material. The equivalent shear modulus in the *x-y* plane is found from Eq. (2),

$$G_{xy,e} = \frac{3\left(2H_e - D_{x,e}\nu_e - D_{y,e}\nu_e\right)}{h_e^3}. \tag{7}$$

Moreover, the equivalent shear moduli in the *x-z* plane and *y-z* plane are obtained from Eq. (3),

$$G_{iz,e} = \frac{\sqrt{E_{i,e}E_{z,e}}}{2\left(1+\nu\right)}, \qquad i = x, y. \tag{8}$$

With these equivalent material parameters, the FE model of a smeared orthotropic plate can represent the vibrational behavior of the stiffened plate.

III. Evaluation of the finite element for smeared plates

This section analyses and evaluates the performance of the proposed method for two different cases of simply supported cross-stiffened thin rectangular plates that include a base plate and rib stiffeners. In the first case the vibration of a relatively large panel is examined numerically. In the second case numerical predictions of a smaller panel are compared with measurements.

A. Vibrations

In the first case the dimensions of the base plate are 516 mm x 430 mm with a thickness of 6 mm. The stiffeners are the same both in the *x* and *y* direction, and the height of the stiffeners is 9 mm, the width is 6 mm, and the stiffener spacing is 86 mm. With half end-spacing it follows that there are 6 stiffeners in the *x* direction and 5 stiffeners in the *y* direction, and the plate is assumed to be simply supported along all four edges. The material properties are for hard polyvinyl chloride (PVC), which has a complex Young's modulus of $E = 3\text{x}10^9(1 + \text{i}0.035)$ N/m^2, a Poisson's ratio of $\nu = 0.33$, and a material density of $\rho = 1360$ kg/m^3.

In order to predict the bending vibration of the panel accurately at frequencies up to, say, 800 Hz, the mesh size limit of the FE calculation is taken to be ten times[8] smaller than the bending wavelength[10] in the base plate at that frequency. This means that at least ten elements are included per wavelength of motion below 800 Hz. For the given material parameters, the wavelength of a bending wave is 155 mm at 800 Hz, and 15 mm is therefore chosen to be the maximum mesh size in the FE models.

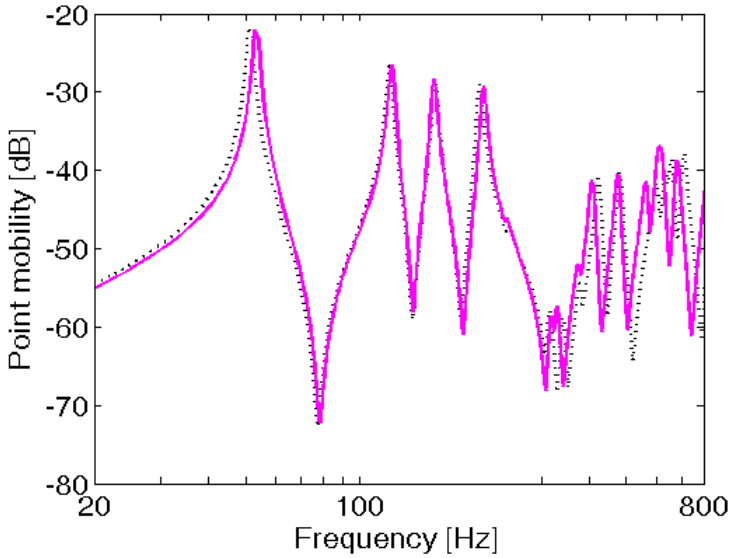

FIG. 1. Calculated point mobility of a simply supported cross-stiffened rectangular plate. The solid line represents the result for the "exact" FE model; the dotted line is for the smeared FE model.

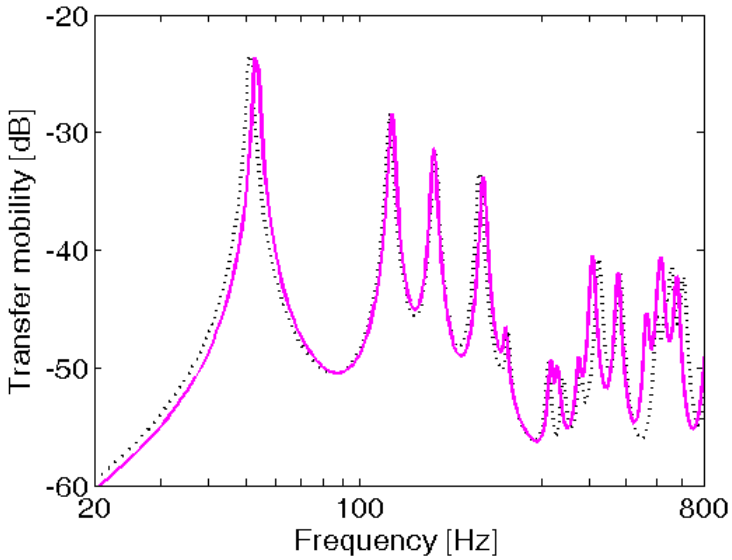

FIG. 2. As in Fig. 1, but for the panel's spatially average mean-square velocity normalized by the square of the driving force.

Forced flexural vibration of the panel is considered in the simulations, which compute the point mobility of the panel and its spatially averaged mean-square velocity. Vibration results of the smeared FE model, which is modeled as an equivalent smeared plate, is compared to an "exact" FE model that contains all stiffener details of the structure. The structure is driven by an unit point force at coordinates (x_0, y_0) = (0.081 m, 0.096 m), where the origin of the coordinate system is at the center plate surface, and the x axis is parallel to the longer edge of the plate. The equivalent material parameters of the smeared model is calculated according to Eqs. (5) to (8); the values are shown in Table 1. The calculated results for the driving point mobility are shown in Fig. 1, where the result of the smeared model is compared with the "exact" model. It can be seen that a good agreement is achieved except for minor deviations, especially at higher frequencies, presumably because the upper frequency limit of the smearing technique is reached. The smearing technique is not expected to work when the frequency is so high that the spacing between the stiffeners is comparable to or larger than half a flexural wavelength in the base plate.

Table 1. The equivalent material properties of the smeared panel.

E_x	5.16e9×(1+i0.035) N/m^2	G_{xy}	9.35e7×(1+i0.035) N/m^2
E_y	5.16e9×(1+i0.035) N/m^2	G_{yz}	1.69e9×(1+i0.035) N/m^2
E_z	3.00e9×(1+i0.035) N/m^2	G_{xz}	1.69e9×(1+i0.035) N/m^2
ν_{xy}	0.33	h_e	7.212e-3 m
ν_{yz}	0.33	ρ	1360 kg/m^3
ν_{xz}	0.33		

Structural acoustic designers are often interested in the spatially averaged velocity of a vibrating panel, for example, for noise control measures. It is therefore of interest to calculate the mean-square vibration velocity averaged over the surface of the plate.[10] This calculation of the mean-square velocity is obtained by averaging over 30 randomly chosen points on the surface of the panel. Figure 2 illustrates the frequency variation of this mean-square velocity normalized by the squared driving force. In this way the result represents the spatially averaged transfer mobility.

Again, the result for the smeared model is seen to be in good agreement with the result for the "exact" model.

B. Sound radiation

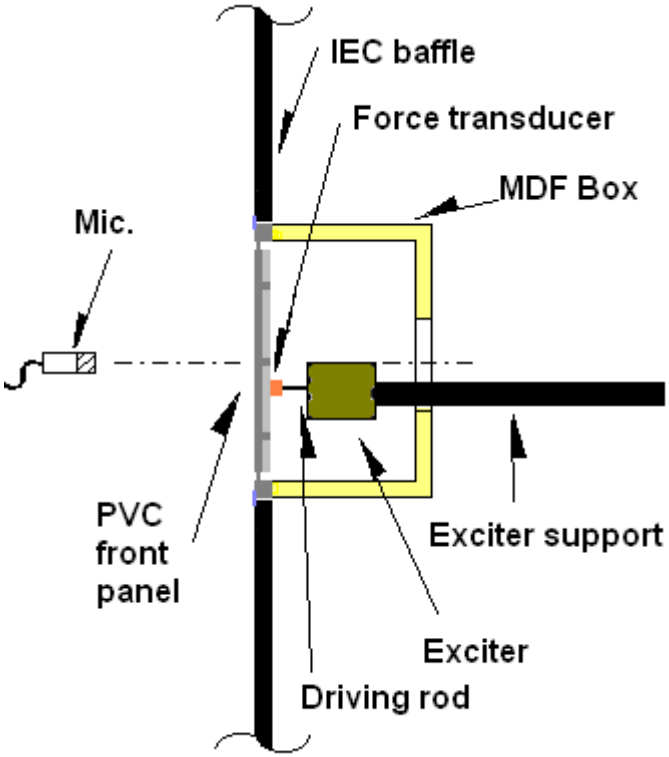

FIG. 3. The experimental setup of an PVC-panel mounted on the box and placed in an IEC baffle.

Predictions of the radiated sound are also of interest. In this section a physical model is used. The sketch of the experimental setup in Fig. 3 shows that the model included a cross-stiffened rectangular test panel of PVC mounted on the front of a supporting, thick-walled open box structure of hard-wood (medium-density fiberboard, MDF). The front panel was fabricated (milled out) from a solid block of hard PVC and comprised an inner panel part, a thin connecting strip, and an outer supporting part. The inner cross-stiffened rectangular plate was supported around the plate perimeter by the thin connecting strip (a machined groove), which was connected to a thick supporting edge. This supporting edge was bolted to a thick-walled hard-wood box. The dimensions of the base plate of the stiffened panel were 344 mm x 258 mm, with a thickness of 6 mm; the stiffeners were identical in the x and y directions with a height of 10 mm, a width of 6 mm, and a stiffener spacing of 86 mm. The thin connecting strip was 2 mm thick and 4 mm wide. The dimensions of the outer supporting part were 390 mm x 325 mm x 18 mm, and the size of the matching open wooden box were 390 mm x 325 mm x 195 mm with a wall thickness of 19 mm. The PVC-panel was screwed on the open front of the wooden box, which had a hole of radius 110 mm located in the center of the rear panel of the wooden box. The material parameters of the PVC-panel were as before, and the material properties of the wooden box were $E = 2.4 \times 10^9(1 + i0.01)$ N/m^2, $\nu = 0.33$, and $\rho = 768$ kg/m^3.

The experimental investigation of the vibration and sound radiation from the panel was carried out in a large anechoic room (with a free volume of 1000 m^3) with the box placed in an free-standing IEC baffle of dimensions 1.35 m x 1.65 m; see Fig. 3. The box was resiliently suspended on soft foam, and the surface of the PVC-panel was located flush with the baffle. The gap between the baffle and the PVC-panel was resiliently sealed in order to avoid transmission of vibration to the baffle. In the experiments the plate was driven by an electrodynamic exciter of type Brüel & Kjær 4810 (B&K, Nærum, Denmark) via a stringer at a stiffener; the coordinates of the drive point were (x_0, y_0, z_0) = (0.043 m, - 0.053 m, 0 m), where the origin of the coordinate system was as previously defined in the center of the plate with the z axis normal to the surface. The input force was measured with a force transducer of type B&K 8200, and the sound pressure was measured with a ½ in. microphone of type B&K 4192 at observation points at a distance of 1 m and 0.3 m from the center of the radiating surface. The force signal was fed to a charge amplifier of type B&K Nexus 2692, and the frequency responses between sound pressure and force were measured using a B&K "PULSE" analyzer 3560 with a frequency resolution of 0.25 Hz.

Vibration estimations determined with an "exact" FE model which includes all details of the stiffened PVC-panel as well as the co-vibrating wooden box are again used as the reference. The air in front of the PVC-panel was modeled as a half sphere with a radius of 0.4 m; and the size of the acoustic finite element was less than 35 mm, which is one sixth of the wavelength at 1600 Hz. Infinite elements were used as boundary conditions at the surface of the half sphere to avoid acoustic reflections. The plane of the half sphere was located in plane with the surface of the PVC-panel, and overlapped areas were coupled; the remaining part of the half sphere plane was modeled as an infinite baffle. The driving position was located on a stiffener of the panel at the same position as with the physical model. The driving force was set to be 1 N, and the estimated results have been normalized by the square of this value. The "exact" FE model and the corresponding smeared FE model were estimated with a commercial software package, ACTRAN, which can solve the sound radiation both in the acoustic near and far field.[8]

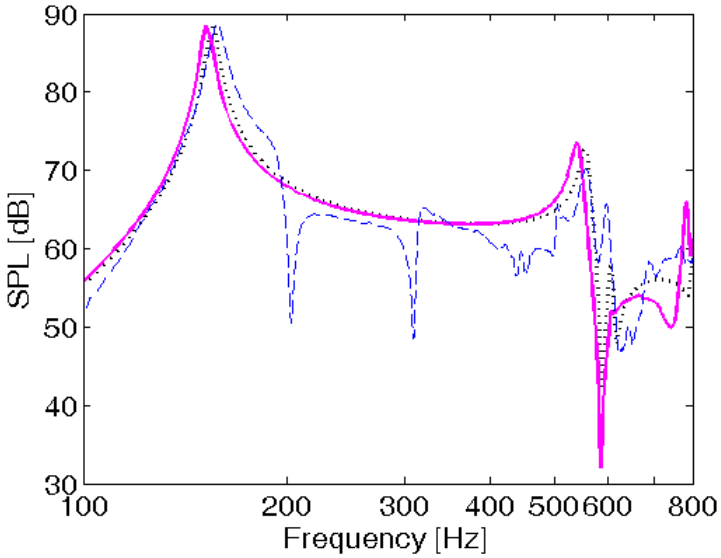

FIG. 4. On-axis sound pressure level at a distance of 1 m, normalized by the driving force, of the models of a cross-stiffened rectangular plate in a box-like structure. The solid line represents the "exact" FE model; the dotted line is for the smeared FE model; the dashed line is the experimental data. The results are referred to a reference of 20 μPa/N.

A smeared FE model for the same case was made with the inner stiffened PVC-panel part modeled as a smeared plate. The equivalent material properties of this smeared model were

obtained in a similar manner as in Section III A, but the results are left out for brevity. In Fig. 4 the results for this smeared FE model are compared with both the experimental data and the “exact” FE results. The figure shows the frequency response of the sound pressure level (normalized by the driving force) at a receiving position placed on the center axis at a position 1 m from the radiating surface of the panel. It is clearly seen that a very good agreement is obtained between the predictions made by the smeared model and the “exact” model. A fairly good overall agreement is also found with respect to the experimental data, but some differences can be observed between the FE models and the experiment. The deviations in all probability are due to shortcomings of the experimental setup, e.g., unintended vibrations in the baffle, sound traveling from the back side of the structure travelling around the baffle, etc. At higher frequencies, the result of the smeared model is slightly different from the “exact” model, presumably because of the limitation of the smearing technique. Figure 5 shows similar results obtained at a receiving position 0.3 m from the radiating surface. The difference between the results estimated by the two FE models and the measurement is observed to be smaller at this receiving position, probably the direct sound is much stronger than the indirect sound compared with the case of 1 m.

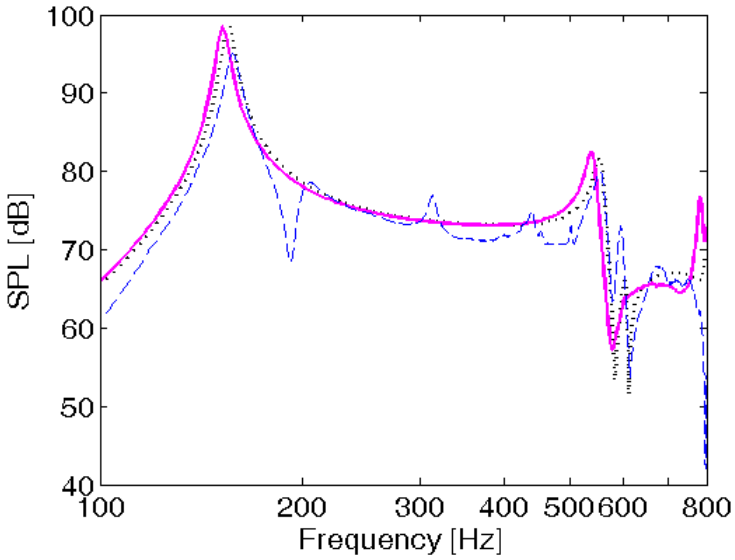

FIG. 5. As in Fig. 4 but at a distance of 0.3 m.

V. CONCLUSIONS

The smearing technique has been employed for determining the equivalent material parameters of cross-stiffened panels. These parameters are then used for modeling the smeared plate by means of a general type of orthotropic finite element. The estimated results are evaluated by comparison with vibration and sound radiation data obtained with “exact” FE models and measurements. For the cases considered it can be concluded that the smeared FE-plate model can estimate the vibration as well as the sound radiation very well up to the frequency limit of the smearing technique.

REFERENCES

[1] P. Lampert, "Postcracking stiffness of reinforced concrete beams in torsion and bending," in R. Szilard, P. Zia, and G. Fisher (eds.), *Analysis of Structural Systems for Torsion*, ACI SP-35 (American Concrete Institute, Detroit, Michigan, 1973).

[2] R. Szilard, *Theories and Applications of Plate Analysis*, Chap. 10, John Wiley & Sons, Hoboken, New Jersey, 2004.

[3] Y. Luan, and M. Ohlrich, "An improvement of the smeared theory for stiffened plates," Proceedings of Noise and Vibration: Emerging Methods 2009, Oxford, England, 2009.

[4] Y. Luan, M. Ohlrich, and F. Jacobsen, "Smearing technique for vibration analysis of simply supported cross-stiffened and doubly curved thin rectangular shells," J. Acoust. Soc. Am.**129** (2), 707-716 (2011).

[5] S. R. Rao, A. H. Sheikh, and M. Mukhopadhyay, "Large-amplitude finite element flexural vibration of plates/stiffened plates," J. Acoust. Soc. Am. **93** (6), 3250-3257 (1993).

[6] A. Berry, J.-L. Guyader, and J. Nicolas, "A general formulation for the sound radiation from rectangular, baffled plates with arbitrary boundary conditions," J. Acoust. Soc. Am. **88**, 2792–2802 (1990).

[7] A. Berry and C. Locqueteau, "Vibration and sound radiation of fluid-loaded stiffened plates with consideration of in-plane deformation," J. Acoust. Soc. Am. **100**, 312-319 (1996)

[8] *ACTRAN 10 User's Manual*, Free Field Technologies, Brussels, 2009.

[9] S. Moaveni, *Finite Element Analysis: Theory and Application with ANSYS*, second ed., pp. 695, Prentice Hall PTR, Upper Saddle River, NJ, 2003.

[10] L. Cremer, M. Heckl, and B.A.T. Petersson, *Structure-Borne Sound*, third ed., pp. 55 and 298, Springer-Verlag, Berlin, 2005.

Bibliography

[1] O. C. Zienkiewicz, *The Finite Element Method*, third ed., McGraw-Hill, New York, 1977.

[2] R. Szilard, *Theories and Applications of Plate Analysis*, Chap. 10, John Wiley & Sons, Hoboken, New Jersey, 2004.

[3] M.S. Troitsky, *Stiffened Plates*, Elsevier, Amsterdam, 1976.

[4] M. Mukhopadhyay and A. Mukherjee, "Recent advances on the dynamic behavior of stiffened plates," The Shock and Vibration Digest **21,** 6-9 (1989).

[5] L. Cremer, M. Heckl, and E. E. Ungar, *Structure-borne sound (2nd ed.)*, pp. 186, Springer, Berlin, 1982.

[6] M. Heckl, "Wave propagation on beam–plate systems," Journal of Acoustical Society of America **33** (5), 640–651 (1961),.

[7] G. Maidanik, "Response of ribbed panels to reverberant acoustic fields," Journal of Acoustical Society of America **34,** 809–826 (1962).

[8] R.S. Langley and K.H. Heron, "Elastic wave transmission through plate/beam junctions," Journal of Sound and Vibration **143** (2), 241–253 (1990).

[9] V. Zalizniak, Y. Tso and L.A. Wood, "Waves transmission through plate and beam junctions, " International Journal of Mechanical Sciences **41**, 831–843 (1991).

[10] T.J. McDaniel and J.P. Henderson, "Review of transfer matrix vibration analysis of Skin–Stringer structures," The Shock and Vibration Digest **6**, 13–19 (1974).

[11] K.M. Liew, Y. Xiang, S. Kitipornchai and M.K. Lim, "Vibration of rectangular Mindlin plates with intermediate stiffeners," Journal of Vibration and Acoustics **116**, 529–535 (1994).

[12] R.B. Bhat, "Vibrations of panels with non-uniformly spaced stiffeners," Journal of Sound and Vibration **84** (3) , 449–452 (1982).

[13] J.R. Wu and W.H. Liu, "Vibration of rectangular plates with edge restraints and intermediate stiffeners," Journal of Sound and Vibration **123** (1), 103–113 (1988).

[14] M. Chiba and I. Yoshida, "Free vibration of a rectangular plate–beam coupled system," Journal of Sound and Vibration **194** (1), 49–65 (1996).

[15] P.A.A. Laura and R.H. Gutierrez, "A note on transverse vibrations of stiffened rectangular plates with edges elastically restrained against rotation," Journal of Sound and Vibration **78**, 139–144 (1976).

[16] G. Asku and R. Ali, "Free vibration analysis of stiffened plates using finite difference method," Journal of Sound and Vibration **48**, 15–25 (1976).

[17] H.L. Cox and W.A. Bernfield, "Vibration of uniform square plates bounded by flexible beams," Journal of Acoustical Society of America **31**, 963–966 (1959).

[18] L. Doze and M. Ricciardi, "Free vibration analysis of ribbed plates by a combined analytical–numerical method," Journal of Sound and Vibration **319**, 681–697 (2009).

[19] H. Zeng and C.W. Bert, A differential quadrature analysis of vibration for rectangular stiffened plates, Journal of Sound and Vibration **241** (2) , 247–252 (2001).

[20] L.X. Peng, K.M. Liew and S. Kitipornchai, Buckling and free vibration analysis of stiffened plates using the FSDT mesh-free method, Journal of Sound and Vibration **289**, 421–449 (2006).

[21] S.B. Hong, A.M. Wang and N. Vlahopoulos, A hybrid finite element formulation for a beam–plate system, Journal of Sound and Vibration **298**, 233–256 (2006).

[22] H. Xu, J. Du, W.L. Li, Vibrations of rectangular plates reinforced by any number of beams of arbitrary lengths and placement angles, Journal of Sound and Vibration **329**, 3759-3779 (2010).

[23] W. H. Hoppmann II, "Some characteristics of the flexural vibrations of orthogonally stiffened cylindrical shells," Journal of Acoustical Society of America **30**, 77–82 (1958).

[24] Manning, J. E., and Maidanik, G., "Radiation Properties of Cylindrical Shells," Journal of Acoustical Society of America **36**, 1691–1698 (1964).

[25] S. A. Rinehart and J. T. S. Wang, "Vibration of simply supported cylindrical shells with longitudinal stiffeners," Journal of Sound and Vibration **24**, 151-163 (1972).

[26] D. J. Mead and N. S. Bardell, "Free vibration of a thin cylindrical shell with discrete axial stiffeners," Journal of Sound and Vibration **111**, 229-250 (1986).

[27] D. J.Mead and N. S. Bardell, "Free vibration of a thin cylindrical shell with periodic circumferential stiffeners," Journal of Sound and Vibration **115**, 499-520 (1987).

[28] B. A. J. Mustafa and R. Ali, "Prediction of natural frequency of vibration of stiffened cylindrical shells and orthogonally stiffened curved panels," Journal of Sound and Vibration **113**, 317-327 (1987).

[29] B. A. J. Mustafa and R. Ali, "Free vibration analysis of multi-symmetric stiffened shells," Computers and Structures **27**, 803-810 (1987).

[30] N. S. Bardell and D. J. Mead, "Free vibration of an orthogonally stiffened cylindrical shell, Part I: Discrete line simple supports," Journal of Sound and Vibration **134**, 29-54 (1989).

[31] N. S. Bardell and D. J. Mead, "Free vibration of an orthogonally stiffened cylindrical shell, Part II: Discrete general stiffeners," Journal of Sound and Vibration **134**, 55-72 (1989).

[32] Z. Mecitoglu and M. C. Dökmeci, "Forced vibrations of stiffened cylindrical elastic panels," Journal of Acoustical Society of America **85**, S118 (1989).

[33] S. P. Cheng and C. Dade, "Dynamic analysis of stiffened plates and shells using spline Gauss collocation method," Computers and Structures **36**, 623-629 (1990).

[34] M. L. Accorsi and M. S. Bennett, "A finite element based method for the analysis of free wave propagation in stiffened cylinders," Journal of Sound and Vibration **148**, 279-292 (1991).

[35] Z. Mecitoglu and M. C. Dokmeci, "Free vibrations of a thin, stiffened, cylindrical shallow shell," *AIAA* J. **30**, 848-850 (1991).

[36] R. S. Langley, "A dynamic stiffness technique for the vibration analysis of stiffened shell structures," Journal of Sound and Vibration **156**, 521-540 (1992).

[37] M. Conti and I. Dyer , "The influence of internal structures on bistatic scatter from finite cylindrical shells near axial incidence (A)," Journal of Acoustical Society of America **94**, 1878 (1993).

[38] D. M. Photiadis, J. A. Bucaro, and B. H. Houston, "Scattering from flexural waves on a ribbed cylindrical shell," Journal of Acoustical Society of America **96**, 2785–2790 (1994).

[39] G. Maze, D. Décultot, A. Klauson, and J. Metsaveer , "Acoustic scattering by immersed circular cylindrical shell stiffened by internal lengthwise rib (A)," Journal of Acoustical Society of America **95**, 2868 (1994).

[40] A. Klauson, G. Maze, and J. Metsaveer , "Acoustic scattering by submerged cylindrical shell stiffened by an internal lengthwise rib," Journal of Acoustical Society of America **96**, 1575 (1994).

[41] A. Klauson, J. Metsaveer, D. Décultot, G. Maze, and J. Ripoche , "Identification of the resonances of a cylindrical shell stiffened by an internal lengthwise rib," Journal of Acoustical Society of America **100**, 3135 (1996).

[42] A. J. Stanley and N. Ganesan, "Free vibration characteristics of stiffened cylindrical shells," Computers and Structures **65**, 33-45 (1997).

[43] D. M. Photiadis and B. H. Houston, "Anderson localization of vibration on a framed cylindrical shell," Journal of Acoustical Society of America **106**, 1377–1391 (1999).

[44] M. H. Marcus, B. H. Houston, and D. M. Photiadis, "Wave localization on a submerged cylindrical shell with rib aperiodicity," Journal of Acoustical Society of America **109**, 865–869 (2001).

[45] M. Tran-Van-Nhieu, "Scattering from a ribbed finite cylindrical shell," Journal of Acoustical Society of America **110**, 2858–2866 (2001).

[46] R. Liétard, D. Décultot, G. Maze, and M. Tran-Van-Nhieu, "Acoustic scattering from a finite cylindrical shell with evenly spaced stiffeners: Experimental investigation," Journal of Acoustical Society of America **118**, 2142–2146 (2005).

[47] D. G. Karczub, "Expressions for direct evaluation of wave number in cylindrical shell vibration studies using the Flügge equations of motion," Journal of Acoustical Society of America **119**, 3553–3557 (2006).

[48] M. Caresta and N. J. Kessissoglou, "Structural and acoustic responses of a fluid loaded cylindrical hill with structural discontinuities," Appl. Acoust. **70**, 954–963 (2009).

[49] Z. Mecitoğlu, "Vibration characteristics of a stiffened conical shell," Journal of Sound and Vibration **197**, 191-206 (1992).

[50] A. N. Nayak and J. N. Bandyopadhyay, "Dynamic response analysis of stiffened conoidal shells," Journal of Sound and Vibration **291**, 1288-1297 (2006).

[51] W. Soedel, *Vibrations of Shells and Plates*, third edition, Chap. 6, Marcel Dekker, Inc.. New York, 1993.

[52] L. Cremer, M. Heckl, B.A.T. Petersson, *Structure-Borne Sound*, third ed. , pp. 55, 123, 298-300, Springer-Verlag, Berlin, 2005.

[53] S. R. Rao, A. H. Sheikh, and M. Mukhopadhyay, "Large-amplitude finite element flexural vibration of plates/stiffened plates," J. Acoust. Soc. Am. **93** (6), 3250-3257 (1993).

[54] A. Berry, J.-L. Guyader, and J. Nicolas, “A general formulation for the sound radiation from rectangular, baffled plates with arbitrary boundary conditions,” J. Acoust. Soc. Am. **88**, 2792–2802 (1990).

[55] A. Berry and C. Locqueteau, “Vibration and sound radiation of fluid-loaded stiffened plates with consideration of in-plane deformation,” J. Acoust. Soc. Am. **100**, 312-319 (1996).

[56] *ACTRAN 10 User's Manual*, Free Field Technologies, Brussels, 2009.

[57] S. Moaveni, *Finite Element Analysis: Theory and Application with ANSYS*, second ed., 695, Prentice Hall PTR, Upper Saddle River, NJ, 2003.

Appendix: Cabinet vibration and sound radiation induced by a loudspeaker unit

This appendix addresses the problem of modeling the structural acoustic properties of a loudspeaker system which comprises a numerically modeled cabinet and a physical loudspeaker unit. This study focuses on the determination of the excitations from the loudspeaker unit that causes unwanted audible vibration and associated sound radiation from the cabinet panels.

The panel vibrations and associated sound radiations described in the main body of this dissertation were generated by a point force acting on the cross-stiffened PVC-panel; in the reported experiments this was mounted as one panel on a wooden box cabinet. This appendix considers a different arrangement where the vibration was generated by a built-in loudspeaker unit mounted in the wooden cabinet at the wooden panel opposite to the mounted PVC-panel. Vibration is thus transmitted from the loudspeaker unit via its frame support to the wooden box, and further to the rear-mounted PVC-panel. In addition to this edge excitation, the PVC-panel is also excited by the high interior sound pressure in the enclosure as caused by the vibrating membrane of the loudspeaker unit.

The steel frame and circular flange of the loudspeaker unit were mounted to the box with six screws around the circumference of the flange. With only four magnet-supporting steel brackets the loudspeaker unit was not fully axis-symmetric in a structural sense. Assuming that the loudspeaker unit (considered as source) is strongly connected to the cabinet (considered as receiver) at the screw positions, the vector of coupled normal velocities $\mathbf{v}_{\mathbf{couple}}$ at these contact points can be calculated to be [52]

$$\mathbf{v}_{\mathbf{couple}} = \mathbf{Y}_{\mathbf{R}} \left[\mathbf{Y}_{\mathbf{S}} + \mathbf{Y}_{\mathbf{R}} \right]^{-1} \mathbf{v}_{\mathbf{free}}, \tag{A.1}$$

where $\mathbf{v}_{\mathbf{free}}$ is the vector of free source velocities, and $\mathbf{Y}_{\mathbf{S}}$ and $\mathbf{Y}_{\mathbf{R}}$ are the mobility matrices of the source and receiver, respectively. It is the voltage-dependent free velocity vector of the source mounting flange and its mobility matrix that characterize the vibrational properties of the loudspeaker unit. With a given physical loudspeaker unit and a cabinet, the elements of the matrices $\mathbf{Y}_{\mathbf{S}}$ and $\mathbf{Y}_{\mathbf{R}}$ can be measured. In a real design process of a loudspeaker cabinet, the loudspeaker unit is usually given. For this, an FE model of the cabinet is generated, and then the $\mathbf{Y}_{\mathbf{R}}$ can be calculated with the FE model. Thus, by solving Eq. (A.1), the coupled velocity at each screw point is obtained, and these velocities may then used as boundary conditions of the FE model of the cabinet. The resulting sound pressure in the air could then be obtained by the FE model combining with air. However, the high sound pressure in the enclosed cabinet has not yet been taken into account in this calculation. A possible way of including the high excitation pressure will be discussed as future work.

A. Vibration experiments

In this section, the mobility matrices of the unit $\mathbf{Y}_{\mathbf{S}}$ and of the cabinet $\mathbf{Y}_{\mathbf{R}}$ have been measured at six screw positions, respectively, as well as the free vibration velocities of the loudspeaker unit and the coupled velocities when the unit was mounted in the box. The analytical coupled velocity

vector obtained by solving Eq. (A.1) is then compared to the measured results. This is done in order to test the utility of Eq. (A.1) with the assumptions of strong connections between the frame and the cabinet, as well as the assumption of neglecting the high sound pressure in the volume of the cabinet.

Figure A-1. The 10 inch loudspeaker unit placed on soft foam.

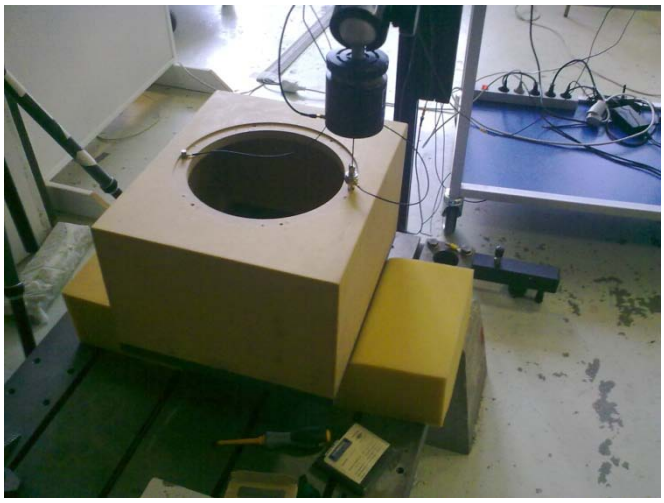

Figure A-2. Loudspeaker cabinet placed on soft foam.

Figure A-1 and Figure A-2 show the loudspeaker unit and the box cabinet placed on soft foam supports that enable mobility measurements under free boundary conditions. The loudspeaker unit has six mounting screw holes on the frame, and these are named position Nos. 1 – 6. The box cabinet has six corresponding screw holes. Since there are six mounting positions, each mobility matrix contains six by six mobility functions. In the mobility measurement, the loudspeaker unit and box were driven via a stringer by an electrodynamic exciter at each of the numbered positions. The input force was measured with a force transducer of type Brüel & Kjær (B&K) 8200, and the response velocities were measured with an accelerometer of type B&K 4393. The force and velocity signals were connected to charge amplifiers of type B&K Nexus 2692, and the frequency responses between force and velocities were measured using a B&K “PULSE” analyzer 3560 with a frequency resolution of 0.25 Hz.

As typical examples, Figure A-3 shows the magnitude and phase of the measured point mobility at position No. 1 of the loudspeaker unit and box cabinet. It is observed that the receiver mobility is lower than the source mobility by about 25 dB in large parts of the low frequency range.

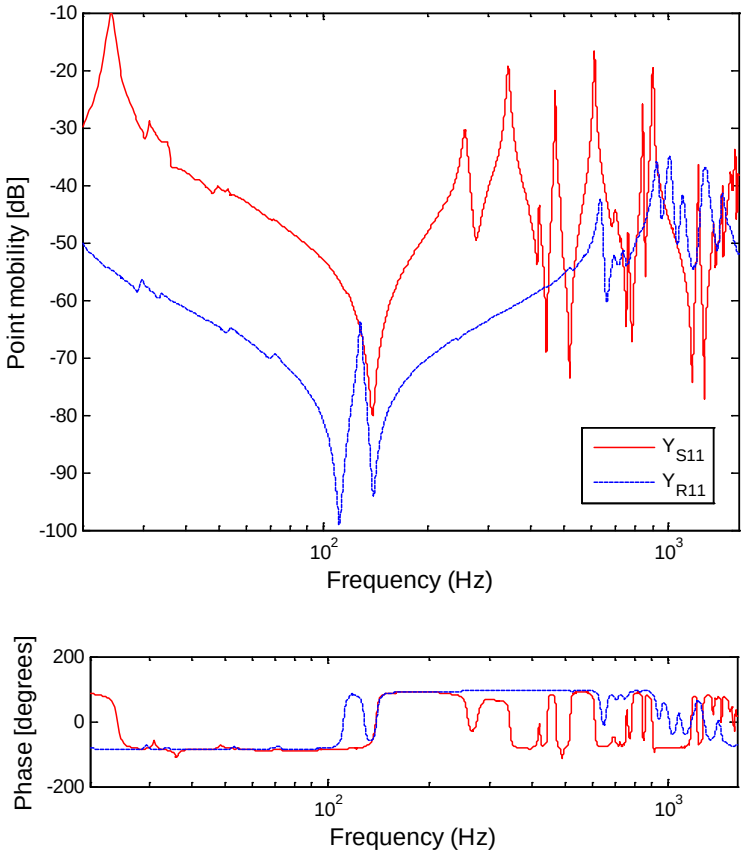

Figure A-3. Point mobility of the loudspeaker unit Y_{S11} and of the box structure Y_{R11} at position No. 1.

Corresponding transfer mobilities between position 1 and the diagonal position 4 are compared with the point mobilities in Figure A-4 and Figure A-5. For the loudspeaker unit the results show that the transfer mobility is of the same level as the associated point mobilities. Moreover, the transfer mobility is seen to be in anti-phase in the frequency range from 25 Hz to 135 Hz where the unit is inertia controlled and undergoing angular (rocking) motion. On the other hand, the transfer mobility of the cabinet is seen to be much lower in level than the point mobilities, but in phase in the mass controlled frequency range. This means that the cabinet primarily vibrates translationally in the mentioned frequency range. At higher frequencies, the frequency variations of the mobilities become more complex as a result of the modal properties of the structures.

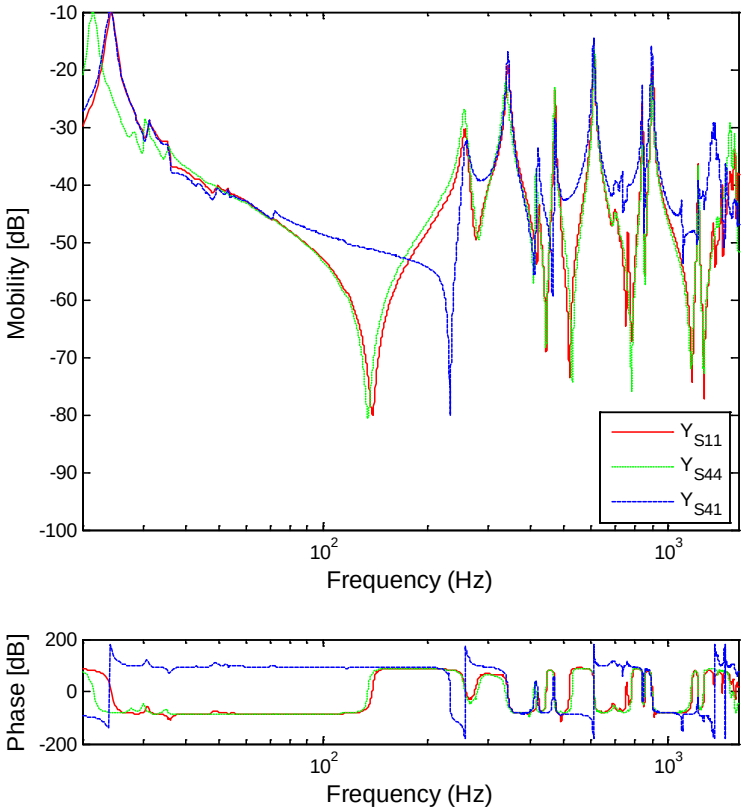

Figure A-4. Point mobilities of the loudspeaker unit at mounting positions 1and 4, and the associated transfer mobility Y_{S41}.

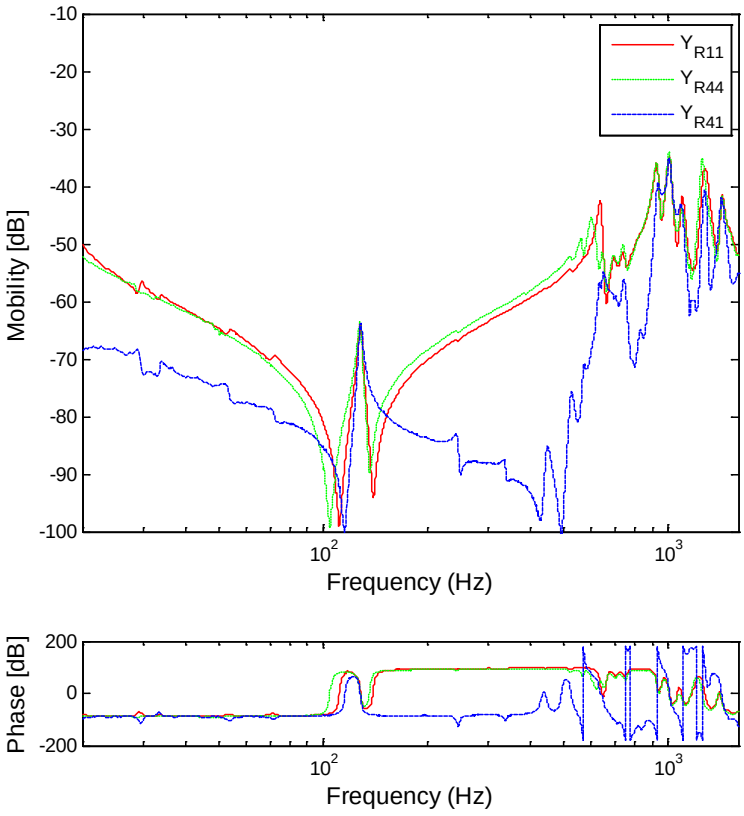

Figure A-5. Point mobilities of the cabinet at mounting positions 1 and 4, and the associated transfer mobility Y_{R41}.

Also measured were the free and coupled vibrations of the loudspeaker unit when this was active and driven by an electrical signal of white noise. Thus, the free velocity of the loudspeaker unit was measured at positions 1 to 6, and so were the corresponding coupled velocities when the loudspeaker unit and cabinet were assembled. Figure A-6 shows the results for position 1. Note that the coupled velocity was measured with the unit mounted in the box cabinet, and hence with the cabinet is actually closed. With the exception of the two peaks at 131 Hz and 172 Hz, it can been seen that the coupled velocity mostly is lower than the free velocity at frequencies below 500 Hz. The former value is the natural frequency mode (1,1) of the stiffened PVC-panel; the latter is estimated to be the natural frequency of an approximate mass-spring-mass system formed by the masses corresponding to the PVC-panel and the moving part of the loudspeaker unit and with the spring caused by the air volume in the closed cabinet.

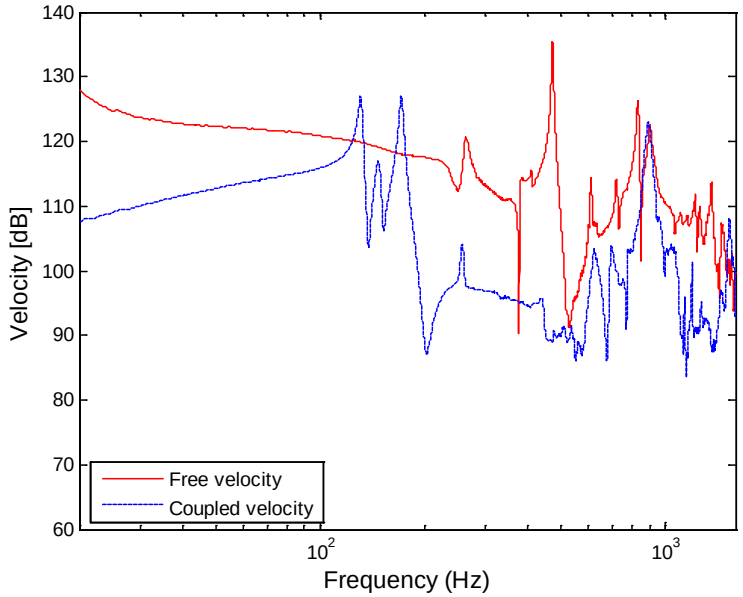

Figure A-6. Free velocity of loudspeaker unit, and coupled velocity of the assembled loudspeaker unit and cabinet at position No. 1. The velocity levels in dB re 1 nm/s are normalized by the input voltage to the loudspeaker unit.

The coupled velocities are obtained by solving Eq. (A.1) and this includes inverting the sum of the six by six mobility matrices. The result for position 1 is shown together with the experimental result in Figure A-7. It is seen that there is some agreement in the overall spectral shape of the results, but significant deviations are found at certain frequencies, for example at about 140 Hz and 450 Hz. The enclosed air in the cabinet has an impedance on the stiffened PVC-panel. This moves the natural frequency of the fundamental mode of the PVC-panel to a lower frequency. Moreover, the mentioned mass-spring-mass system for the measured coupled velocity has not been taken into account in the analytical result, and therefore the peak at 172 Hz in the experimental result (blue curve) has no corresponding peak in the analytical result (red curve). Furthermore, the deviation around 450 Hz is assumed to be caused by the high sound pressure in the closed air volume in the cabinet, which was not included in the calculation. Therefore, the pressure excitation needs to be taken into account in the calculation; this study is left for future work.

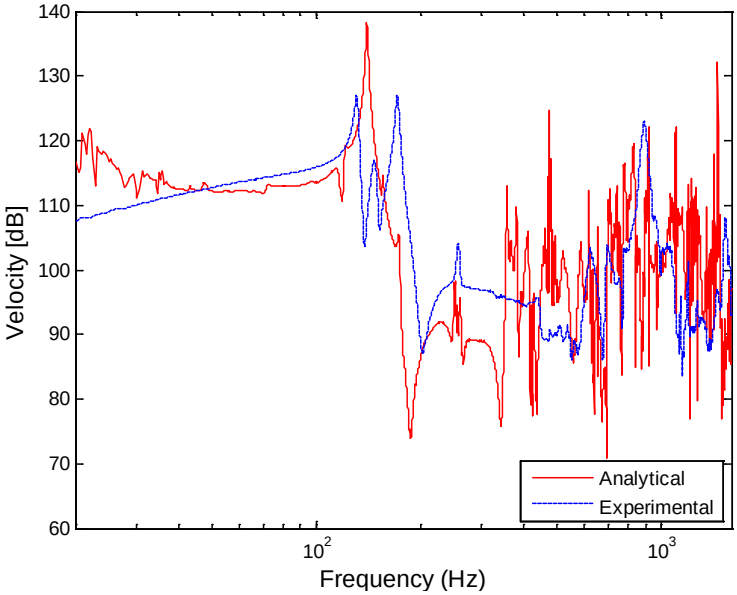

Figure A-7. Comparison of experimental and analytical coupled velocity normalized by input voltage to the loudspeaker unit; results for position 1.

B. Experiments of sound radiation

This section presents the experiments for investigating the sound radiation of the PVC-panel when the built-in loudspeaker unit is acting. The experimental setup in Section 4.2 is employed again, but with the loudspeaker unit mounted in the box and activated by white noise, i.e. with the exciter removed, see Figure B-1. Measurement of the unwanted sound radiation from the 'rear' PVC-panel with the operating built-in loudspeaker unit is a difficult task, even when the PVC-panel placed in a baffle. This is because the very strong sound pressure from the loudspeaker unit will contribute to the sound pressure on the 'rear' side because of diffraction and possibly acoustic excitation of the baffle.

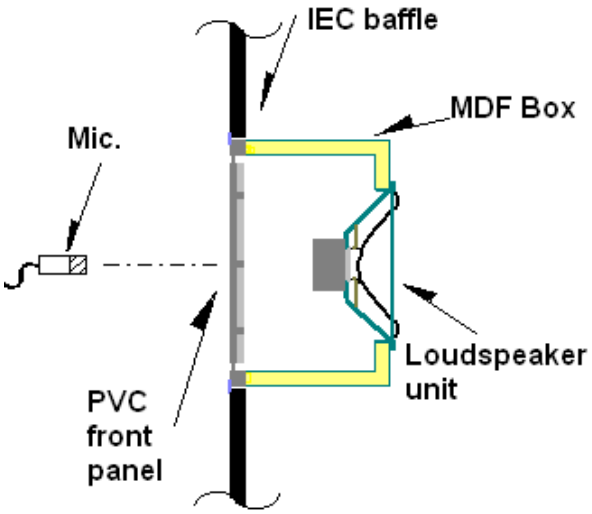

Figure B-1. Experimental setup for sound radiation of the PVC-panel

In order to minimize the influence of radiation and diffraction of sound from the loudspeaker unit, the baffle was extended with 40 cm on the two shorter sides in Figure B-2. This was expected to reduce the sound by a longer travel distance. Moreover, a rectangular tube-baffle over the cabinet and loudspeaker unit was placed to isolate the sound from the loudspeaker unit; the connection was resiliently sealed by type. The open ended tube was anechoicly terminated by a 1 m long wedge of mineral wool. This experimental setup is shown in Figure B-3. In this way, the sound from the loudspeaker unit is somewhat isolated, and its associated acoustic excitation of the baffle structure is also minimized. The frequency responses of the measured sound pressure at 2 m in front of the PVC-panel are shown in Figure B-4 for the experimental arrangements with the mentioned baffles. The resulting pressure curve of the final setup is obviously lower than the other results by about 10 dB overall, and therefore, the sound from the loudspeaker unit and the acoustic excitation of the baffle is seen to be very much reduced.

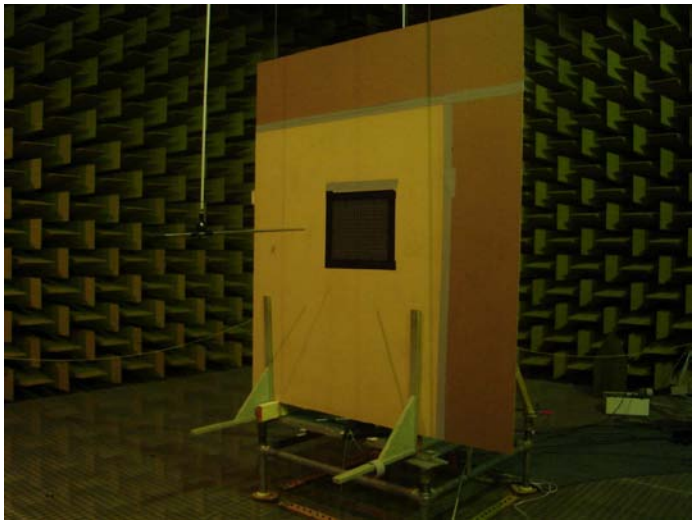

Figure B-2. Extended baffle.

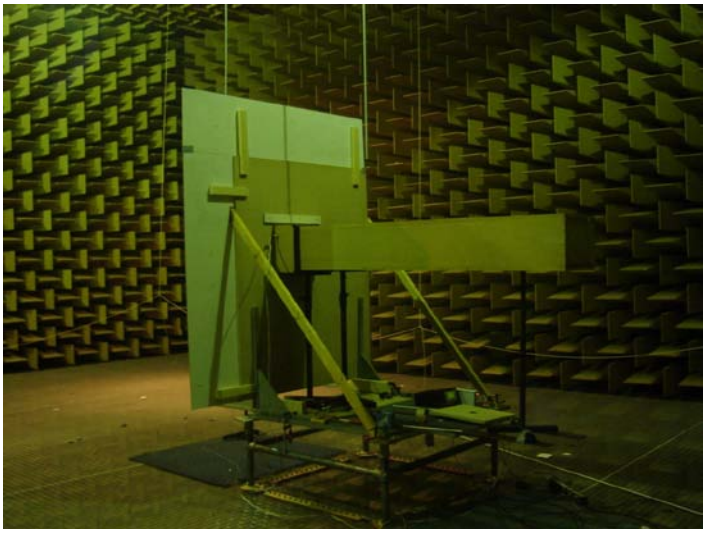

Figure B-3. Experimental setup with extended baffle and tube for measuring the sound pressure of a loudspeaker cabinet.

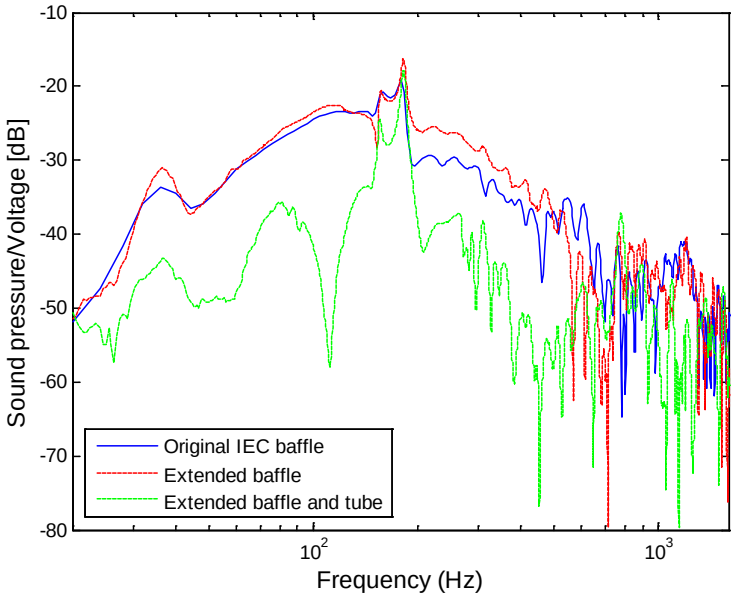

Figure B-4. Frequency responses of sound pressure with different baffles at 2 m in front of the PVC-panel normalized by the input voltage to the loudspeaker unit.

Figure B-5 illustrates the sound pressures measured at a position 1 m in front of the stiffened PVC-panel and in front of the loudspeaker unit. These results are normalized by the input voltage to the loudspeaker unit. This is done in order to illustrate how much the baffles reduce the sound radiated by the loudspeaker unit. It is seen that the result in front of the PVC-panel obtained without the extended baffle and tube baffle is less than 10 dB lower than the result in front of the loudspeaker unit at frequencies lower than 140 Hz, and the results with the baffles mostly is more than 20 dB reduced in the same frequency range. A similar comparison with a slightly better reduction of sound is obtained at higher frequencies from 200 Hz to 500 Hz. At still higher

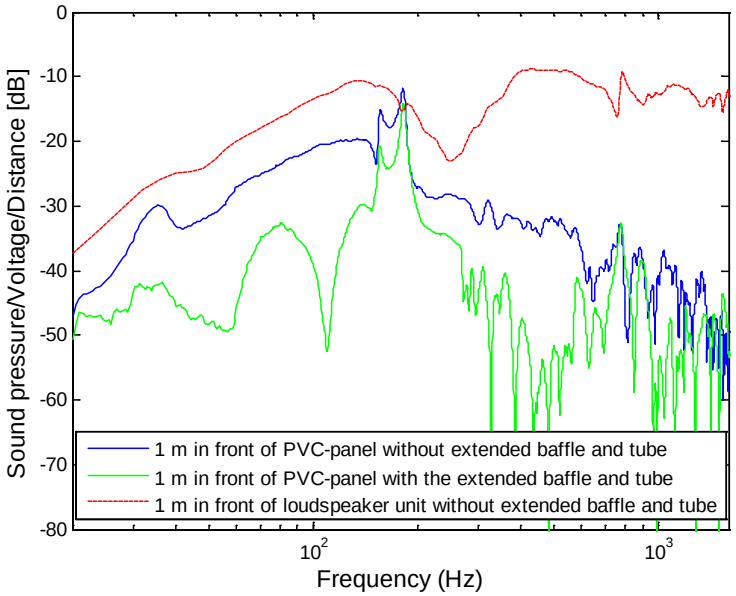

Figure B-5. Frequency responses of sound pressure measured at different positions normalized by the input voltage to the loudspeaker unit.

frequencies, the sound from the loudspeaker unit cannot diffract even at the edges of the original IEC baffle according to the short sound wavelength in the air. However, the two peaks at 131 Hz and 172 Hz in the results in front of the PVC-panel are seen to be very high. They are, as previously mentioned, caused by the sound radiated by the vibrating PVC-panel, and therefore, the baffles cannot reduce them.

With the final experimental setup, Figure B-6 shows the sound pressure measured at a distance of 1, 2, and 4 m in front of the stiffened PVC-panel. These results is normalized in the same way as mentioned. It is anticipated that these curves can be used in future work as references to evaluate the FE model results.

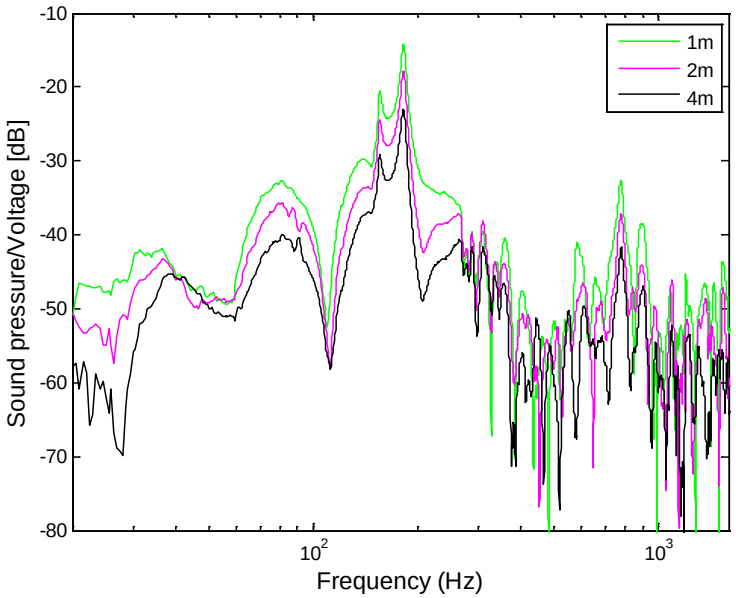

Figure B-6. Sound pressure at 1/2/4 m in front of the stiffened PVC-panel normalized by the input voltage to the loudspeaker unit.

Also for future work, an FE model of the cabinet needs to be generated. As to the numerical modeling of the cabinet each term of $\mathbf{Y_R}$ at each screw position can be calculated from a forced response simulation and substituted into Eq. (A.1) together with the measured $\mathbf{v_{free}}$ and $\mathbf{Y_S}$ of the loudspeaker unit to get the coupled velocity. This is then used as a boundary condition to the FE model of the cabinet combined with air to estimate the sound radiation. Still, the high sound pressure in the box is a challenge. It could be predicted by modeling the air volume in the cabinet box in the FE model.

www.elektro.dtu.dk
Department of Electrical Engineering
Acoustic Technology
Technical University of Denmark
Ørsteds Plads
Building 348
DK-2800 Kgs. Lyngby
Denmark
Tel: (+45) 45 25 38 00
Fax: (+45) 45 93 16 34
Email: info@elektro.dtu.dk

ISBN 978-87-92465-98-6